Electronic Thesis and Dissertation Repository

6-17-2024 1:00 PM

Cortical Thickness Changes as a Potential Biomarker for Epilepsy in People with First-Time Unprovoked Seizure

Keza T. Motlana, *Western University*

Supervisor: Khan, Ali, *The University of Western Ontario*
Co-Supervisor: Mirsattari, Seyed, *The University of Western Ontario*
A thesis submitted in partial fulfillment of the requirements for the Master of Science degree in Neuroscience
© Keza T. Motlana 2024

Follow this and additional works at: https://ir.lib.uwo.ca/etd

Part of the Neuroscience and Neurobiology Commons

Abstract

Accurate epilepsy diagnosis after a First-Time Unprovoked Seizure (FTUS) remains challenging as the epileptogenic abnormalities and epileptiform EEG abnormalities used for such diagnoses infrequently occur and are often missed or misinterpreted. Expanding the scope of diagnostic abnormalities to include cortical thickness changes could enhance diagnostic efficacy. This is because cortical thickness changes are a significantly prevalent pathophysiological change that occurs in cases of epilepsy progressively, independent of seizure frequency, drug load and age. These changes are theorised to be a product of epileptogenesis, the process in which brain networks undergo disruptions becoming epileptic. This study aims to investigate whether these changes can be used for epilepsy diagnosis by determining if epileptogenic brain network changes and cortical thickness changes are present as early as the FTUS of epilepsy. In this study, 16 healthy controls and 16 FTUS patients were recruited and underwent 7T structural Magnetic Resonance Imaging (MRI) scans; of the 16 FTUS patients, six were confirmed to be epileptic (CE). The participants' MRI scans were parcellated using the 17-network Schaefer 200 and 100 parcellation maps. Within these maps, the average cortical thicknesses per region were measured for each participant group and used for between-group comparisons. These comparisons contrasted the cortical thicknesses of the FTUS patients with their age- and sex-matched healthy controls (HC) and the cortical thicknesses of solely the CE patients with their age- and sex-matched HC. Each between-group comparison included both mixed-sex and sex-based comparisons. The cortical thickness measures were used for structural covariance analysis, with the calculated nodal and global measures undergoing the same set of between-group comparisons conducted for the cortical thickness measures. No statistically significant differences in cortical thickness were observed in any of the comparisons. At both parcellation levels, the CE patients displayed sex-dependent statistically significant differences in their structural covariance nodal measures. These differences indicate that brain network changes are present as early as the FTUS and support the theory that the cortical thickness changes observed in people with epilepsy are a byproduct of the network disruptions observed in epilepsy. Indicating that cortical thickness changes are not an ideal diagnostic symptom for epilepsy.

Keywords: MRI, Epilepsy, Seizures, Cortical thickness, Structural covariance analysis

Summary for Lay Audiences

When an individual experiences a seizure for the first time in their life, there is no guarantee that the seizure occurred due to epilepsy. As a result, individuals who have experienced a seizure undergo a series of medical exams and neuroimaging scans to determine if such seizures are due to epilepsy. However, accurate and prompt epilepsy diagnosis is still an ongoing issue as the current definitive indicators of epilepsy are not universal; as such, there is a need for additional epilepsy indicators that can be noticed as early as the first-time unprovoked seizure (FTUS). One such indicator could be cortical thickness changes, as past research on people with epilepsy (PWE) has shown it to occur progressively in PWE regardless of age and seizure frequency. This research study aims to investigate whether cortical thickness changes can be used as an observable epilepsy symptom for diagnosis by evaluating the cortical thicknesses of individuals who have experienced a first-time seizure. Additional research looking into the brain networks of the participants will be conducted as past research has indicated that the cortical thickness changes occurring in PWE are a product of brain network changes. The cortical thicknesses of individuals who have experienced a first-time seizure were measured via 7T MRI scans, the strongest human MRI scan available, and compared with healthy participants of the same age and sex as the patients. These comparisons were conducted once for all of the FTUS patients and then once again for the FTUS patients who were confirmed to have epilepsy. These cortical thickness measures were then used for structural covariance analysis, which uses the biological phenomenon of brain morphological features, like cortical thickness, reflecting brain networks to quantify and evaluate brain networks. This study's results indicated no cortical thickness changes could be detected at the FTUS stage. Still, the data did suggest that there were observable brain network changes in the FTUS patients who were confirmed to have epilepsy.

Acknowledgements

Table of Contents

Lists of Tables

List of Figures

List of Appendices

List of Abbreviations

AED/ASM	Anti-epileptic drug/Anti-seizure medication
AFNI	Analysis of functional neuroimages
B_0	Initial MRI magnetic field
$B_1{}^+$	Homogenous radiofrequency transmit field
CE	(subjects) Confirmed to be epileptic
EEG	Electroencephalogram
FDR	False discovery rate
FoV	Field of view
FLE	Frontal lobe epilepsy
fMRI	Functional magnetic resonance imaging
FTUS	First-time unprovoked Seizure
GRE	Gradient-recalled echo
gwMRF	Gradient-weighted markov random Field
HARNESS	Harmonized Neuroimaging of Epilepsy Structural Sequences
HC	Healthy controls
HCP-MMP	Human connectome project multi-modal parcellation
IGE	Idiopathic generalised epilepsy
ILAE	International league against epilepsy
L-TLE	Left temporal lobe epilepsy
MCD	Malformations of cortical development
mm	Millimeter
MNI	Montreal neurological institute
MNI	Montreal neurological institute
MP-RAGE	Magnetization Prepared-rapid Gradient Echo
MP2RAGE	Magnetization Prepared 2-rapid Gradient Echo
MRI	Magnetic resonance imaging
ms	Milisecond
M_{xy}	Transverse plane longitudinal magnetisation
M_z	Net longitudinal magnetisation
NMR	Nuclear magnetic resonance

PET	Positron emission tomography
PWE	People with epilepsy
QoL	Quality of life
R-TLE	Right temporal lobe epilepsy
RF	Radiofrequency
ROI	Region of interest
rs-fMRI	Resting state functional magnetic resonance imaging
SA2RAGE	Saturation-prepared with 2 rapid Gradient Echoes
SCN	Structural covariance brain network
SCONA	Structural covariance brain network analyses
SNR	Signal-to-noise ratio
T	Tesla
T1w	T1-weighted
T2w	T2-weighted
TE	Echo time
TLE	Temporal lobe epilepsy
TR	Repetition time
UNI	Uniform image

1. Chapter 1: Introduction and Background

1.1. Introduction

1.1.1. Epilepsy and Seizures

Epilepsy is one of the most common neurological disorders in the world, affecting 6.38 people per 1,000 persons with an incidence rate of 61.44 people per 100,000 persons per year, for an estimated total of 50 million people with epilepsy (PWE) internationally (Beghi, 2019; Fiest et al., 2016; World Health Organization, 2019). Also known as a seizure disorder, epilepsy is characterised by recurrent and unprovoked seizures, temporary disruptions of neurological function occurring due to abnormal excessive or hypersynchronous firing of cortical neurons in abnormal patterns (Fisher et al., 2017). These unprovoked epileptic seizures can occur due to any number of reasons ranging from brain injuries such as head trauma and brain lesions to reasons currently unknown (Egesa et al., 2022). The underlying causes of these seizures significantly influence how they manifest as seizure type is dependent on onset location, propagation pattern, as well as the patient's sleep cycle, brain maturity and medical history (Egesa et al., 2022; Fisher et al., 2017; Fisher et al., 2005). Seizure cause and type, in turn, influence their effect on PWE's memory, behaviour, sensory perception, motor capabilities or automatic functions, emotional state, cognitive capacity or consciousness (Fisher et al., 2017; Fisher et al., 2005).

As a disorder, epilepsy does not refer to a single disease but rather a complex network of numerous biological disorders and diseases centralised around the primary symptom of recurring seizures (Behr et al., 2016; Fisher et al., 2014). As a result, there is a wide array of epilepsy types, and it is due to this extreme variation that epilepsy diagnosis depends not on whether a seizure has occurred but rather on the chance of seizure recurrence. Cases of epilepsy in adults are typically identified and diagnosed following the occurrence of a First-Time Unprovoked Seizure (FTUS) through the use of the International League Against Epilepsy's (ILAE) three diagnostic criteria (Fisher et al., 2014). These diagnostic criteria are used because although seizures are the primary symptom of epilepsy, epilepsy is not the sole reason a seizure can occur: after an FTUS, there is only a 30-50% chance of a second seizure occurring in the next five years (Berg, 2008; Pohlmann-Eden et al., 2006). It is only after the second seizure

occurs that the chance of subsequent seizures occurring drastically increases, and it can be said with confidence that the individual has epilepsy as there is a 70-80% chance of subsequent seizures occurring after the second unprovoked seizure (Berg, 2008; Fisher et al., 2014; Hauser et al., 1998; Neligan et al., 2023; Pohlmann-Eden et al., 2006).

1.1.2. Epilepsy Diagnosis after a First-Time Unprovoked Seizure

As stated earlier, epilepsy is diagnosed based on an individual meeting one of the ILAE's three diagnostic criteria after experiencing an FTUS (Fisher et al., 2014) (Table 1.1). The first of these diagnostic criteria is whether the patient has experienced two unprovoked seizures a minimum of 24 hours apart (Fisher et al., 2014). This 24-hour minimum is specified to ensure that subsequently observed seizures are not the product of seizure clusters and, thus, the seizure is not an isolated incident since there is a significantly higher chance of seizure recurrence after a second unprovoked seizure (Fisher et al., 2014; Hauser et al., 1998; Mesraoua et al., 2021; Neligan et al., 2023). The second criterion is whether the patient has experienced an FTUS and has at least a 60% chance of subsequent seizures occurring in the next ten years, a probability threshold based on the seizure recurrence rate observed in the 1990 MESS study (Fisher et al., 2014; Shinnar et al., 1990).

The seizure recurrence probability of FTUS patients is determined through an examination of their medical history, both individual and familial, and assessments of the patient's neuroimaging for epileptiform abnormalities (Fisher et al., 2014; Kim et al., 2006; Pohlmann-Eden et al., 2006; Vergara López et al., 2021). Such evaluations allow for the detection of genetic predispositions towards epilepsy and secondary epileptogenic conditions, both of which indicate a higher chance for subsequent seizures to occur and contribute to the overall estimated probability of subsequent seizure occurrence (Ben-Ari & Dudek., 2010; Pohlmann-Eden et al., 2006; Vergara López et al., 2021). While the ILAE specify a recurrence probability threshold of 60% for epilepsy diagnosis, it is rarely utilised in clinical settings as, currently, there are no definitive frameworks or guidelines that assign probability quantifiers to specific risk factors (Fisher et al., 2014; Krumholz et al., 2015; Rizvi et al., 2017). Instead, epilepsy diagnoses utilising this diagnostic criterion are predominantly dependent on the diagnosing physician or epileptologist's estimation of seizure recurrence risk based on the aforementioned medical evaluations (Fisher et al., 2014; Krumholz et al., 2015;

Rizvi et al., 2017). The third criterion is whether the patient has received an epilepsy syndrome diagnosis (Fisher et al., 2014). Epilepsy syndromes can be diagnosed after an FTUS when an individual is identified as possessing a specific cluster of clinical features and symptoms linked to a specific epilepsy syndrome, typically based on the patient's seizure type, age of onset, seizure aetiology and medical history (Dreifuss et al., 1985; Fisher et al., 2014; Ono & Galanopoulou, 2012; Pohlmann-Eden et al., 2006).

Table 1.1: ILAE Operational (Practical) Clinical Epilepsy Diagnostic Criteria
1. At least two unprovoked (or reflex) seizures occurring more than 24 hours apart
2. One unprovoked (or reflex) seizure and a probability of further seizures similar to the general recurrence risk (at least 60%) after two unprovoked seizures, occurring over the next 10 years
3. Diagnosis of an epilepsy syndrome
(Fisher et al., 2014)

1.1.2.1. Categorisation and Treatment of Epilepsy Following Diagnosis

After a case of epilepsy is diagnosed, it is classified according to the three levels of the ILAE epilepsy categorisation (Fisher et al., 2017). The first level of categorisation is seizure type, which is based on whether the seizure originates and remains in a specific hemisphere's network (focal onset), propagates into bilaterally distributed networks (generalised onset) or originates from an unknown network (unknown onset) (Fisher et al., 2017; Scheffer et al., 2017). The second level of categorisation is epilepsy type, which is based on the patient's electroencephalogram (EEG) activity; it is Generalized Epilepsy if generalised spike activity is present, Focal Epilepsy if the epileptiform activity is in specific regions, Combined Generalized and Focal Epilepsy if both are present, and Unknown Epilepsy if no abnormalities are detected or an EEG has not been taken (Scheffer et al., 2017). The final level of categorisation is determining the presence and type of epilepsy disorder/syndrome; this is based on the seizure types, EEG and imaging features, age of onset, awareness level, and seizure triggers (Riney et al., 2022; Scheffer et al., 2017).

Once a formal epilepsy diagnosis is made, the clinical recommendation for adult patients is for them to undergo anti-epileptic drug/anti-seizure medication (AED/ASM) therapy; the type of AED/ASMs prescribed is based on lifestyle, medical history, and

patient preferences (Liu et al., 2017; Tomson et al., 2022). Treatment with AED/ASM is not considered for adult patients until after they have received a formal epilepsy diagnosis, as there is a 7-to-31% risk of AED/ASM patients experiencing adverse side effects, and the risk of experiencing such effects are only worthwhile when preventing the occurrence of further epileptic seizures (Liu et al., 2017; Tomson et al., 2022).

Unfortunately, while medical treatment with AED/ASM can help mitigate and prevent seizure occurrence, an estimated 30% of PWE are considered drug-resistant (Fattorusso et al., 2021; Liu et al., 2017; Kwan & Brodie, 2006). Once categorised as drug-resistant, PWE qualify for more invasive forms of epilepsy treatment, such as resective surgeries in which structural epileptogenic abnormalities are identified, located and removed through the use of extensive neuroimaging, including EEG, functional Magnetic Resonance Imaging (fMRI), positron emission tomography (PET), MRI scans and more (Guery & Rheims, 2021; Pittau et al., 2014).

1.1.3. Quality of Life after First-Time Unprovoked Seizure

The occurrence of an FTUS and an epilepsy diagnosis can be a major disruptive force to an individual's life as it has been well-documented that such events can lead to a notable decrease in quality of life (QoL) due to their threatening the physical, mental and social well-being of the patient (Foster et al., 2019; Siebenbrodt et al., 2023). One of the first QoL challenges FTUS patients experience is the suspension of their driving privileges until they remain seizure-free for a specific duration, for fear of subsequent seizures occurring while driving (Abdennadher et al., 2021; Asadi-Pooya et al., 2022; Foster et al., 2019). Such worries are not limited to the doctors and lawmakers behind such legal restrictions as FTUS patients report feeling significantly diminished control over their lives and heightened anxiety about the prospect of experiencing another seizure at any point, not just when driving (Foster et al., 2019; Velissaris, 2007). These concerns are not unfounded as PWE, especially those who experience generalised tonic-clonic seizures, face increased risks of head and extremity injuries as well as possess a standardised mortality ratio of 2.3, indicating that they have a mortality rate 2.3 times higher than the general population (Mesraoua et al., 2020; Nashef et al., 2011; Neligan et al., 2011).

Due to the negative impacts an FTUS can have on an individual's QoL, prompt epilepsy diagnosis is essential as it allows for swift medical intervention, which can

reduce the occurrence of seizures in the next two years, improving the patient's QoL (Marson et al., 2005). Quick epilepsy diagnosis might also encourage patients to start engaging in lifestyle changes that reduce seizure frequency, such as reducing alcohol intake and increasing sleep (Kobau & DiIorio, 2003; Velissaris, 2007). It has been shown that when PWE receive medical treatment and engage in lifestyle changes promptly after an FTUS and epilepsy diagnosis they display a notable QoL improvement (Jacoby et al., 2007; Velissaris, 2007). This is because such interventions help PWE redevelop their sense of control over their lives as well as reduce their seizure anxiety and depression (Jacoby et al., 2007; Velissaris, 2007). Furthermore, it is essential to note that 50-70% of FTUS cases are non-epileptic; thus, ruling out epilepsy as the cause of seizures allows for the exploration of alternative causes and facilitates prompt medical intervention (Berg, 2008; Pohlmann-Eden et al., 2006). As such, it is of significant importance that cases of epilepsy are identified and diagnosed as promptly as possible.

1.1.4. Limitations of Current Epilepsy Diagnosis Standards

1.1.4.1. First-Time Unprovoked Seizure Diagnostic Procedure

The quickest way an individual can attain an epilepsy diagnosis and subsequent medical treatment after an FTUS is for them to meet either the second diagnostic criterion, via the diagnosing physician or epileptologist determining the patient to be at high risk of subsequent seizures occurring in the next ten years, or the third diagnostic criterion by being diagnosed with an epilepsy syndrome (Fisher et al., 2014; Krumholz et al., 2015; Rizvi et al., 2017; Vergara López et al., 2021). These epilepsy diagnoses in adult FTUS cases typically occur after an FTUS patient is admitted into a hospital and undergoes a series of diagnostic procedures (Pohlmann-Eden et al., 2006). These diagnostic procedures consist of physical examinations, medical history evaluations, cerebrospinal fluid assessments, drug screening, an assessment of the seizure's features (seizure semiology) and clinical neuroimaging via EEG and/or MRI scans (Foster et al., 2019; Galizia & Faulkner, 2018; Pohlmann-Eden et al., 2006). These diagnostic procedures are used to determine whether the patient's FTUS is the product of a provoking factor or event, such as drug use or head trauma, or if the seizure is truly unprovoked and caused by something beyond an acute provoking factor/event (Pohlmann-Eden et al., 2006). An estimated 3-10% of first-time seizures are

attributable to the presence or occurrence of a seizure-provoking factor or event (Pohlmann-Eden et al., 2006). It is at this stage that an epilepsy diagnosis could first be made through the identification of specific symptoms, signs, and the patient's medical history (Fisher et al., 2014; Panayiotopoulos, 2005; Dreifuss et al., 1985).

1.1.4.2. Epilepsy Diagnosis after First-Time Unprovoked Seizure

When neither an acute cause nor an epilepsy syndrome is recognised through the patient's signs, symptoms and medical history examinations, clinical neuroimaging becomes especially crucial as it plays a significant role in determining whether an individual has epilepsy (Bernasconi et al., 2019; Pohlmann-Eden et al., 2006). As stated earlier, the second diagnostic criterion of epilepsy requires a diagnosing physician/epileptologist to determine that there is a high chance of subsequent seizures occurring, while the third criterion requires the presence of specific symptoms or abnormalities that can be used for an epilepsy syndrome diagnosis; either of these criteria can be met through the detection of epileptogenesis features (Bernasconi et al., 2019; Fisher et al., 2014; Krumholz et al., 2015; Rizvi et al., 2017; Vergara López et al., 2021).

Epileptogenesis refers to the process in which typical brain functions and networks are altered, disrupting the balance of excitation and inhibitory activity in an individual's brain, resulting in increased seizure susceptibility and unprovoked recurrent seizures (Banerjee et al., 2014; He et al., 2020; Ono & Galanopoulou, 2012; Pitkänen et al., 2015). Two significant indicators of epileptogenesis are EEG-detected epileptiform discharges and epileptogenic lesions identified in structural MRI scans, as their presence indicates underlying brain network dysfunction and disruption (Scharfman, 2007; Stafstrom & Carmant, 2015; Britton et al., 2016). EEG-detected epileptiform discharges and abnormalities typically manifest as focal spikes or waves or diffuse bilateral spike waves and are theorised to reflect such network disruptions (Britton et al., 2016; Stafstrom & Carmant, 2015). Epileptogenic lesions refer to congenital or acquired structural abnormalities; they are typically identified through MRI scans and are theorised to be a driving force for the network disruptions and subsequent seizures observed in epilepsy (Adamczyk et al., 2021; Stafstrom & Carmant, 2015). The presence of either or both of these features can be used for an epilepsy diagnosis through the second criterion, as they are the strongest indicators for subsequent seizures

occurring (Fisher et al., 2014; Pohlmann-Eden et al., 2006). While these features can also be used for an epilepsy syndrome diagnosis, such diagnoses can only be made when specific lesions or EEG patterns are identified (Ono & Galanopoulou, 2012; Panayiotopoulos, 2005; Riney et al., 2022; Smith et al., 2005).

However, neither the identification of epileptiform EEG abnormalities nor epileptogenic lesions are universal methods for epilepsy detection since they are not present in all cases of epilepsy (Bernasconi et al., 2019; Fisher et al., 2014; López-Rivera et al., 2022; Pohlmann-Eden et al., 2006).

Epileptogenic Lesions

The most common manifestations of epileptogenic lesions are hippocampal sclerosis, the occurrence of neuron loss and gliosis in the hippocampus, and malformations of cortical development (MCD): a range of cortical abnormalities that arise from molecular disruptions to brain development (Behr et al., 2016; Bernasconi et al., 2019; Desikan & Barkovich, 2016; Lopez-Rivera et al., 2022; Woermann et al., 1999). In cases of adult focal epilepsy, an estimated 26-44% of individuals have hippocampal sclerosis, while an estimated 12-32% possess MCD (Behr et al., 2016; Lopez-Rivera et al., 2022; Thom, 2014). As stated earlier, the presence of epileptogenic lesions can be used for epilepsy diagnosis to a reliable degree in cases of FTUS, but they are not present in all cases of epilepsy (Behr et al., 2016; Lopez-Rivera et al., 2022; Thom, 2014). Moreover, even in cases in which epileptogenic lesions are present, there is a high probability that such lesions will go unnoticed as standard MRI protocols, which typically include only T_1-weighted and T_2-weighted sequences, are typically used in clinical settings instead of an epilepsy-dedicated MRI protocol such as the ILAE Harmonized Neuroimaging of Epilepsy Structural Sequences MRI (HARNESS-MRI) protocol (Bernasconi et al., 2019; Spencer, 2014; Von Oertzen et al., 2002). When standard 1.5T MRI protocols are used, an estimated 30-57% of epilepsy cases go undiagnosed due to radiologists' uncertainty or failure to detect the presence of epileptogenic lesions; this is especially the case among inexperienced radiologists (Bernasconi et al., 2019; Spencer, 2014; Ponnatapura et al., 2018; Von Oertzen et al., 2002). This is also the case with 3T MRIs as demonstrated in the study by Ahmed et al. (2018), in which epileptogenic lesions were identified in 66% of PWE participants only when an epilepsy-dedicated MRI protocol was used. This finding contrasted with the

PWE participants' initial epilepsy categorisation as MRI-negative, epilepsy with no epileptogenic abnormalities detected via MRI, when standard MRI protocols were used (Ahmed et al., 2018). This improved epileptogenic lesion detection was attributed to the epilepsy-dedicated MRI protocol increasing MRI sensitivity for epileptogenic lesions by 32.8% (Ahmed et al., 2018).

Epileptiform Electroencephalogram Abnormalities

Similar difficulties occur regarding the use of epileptiform EEG abnormalities for epilepsy diagnoses as such abnormalities are not pathogenic symptoms of epilepsy, nor are they reliably identified in FTUS patients. In 32.3% of FTUS cases, epileptiform EEG abnormalities remain undetectable until after three separate EEGs, while an estimated 10% of PWE never display any epileptiform abnormalities (Baldin et al., 2014; Smith, 2005; Panayiotopoulos, 2005). These issues are even worse in cases of FTUS patients who possess EEG epileptiform abnormalities but whose medical histories do not indicate a predisposition for epilepsy, such as having experienced a stroke or possessing a genetic predisposition (Baldin et al., 2014; Smith, 2005; Panayiotopoulos, 2005). This is because in approximately 25-30% of such cases the observed epileptiform abnormalities are false positives, in which benign variant EEG patterns were misinterpreted as epileptiform abnormalities (Baldin et al., 2014; Smith, 2005; Panayiotopoulos, 2005). These false positives can potentially exert significant negative impacts on patients' lives as they can lead to false positive epilepsy diagnoses resulting in delayed medical treatment for the underlying conditions that initially triggered their seizures as well as risk the patient enduring a substantial decline in their mental health and QoL as a result of the diagnosis (Benbadis, 2007; Foster et al., 2019).

Second Seizure Occurrence

Should a diagnosis of epilepsy not be possible through the diagnostic criteria discussed above, the remaining criterion that could be met is for the patient to wait upwards of 2 years for a second unprovoked seizure to occur, as the chance of subsequent seizures occurring afterwards significantly decreases (Berg, 2008). However, as stated earlier, such a wait for subsequent seizures to occur can lead to profound stress and anxiety while also running the risk of an individual failing to recognise subsequent seizures, as PWEs have been shown to fail to report

approximately 29.9-50.5% of their seizures (Hoppes et al., 2007; Schulze-Bonhage et al., 2023).

1.1.5. Structural Abnormalities in Epilepsy as a Network Disorder

1.1.5.1. Epilepsy as a Network Disorder

As stated earlier, MRIs are an essential tool in the clinical diagnosis and treatment of epilepsy as well as in the field of epilepsy research, investigating its symptoms and underlying causes. In recent years, epilepsy research using neuroimaging technologies have provided evidence that epilepsy is not a neurological disorder originating solely from a singular seizure focus but is instead a network disease in which brain networks, systems of cortical and sub-cortical brain regions connected bilaterally, functionally and/or structurally, experience disruptions which cause them to become epileptic (Bartolomei et al., 2017; Lehnertz et al., 2023; Sinha et al., 2022; Spencer, 2002; Van Diessen et al., 2013). The connections and dynamics between the brain regions of networks allow for the smooth communication and processing of information; such collaboration between both brain regions and brain networks allows for the generation of macro-level functions and behaviours, large-scale tasks and actions such as higher-order cognitive functions, sensory processing and motor control (Bullmore & Sporns, 2009; Lehnertz et al., 2023; Royer et al., 2021; Sinha et al., 2022; Suárez et al., 2020; Spencer, 2002; Van Diessen et al., 2013). These networks rely on stable synchronisation of neural activity because their interconnectedness allows the activity of any single brain region within a network to affect the activity of all the others (Lehnertz et al., 2023; Royer et al., 2021; Sinha et al., 2022; Spencer, 2002; Suárez et al., 2020; Van Diessen et al., 2013). Thus, when network disruptions occur, brain networks become more susceptible to abnormal neural activity occurring within, propagating throughout and interrupting the network, resulting in a disruption of macro-level functions known as a seizure (Bartolomei et al., 2017; Lehnertz et al., 2023; Royer et al., 2021; Sinha et al., 2022; Spencer, 2002; Suárez et al., 2020). These network disruptions linked to seizures have been observed to manifest in ways beyond the expected abnormal patterns of neuroactivity, as PWE often display a multitude of neuroanatomical deviations, such as cortical thickness changes (Engel et al., 2013; Kramer & Cash, 2012; Pitkänen et al., 2015; Royer et al., 2021; Van Diessen et al., 2013).

Cortical Thickness Changes in Epilepsy

Changes in cortical thickness are well-documented in PWE, with early 1.5T MRI epilepsy research finding patterns of cortical thinning in the entorhinal cortex and temporal lobe cortex in individuals with Temporal Lobe epilepsy (TLE), one of the most common types of epilepsy (Behr et al., 2016; Bernasconi et al., 1999; Lee et al., 1998). Bernasconi et al. (2004) further explored this pattern of cortical thinning by conducting a whole-brain voxel-based analysis, in which they identified cortical thinning occurring in the temporolimbic and frontal cortical regions of TLE patients. These findings were reiterated by the 1.5T MRI Bernhardt et al. (2010) study, which also found that individuals with TLE possessed significantly lower levels of cortical thickness in the frontocentral and temporolateral regions.

The cortical thinning in PWE is not limited to TLE cases as cortical thickness changes have been observed to occur in cases of frontal lobe epilepsy (FLE) and idiopathic generalised epilepsy (IGE) (Galovic et al., 2019; Whelan et al., 2018). In the 3T MRI study by Galovic et al. (2019), it was noted that in cases of focal epilepsy, FLE and TLE, PWE displayed bilateral progressive cortical thinning in their frontal and temporal brain regions, with the cortical thinning being more pronounced in regions ipsilateral to the seizure focus. The 2018 multi-site ENIGMA study showed similar thinning patterns in TLE and that IGE cases exhibit more significant bilateral precentral gyrus thinning (Whelan et al., 2018). Additionally, while both studies identified that the cortical thinning was progressive and increased with epilepsy duration, Galovic et al. (2019) highlighted that such progression was independent of the PWEs' seizure status and frequency as well as their age and medication load.

Epilepsy-linked cortical thinning being independent of seizure status and seizure frequency was also identified in the Coan et al. (2014) and Labate et al. (2010) studies, both of which noted that while seizure frequency influences the severity of the progressive cortical thinning, it is not the sole cause behind it as it was still present in seizure-free PWE. Due to these patterns of cortical thinning being independent of seizure frequency and medication intake, it was hypothesised that they are a product of the epileptogenic neurodegeneration of epilepsy rather than a product of the seizures (Galovic et al., 2019). This theory has been further supported by the 3T MRI longitudinal Gugger et al. (2023) study, which found that individuals with late-onset epilepsy displayed patterns of cortical thinning in their temporal and frontal regions prior to epilepsy onset (Gugger et al., 2023). This cortical thinning has also been shown

to be independent of the presence of epileptogenic lesions, such as hippocampal sclerosis, as Coan et al. (2014), Bernhardt et al. (2010), and Alvim et al. (2016) found that TLE cases present similar patterns of cortical thinning regardless of hippocampal lesion presence. It has also been found that cortical thickness changes in PWE are not limited to cortical thinning. The 3T MRI Ogren et al. (2018) study noted that PWE experiencing generalised tonic-clonic seizures displayed sex- and hemisphere-dependent cortical thickening and thinning patterns. However, unlike the patterns of cortical thinning observed in past research, these patterns of cortical thickening were shown to be influenced by seizure frequency, as the insular cortical thickening was more pronounced in subjects with more frequent seizures, suggesting such thickening is potentially a compensatory response. Overall, past epilepsy research has indicated that while cortical thickness changes in PWE are influenced by seizure occurrence, with cortical thinning linked to seizure-induced excitotoxicity and cortical thickening linked to inflammatory responses and cell swelling, they are linked to epileptogenic changes to a greater degree (Bonilha et al., 2006; Coan et al., 2009; Coan et al., 2014; Ogren et al., 2018, Kemmotsu et al., 2011).

Network Changes in Epilepsy

As can be expected of a network disorder, the aforementioned patterns of epilepsy-associated cortical thickness changes are not isolated from one another (Bartolomei et al., 2017; Bernhardt et al., 2011; Lehnertz et al., 2023; Spencer, 2002). When using structural MRI scans, these epileptic networks can be studied and analysed using graph theoretical analysis (Sporns, 2018). Graph theoretical analysis, graph theory, is a form of mathematical analysis that conceptualises the human brain as a connectome matrix, with nodes representing distinct brain regions and edges signifying anatomical or functional connections between these regions (Bassett & Sporns, 2017; Sporns, 2018). The use of graph theory to characterise and analyse brain networks has allowed for the development of comprehensive frameworks to understand the intricate network architecture of the human brain and how neurodegenerative diseases like epilepsy impact it (Bernhardt et al., 2011; Bernhardt et al., 2013; Larivière et al., 2022; van Diessen et al., 2013; Yasuda et al., 2015). One such way that graph theory has already been useful is in identifying small-world networks within the brain, which are networks consisting of brain regions highly interconnected with short paths and notable levels of clustering (Bernhardt et al., 2011; Bernhardt et al., 2013).

Structural Covariance Analysis

One type of graph theory employed in epilepsy research is structural covariance analysis. Structural covariance refers to a morphological phenomenon in which specific brain regions co-vary in their morphological measures, reflecting neurodevelopmental patterns of synchronised anatomical changes as well as the functional and structural patterns of brain networks (Alexander-Bloch et al., 2013; Larivière et al., 2022). Structural covariance analysis uses these co-variations to identify and examine brain networks as well as the impact neurological diseases have on them (Alexander-Bloch et al., 2013; Bernhardt et al., 2013; Duan & Wen, 2023; Larivière et al., 2022).

When used as a cross-sectional group-based analysis method, as it is in this study, structural covariance analysis requires the datasets of multiple participants to determine the correlation of structural changes across the group (Alexander-Bloch et al., 2013; Bernhardt et al., 2011; Bernhardt et al., 2013; Duan & Wen, 2023; Larivière et al., 2022). When using this form of analysis there is a risk of group datasets can obscure individual variations, and there are limitations to the types of statistical analyses that can be utilised as the most commonly used statistical analysis tests for structural covariance analyses utilise null distributions generated from randomised subject data (Alexander-Bloch et al., 2013; Bernhardt et al., 2011; Bernhardt et al., 2013; Duan & Wen, 2023; Larivière et al., 2022). These null distributions must accurately reflect the distances between of brain regions as such distances heavily influence structural covariance, the closer two brain regions are the more they covary in morphological measures (Alexander-Bloch et al., 2013; Artzy-Randrup et al., 2004; Bernhardt et al., 2011; Bernhardt et al., 2013; Duan & Wen, 2023; Larivière et al., 2022). If this proximity is not properly accounted for there is a possibility that any observed statistically significant differences between the subject datasets and the null distributions may be due to randomised networks being implausible brain networks (Alexander-Bloch et al., 2013; Artzy-Randrup et al., 2004). Despite this the utilisation of multiple datasets for group-based structural covariance analysis allows researchers to develop an understanding of the pathogenesis of neurological disorders like epilepsy by identifying brain network changes that occur in the subjects of interest, PWE (Alexander-Bloch et al., 2013; Artzy-Randrup et al., 2004; Bernhardt et al., 2011; Bernhardt et al., 2013; Duan & Wen, 2023; Larivière et al., 2022).

Epilepsy research using structural covariance analysis on the cortical thickness measures of PWE, researchers have provided evidence that PWE experience epilepsy-type dependent disruptions and changes to their structural covariance brain networks when compared to their healthy counterparts (Bernhardt et al., 2011; Bernhardt et al., 2013; Larivière et al., 2022). Individuals with TLE exhibit disruptions to their small-world networks as changes in the distribution of their hubs- nodes with high levels of betweenness centrality- which shift from being evenly distributed to being more concentrated in the limbic, paralimbic and temporal cortices (Bernhardt et al., 2011; Bernhardt et al., 2013; Larivière et al., 2022; van Diessen et al., 2013; Yasuda et al., 2015). Individuals with TLE also experience increases in the clustering coefficients and shortest path lengths of the orbitofrontal and temporal regions, as well as the average clustering coefficients and average shortest path lengths of the whole network (Bernhardt et al., 2011; Bernhardt et al., 2013; Larivière et al., 2022; van Diessen et al., 2013; Yasuda et al., 2015). These changes were noted to represent a disruption to the participants' small-world network and vary between right TLE (R-TLE) and left TLE (L-TLE), as L-TLE cases demonstrate increases in the occipital lobes while R-TLE cases demonstrate increases in the limbic and temporal regions contralateral to their seizure focus (van Diessen et al., 2013; Yasuda et al., 2015). Overall, the changes occurring in TLE increased local connectivity but interfered with network information flow, decreasing global efficiency and disrupting the small-world network (Bernhardt et al., 2011; Bernhardt et al., 2013; Larivière et al., 2022; van Diessen et al., 2013; Yasuda et al., 2015). Structural covariance brain network changes are not limited to cases of TLE. Those with IGE exhibit significant levels of small-world network disruptions, as they display notably lower local connectivity and global efficiency, especially in the temporal, frontal, and parietal cortices (Larivière et al., 2022; Pegg et al., 2020). Structural covariance brain network changes were also seen in the Liu et al. (2023) study on FLE. Individuals with FLE exhibited significant increases in the clustering and local efficiency of the pre-central gyrus in the frontal lobe but decreases in the temporal pole, as well as decreases in network hubs as they shifted away from the frontal lobe (Liu et al., 2023).

1.1.6. Research Motivation

An epilepsy diagnosis can occur after an initial FTUS when the patient is determined by their physician/epileptologist to have a high chance of subsequent seizures occurring (Fisher et al., 2014; Krumholz et al., 2015; Rizvi et al., 2017; Vergara López et al., 2021). The probability estimations of the diagnosing physician/epileptologist are based on the patient's medical examinations; this is especially the case for the patient's neuroimaging scans as they can indicate the presence of epileptogenesis features (Amin & Benbadis, 2019; Fisher et al., 2014; Krumholz et al., 2015; Pohlmann-Eden et al., 2006; Rizvi et al., 2017; Vergara López et al., 2021). While the methods for detection of epileptogenesis indicators are effective to some degree, there are still a multitude of cases in which they either fail to correctly identify the indicators, resulting in a failure to diagnose epilepsy or, worse still, misidentify typical neuroactivity as epileptogenic, resulting in a false epilepsy diagnosis (Amin & Benbadis, 2019; Benbadis, 2007; Benbadis & Tatum, 2003). As such, there is a need for additional epilepsy indicators present as early as the FTUS that can be used as markers of an epilepsy predisposition (Fisher et al., 2014). One indicator that could be used is cortical thickness changes. Collectively, PWE have a long-documented history of experiencing both cortical thickness increases and decreases independent of the typical age-related cortical thinning; moreover, such changes have been shown to be present prior to epilepsy onset, occurring progressively and at its most prominent in the first five years after the initial epilepsy diagnosis (Bernhardt et al., 2010; Galovic et al., 2019; Gugger et al., 2023; Ogren et al., 2018). These PWE cortical thickness changes indicate that such changes can be identifiable as early as the FTUS, especially in those experiencing tonic-clonic seizures. This research study investigates the cortical thickness changes of individuals who have experienced an FTUS using 7T MRI scans, taking advantage of their higher signal-to-noise ratio (SNR).

1.2. Background

1.2.1. Magnetic Resonance Imaging Physics

MRI is a non-invasive imaging method that uses powerful magnets and radiofrequency pulses to generate detailed anatomical images (Robitaille & Berliner, 2006). When conducting an MRI scan, an initial strong magnetic field (B_0) is

implemented to align the protons of the patient either parallel or anti-parallel to it, during which the protons precess either in a parallel spin-state or anti-parallel spin-state (Berger, 2002; McRobbie et al., 2017; Robitaille & Berliner, 2006). Both the strength of the B_0 magnetic field and the frequency at which the protons precess are dependent on the strength of MRI magnets, the strength of which is measured in Tesla (T); with clinical MRIs typically ranging from 0.5T to 3T (Berger, 2002; McRobbie et al., 2017; Robitaille & Berliner, 2006). The summation of all the parallel aligned protons' magnetic moments results in a net longitudinal magnetisation (M_z), the magnitude of which is dependent on the strength of the B_0 magnetic field (McRobbie et al., 2017; Robitaille & Berliner, 2006).

To generate MRI images, radiofrequency pulses (RF) are applied to the patient by transmit RF coils, generating a homogenous RF transmit field (B_1^+) and tipping the longitudinal magnetisation into the transverse plane (M_{XY}), at an angle dependent on the RF pulse's strength, and causing it to precess (Gruber et al., 2018; McRobbie et al., 2017; Robitaille & Berliner, 2006; Vaidya et al., 2016). The precession of the M_{XY} magnetisation changes the magnetic field of the MRI machine and generates electrical currents in nearby coils, which are recorded as Nuclear Magnetic Resonance (NMR) signals (McRobbie et al., 2017; Redpath, 1998; Robitaille & Berliner, 2006). Upon the end of the RF pulse, the electrical currents generated by the M_{XY} magnetisation begin to decline as it returns to its original M_z alignment in a process called 'relaxation' (McRobbie et al., 2017; Robitaille & Berliner, 2006).

The duration of this relaxation is measured in two ways: T_1, the time it takes the M_z magnetisation to recover to approximately 63% of its initial M_0 magnetisation, and T_2, the time it takes the M_{xy} magnetisation to decay to approximately 37% of its initial value (McRobbie et al., 2017; Robitaille & Berliner, 2006). The MRI uses additional magnetic gradients to be able to localise the generated NMR signals in space; their location and intensity, calculated using the Fourier transformation, are then used to generate an image (McRobbie et al., 2017; Robitaille & Berliner, 2006). By varying the sequence of RF pulses, different types of MRI images can be generated (McRobbie et al., 2017; Robitaille & Berliner, 2006). These sequences are made by modifying the time between successive RF pulses (repetition time or TR) and adjusting the time between RF pulse delivery and the measurement of the resulting relaxation signal (Echo Time or TE) (McRobbie et al., 2017; Robitaille & Berliner, 2006).

1.2.2. Anatomical Imaging with T1-weighted and T2-weighted Images

The most basic sequence types used for MRI image generation are T1-weighted (T1w) sequences and T2-weighted (T2w) sequences, both of which take advantage of tissue-specific relaxation times to generate images with varying contrasts (McRobbie et al., 2017; Robitaille & Berliner, 2006). These tissue-specific relaxation times occur due to the varying proton densities and their interactions, as such fatty tissues like myelin and white matter possess short T_1 relaxation times while fluids such as cerebrospinal fluid possess longer T_1 relaxation times (McRobbie et al., 2017; Robitaille & Berliner, 2006). T1-weighted images are generated by T1w sequences that use short TE and TR sequences for quick signal acquisition, emphasising signal acquisition from tissues with short T_1 relaxation times over tissues and bodily fluids with longer T_1 relaxation times (Kawahara & Nagata, 2021; McRobbie et al., 2017; Robitaille & Berliner, 2006). T2-weighted images are generated by T2w sequences using longer TE and TR sequences for more pronounced M_{xy} decay, emphasising signal acquisition from tissues with longer T_2 relaxation times over tissues with shorter T_2 relaxation times (Kawahara & Nagata, 2021; McRobbie et al., 2017; Robitaille & Berliner, 2006).

The most commonly used T1w sequences in clinical and research settings are the Magnetization Prepared-RApid Gradient Echo (MP-RAGE) sequence and the turbo field echo sequence (Bernasconi et al., 2019; McRobbie et al., 2017; Mugler & Brookeman, 1991). Both generate 3D T1w anatomical images with emphasised grey and white matter, allowing for efficient brain analysis (Bernasconi et al., 2019; McRobbie et al., 2017; Mugler & Brookeman, 1991; Wang et al., 2020a).

1.2.3. Opportunities and Challenges with 7-Tesla MRI

3T MRI scanners are becoming more commonly used in clinical and research settings, but more recently, 7T MRI scanners have become available for human scanning, although they are much less common (McRobbie et al., 2017; Viessmann & Polimeni, 2021). These 7T MRI scanners possess significantly stronger magnets than their 3T counterparts, resulting in stronger B_0 magnetic fields aligning more protons, generating stronger M_z, and causing them to precess at higher frequencies (Redpath, 1998; Viessmann & Polimeni, 2021). The higher B_0 magnetic field strength and

resulting precessing frequencies allow for shorter T_1 relaxation times, resulting in stronger NMR signals (Karamat et al., 2016; Redpath, 1998). These stronger NMR signals lead to a higher SNR, higher signal contrast and, thus, better spatial resolution and identification of unwanted noise artefacts (Barisano et al., 2019; McRobbie et al., 2017; Redpath, 1998; Viessmann & Polimeni, 2021). Overall allowing for the generation of T1w images of significantly higher quality, resulting in better diagnostic confidence and identification of epileptogenic lesions (Isaacs et al., 2020; Springer et al., 2016; Wang et al., 2020b).

However, it should be noted that while 7T MRI scans allow for the generation of T1w images with higher spatial resolutions than their lower field strength counterparts, they are not without limitations (Karamat et al., 2016). Due to the strength of their B_0 magnetic field, the RF transmit field wavelengths used are significantly smaller than those used in 3T MRI scans and thus, B_1 inhomogeneities are much more likely to occur, causing abnormal variations in signal intensities and image contrast (Hwang et al., 2019; Karamat et al., 2016). Additionally, 7T MRI scans are much more susceptible to geometric distortions, either due to gradient coil non-linearities in head-only systems, in which gradient coil imperfections cause spatial inaccuracies and image distortions, or due to magnetic susceptibility artifacts, in which image distortions occur due to changes in magnetic properties at tissue interfaces (Collins et al., 1998; Karamat et al., 2016; Lau et al., 2016).

Despite these issues, 7T MRIs are still being turned to more and more for MRI research due to their higher spatial resolution, allowing for more in-depth investigation and analysis while compensating for these issues by implementing gradient non-linearities corrective applications and using sequences less sensitive to B_1^+ inhomogeneity (Eggenschwiler et al., 2012; Haast et al., 2018; Khan & Haast, 2020; Marques et al., 2010; Oliveira et al., 2021).

1.2.4. Anatomical Imaging Sequences at 7 Tesla

The Magnetization Prepared 2-RApid Gradient Echo (MP2RAGE) sequence is an altered version of the 3D MP-RAGE sequence designed to mitigate B_1 inhomogeneities (Marques et al., 2010; McRobbie et al., 2017). In this MRI sequence, an initial magnetisation preparation pulse is implemented, followed by two separate RF pulses, each after a specific amount of time (inversion times), generating two gradient-

recalled echo (GRE) images (Marques et al., 2010; Metere et al., 2017). The first GRE image is generated after a short inversion time to optimise the SNR, while the second GRE image has a longer inversion time to optimise tissue contrast (Marques et al., 2010; Metere et al., 2017). The GRE images are then combined to make a T1w uniform image (UNI) with optimised SNR and tissue contrast, both of which mitigate the impact of B_1 inhomogeneities (Marques et al., 2010; Metere et al., 2017).

1.2.5. Quantifying Structural Abnormalities with T1w MRI

As highlighted in the introduction, T1w MRI images have been extensively employed in epilepsy research to investigate the various structural abnormalities associated with epilepsy. These structural MRI research studies typically use one of three neuroimaging analysis methods: region of interest (ROI) based volumetry, voxel-based morphometry, or cortical thickness analysis.

ROI-based volumetry is an MRI analysis method in which ROIs are outlined and their volume measured on an MRI scan (Emerton et al., 2009). In voxel-based morphometry, the density or volume of brain regions, typically grey matter regions, is measured on a voxel-wise basis in a standardised space (Ashburner & Friston, 2000). In cortical thickness analysis, the cortical thickness is measured either through voxel-based analysis or via surface-based analysis, in which the pial surface and white matter surfaces are identified, and the distance between the two is measured (Fischl & Dale, 2000; Hutton et al., 2008). Cortical thickness analyses are often considered the more sophisticated MRI analysis method as they allow for more nuanced and comprehensive data collection and analysis in comparison to other MRI analysis methods (Hutton et al., 2009; Winkler et al., 2019). For this reason, cortical thickness measures have been the focus of several epilepsy studies, including this one.

1.2.5.1. MRI Surface Processing Pipeline

To measure cortical thickness, T1w images must undergo a series of image-processing steps; some of the most commonly used processing pipelines are those of FreeSurfer (Dale et al., 1999). FreeSurfer is a software tool used to analyse and visualise structural and functional brain imaging data, and its Surface-based analysis pipeline is commonly used to reconstruct the cortical surface and measure cortical

features such as cortical thickness, surface area and curvature at each vertex of the cortex (Dale et al., 1999; Fischl, 2012). In this processing pipeline, the MRI image volumes are affine registered to the Montreal Neurological Institute (MNI) MNI305 atlas, after which the image undergoes skull-stripping, in which the extra-cerebral voxels are identified and removed (Collins et al., 1994; Dale et al., 1999; Ségonne et al., 2004). Afterwards, the remaining voxels of the image are classified as either white matter or non-white matter based on their signal intensities, after which the hemispheres are separated based on the voxels' signal intensities and the MNI305 coordinates of the corpus callosum and pons (Dale et al., 1999; Ségonne et al., 2004). Once the hemispheres are separated and classified, the pipeline generates the white matter surface by tessellating the edge between the white matter voxels and the non-white matter voxels with a triangular mesh generating a wall separating the two voxel types (Dale et al., 1999). Within the triangular mesh, each triangle consists of three coordinate points called vertices (singular vertex) (Dale et al., 1999). The pial surface is then generated by 'pushing', adjusting towards, the white matter surface towards the intensity gradients of the cerebrospinal fluid and grey matter (Dale et al., 1999). Once the white and pial surfaces are generated, they are then marked out on the original T1-weighted image and used to determine cortical measures such as cortical thickness by measuring the distance between the pial and white matter surfaces (Dale et al., 1999; Fischl & Dale, 2000). Once the FreeSurfer Surface-based pipeline has generated the pial surface, it can be delineated to map every cortical region of the MRI brain image based on a predefined brain atlas in a process called brain parcellation (Fischl et al., 2004; Schaefer et al., 2018).

1.2.5.2. Cortical Parcellation with Brain Atlases

The brain atlases used to parcellate brain scans are created by researchers, with each distinct region designed to be homogenous regarding either their functional, architectural, connectivity or topographical features (Eickhoff et al., 2018). The regions of these atlases, known as parcels, are determined based on the brain's structural, functional, connectivity features or a combination of all three (Fischl et al., 2004; Schaefer et al., 2018). The default brain atlas used in FreeSurfer is the Desikan-Killiany atlas, which divides the cortex into 34 parcels per hemisphere based on the gyri and sulci structural landmarks of the brain (Desikan et al., 2006;). Other commonly used

brain atlases are the Human Connectome Project Multi-Modal Parcellation (HCP-MMP) map and the Schaefer 2018 parcellation map (Glasser et al., 2016; Schaefer et al., 2018). The HCP-MMP map delineates the cortex into 180 parcels per hemisphere, the borders of which are based on where acute changes in cortical architecture, function, connectivity or topography occur (Glasser et al., 2016). The Schaefer 2018 parcellation map is generated using the gradient-weighted Markov Random Field (gwMRF) model, which parcellates the cortex based on resting-state functional connectivity; patterns of resting-state fMRI (rs-fMRI) signal synchronisation between brain regions (Schaefer et al., 2018). Each parcel is then further classified into a functional network based on rs-fMRI patterns, either using a 7-network or 17-network categorisation scheme (Schaefer et al., 2018; Yeo et al., 2011). The Schaefer 2018 map is unique from other parcellation maps as it can be generated at varying resolution levels, ranging from 50 to 500 parcels per hemisphere (Schaefer et al., 2018).

This study uses the 50-parcels per hemisphere and 100-parcels per hemisphere Schaefer atlases, referred to respectively as the 100-parcel and 200-parcel Schaefer 2018 parcellation maps at the 17-network categorisation level (Schaefer et al., 2018) (Figure 2.1.). The 200-parcellation Schaefer 2018 map will be used as Fürtjes et al. (2023) have indicated that more finely segmented cortical maps allow for superior detection of subtle inter-individual morphometric changes (Fürtjes et al., 2023). The 100-parcel Schaefer 2018 parcellation map will be used as its coarser cortical segmentation is more in line with past epilepsy research, making it easier to compare the results with past research as well as potentially allowing for the identification of clearer distinctions between major brain areas in subjects (Fürtjes et al., 2023).
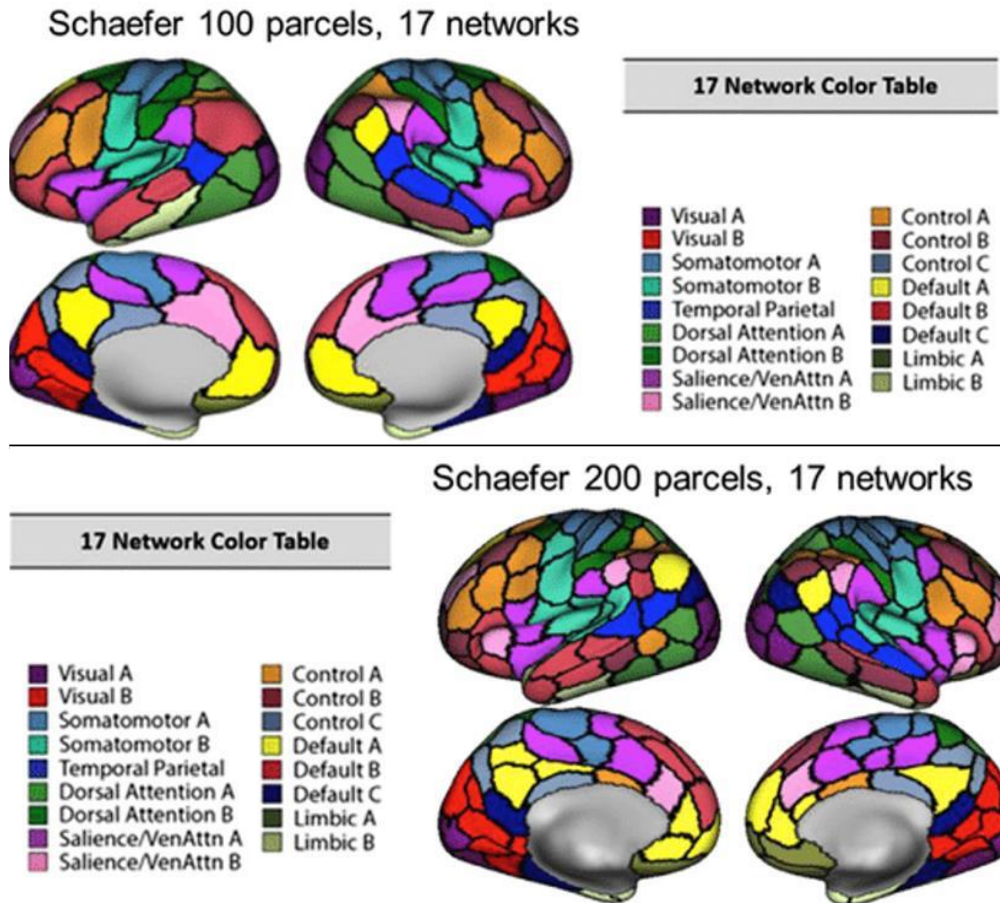
Figure 1.1 The Schaefer 2018 100-parcel map (top) and the Schaefer 2018 200-parcel map (bottom)

(Schaefer et al., 2018; Rieck et al., 2021)

1.2.6. Structural Covariance Analysis

As stated earlier, graph theory is an incredibly useful tool for analysing brain network disruptions and changes via structural MRI scans that has been used in several epilepsy research papers as it allows for the investigation of how neurological disorders impact brain networks (Bernhardt et al., 2011; Bernhardt et al., 2013; Duan & Wen, 2023; Larivière et al., 2022; Liu et al., 2023; Yasuda et al., 2015).

1.2.6.1. Structural Covariance Connectivity Matrix

When conducting structural covariance analysis, the first step is to calculate the correlations of anatomical features measured via structural MRI scans- cortical thickness in this study- between brain regions (Alexander-Bloch et al., 2013). These correlations are used to generate a connectivity matrix (A_{ij}), a two-dimensional matrix

in which each row and column component represents a specific node (Alexander-Bloch et al., 2013; Fornito et al., 2016). Within this matrix, the intersection of each row and column contains the measure of cortical thickness correlation between the row's node (i) and the column's node (j) (Alexander-Bloch et al., 2013; Fornito et al., 2016).

1.2.6.2. Thresholding and Binarization

Once the connectivity matrix is constructed, a filtering process known as thresholding is applied, in which a percentage of the weakest edges are excluded from further analysis (Fornito et al., 2016). Before the thresholding is implemented, the absolute value of each edge is calculated to generate an absolute connectivity matrix consisting of non-negative values (Bernhardt et al., 2011; Bernhardt et al., 2013; Fornito et al., 2016). This prevents strong inverse correlations between nodes from being excluded from further analysis due to their negative values (Bernhardt et al., 2011; Fornito et al., 2016).

Thresholding is applied since mathematical calculations of correlations between brain regions will often generate non-zero correlation matrices between every off-diagonal brain region, implying a fully interconnected brain network (Fornito et al., 2016). However, such levels of interconnectedness are improbable as even simpler organisms, such as macaque monkeys, do not possess fully connected networks when investigated using viral tract tracing (Fornito et al., 2016). As such, it is theorised that a portion of the non-zero correlation matrices are spurious connections and, thus, should be labelled as noise (Fornito et al., 2016). To minimise the impact of this noise on subsequent evaluations and analyses, a threshold value (τ) is selected and all edges in the connectivity matrices with values below the threshold are eliminated as 'noise' (Fornito et al., 2016). The threshold value implemented on a connectivity matrix is typically determined either through a weight-based or a density-based thresholding strategy (Fornito et al., 2016). In the weight-based thresholding strategy, the researcher determines τ based on the correlation matrices' weight, prior research, or adherence to statistical significance criteria (Fornito et al., 2016). This form of thresholding is straightforward and allows for the focus to be placed on the stronger edges of the matrix (Fornito et al., 2016). However, it has limitations when comparing connectivity matrices across different individuals or population groups, as it does not consider variations in connection densities between the groups (Fornito et al., 2016).

In density-based thresholding, the threshold varies between matrices to ensure all connectivity matrices possess the same specific connectivity density (C_d), the proportion of non-zero connections out of the total potential connections that could be made in the network (Fornito et al., 2016). The connectivity density is defined below:

$$C_d = \frac{E_\tau}{N(N-1)}$$

Where E_τ is the total number of edges above the threshold τ, and N is the total number of nodes in the network (Fornito et al., 2016). While this strategy prevents over-filtering low connectivity density matrices, it does risk allowing more noise edges to be included in the final dataset (Fornito et al., 2016).

After applying the threshold to the absolute connectivity matrix (A_{ij}), the matrix is transformed into a binary graph (Fornito et al., 2016). In this graph, all values above the threshold (τ) are assigned the value one, while those below the threshold are designated as zero, as shown in the equation below:

$$A_{ij} \begin{cases} if \ (C_{ij} \geq \tau) = 1 \\ if \ (C_{ij} < \tau) = 0 \end{cases} \text{(Fornito et al., 2016)}$$

Within this graph, the total number of edges connected to each node (i) is represented by (E_i) (Fornito et al., 2016).

1.2.6.3. Nodal Measures of Graph Theory

The generated binary matrix is then used to determine the topological properties of the brain networks and interrelatedness in the regions within that network. Within the generated binary matrix, the network properties of each node were evaluated individually through the nodal measures of degree, betweenness centrality, shortest path length, clustering coefficient and participation coefficient (Bernhardt et al., 2011; Fornito et al., 2016; Yasuda et al., 2015).

Degree

In graph theory, degree (k_i) is a simple measure of connectivity between an individual node and all nodes in the network by calculating the sum of edges in the binary matrix connecting to the node (i). The degree (k) measure for node i is calculated through the following equation:

$$k_i = \sum_{j=i} A_{ij}$$

In this equation, A_{ij} represents the total binary matrix (Fornito et al., 2016). A high nodal degree indicates a node is highly connected and likely a network hub, while a low nodal degree indicates that a node has very few with other nodes (Fornito et al., 2016).

Shortest Path Length

Shortest path length (L_{ij}), like degree, is one of the simpler measures of connectivity as a measure of the shortest path between an individual node and all other nodes; this measure is based on the coordinates of the nodes that are connected by an edge in the matrix (Fornito et al., 2016). The following equation defines shortest path length (L_{ij}):

$$L_{ij} = min_{p_{ij}} \left(\sum_{k=1}^{N-1} w_{p_{k,p_{k+1}}} \right)$$

In which $min_{p_{ij}}$ represents the minimum paths (p) that connect node i to node j, $w_{p_{k,p_{k+1}}}$ is the weight of the edge connecting these nodes (Fornito et al., 2016). The shortest path length is typically interpreted as an indicator of information transfer efficiency in a network, as it is assumed that information will travel through the shortest possible path in a network (Fornito et al., 2016). Increases in the measured shortest path length are interpreted as increases in structural connectivity and efficient communication with a node in a network and vice versa for decreases in shortest path lengths (Fornito et al., 2016; Yasuda et al., 2015).

Betweenness Centrality

Betweenness centrality (C_B) is a metric measuring the number of shortest paths that pass through a node (i), quantifying the importance of the node in facilitating the flow of information in a network (Bernhardt et al., 2011; Yasuda et al., 2015). This measure is based on the aforementioned assumption that information will always travel through the shortest path; thus, should a node lay at the centre of several short paths, it is reasonable to presume the node to be a central or bottle-neck component of a network (Fornito et al., 2016). Betweenness centrality is calculated through the following equation.

$$C_B(i) = \frac{1}{(N-1)(N-2)} \sum_{h \neq i, h \neq j, j \neq i} \frac{\rho_{hj}(i)}{\rho_{hj}}$$

This equation determines the proportion of shortest paths between nodes j and h (ρ_{hj}) that connect through node i ($\rho_{hj}(i)$) (Fornito et al., 2016).

Clustering Coefficient

The clustering coefficient (Cl) is a measure that quantifies the level of local clustering or transitivity in the network by measuring how interconnected a node is to its neighbours (Bernhardt et al., 2011; Fornito et al., 2016; Yasuda et al., 2015). This interconnectedness is measured by determining the probability of the nodes neighbouring the i node being connected to each other through the equation below (Arora & Majumdar, 2022; Bhattacharya et al., 2023; Fornito et al., 2016; Kong et al., 2019). In this equation E_i represents the number of edges connected to node i while k_i represents the degree of node i (Arora & Majumdar, 2022; Bhattacharya et al., 2023; Fornito et al., 2016; Kong et al., 2019).

$$Cl(i) = \frac{2E_i}{k_i(k_i - 1)}$$

Participation Coefficient

The participation coefficient (P) measures how distributed and diverse a node's connections are to modules, which are the well-connected communities within a network (Fornito et al., 2016; Yasuda et al., 2015). It is calculated by determining the portion of node i's connectivity that can be attributed to each module in the following equation:

$$P = 1 - \sum_{m=1}^{M} \left(\frac{k_i}{k_i}\right)^2$$

In this equation, M is the total number of modules in the network, $k_i(m)$ is the number of connections between the node i and the other nodes in module m (Fornito et al., 2016). In this measure, higher participation coefficients indicate higher levels of diverse structural connectivities as these regions are possibly becoming more connected with and integrated into the network (Fornito et al., 2016; Yasuda et al., 2015).

Once the nodal measures for each of the individual nodes are determined, the measures for the overall brain network are evaluated through the global measures of average clustering, average shortest path length, assortativity, modularity and global efficiency (Bernhardt et al., 2011; Fornito et al., 2016; Yasuda et al., 2015).

Average Clustering Coefficient

The average clustering coefficient ($Cl_{\bar{x}}$) is a measure of the average clustering within the network, quantifying how densely interconnected the nodes of the network are (Bernhardt et al., 2011; Fornito et al., 2016; Yasuda et al., 2015). It is calculated by determining the average clustering coefficient per node in the through equation:

$$Cl_{\bar{x}} = \frac{\sum_{i \in N} Cl(i)}{N} = \frac{1}{N}\left(\sum_{i \in N} \frac{2E_i}{k_i(k_i - 1)}\right)$$

Average Shortest Path Length

The average shortest path length (L) is a measure of the average shortest length path in the network, reflecting information transfer efficiency within the network (Fornito et al., 2016). It is calculated through the following equation, in which $d(j, i)$ represents the distance between node i and j:

$$L = \frac{\sum_{i \neq j} d(j, i)}{N(N - 1)}$$

(Fornito et al., 2016).

Assortativity

Assortativity (a) is a measure, in graph theory, of whether nodes with similar structural properties tend to connect more often; it is based on the tendency of high-degree nodes to connect with other high-degree nodes and for low-degree nodes to connect with other low-degree nodes (Fornito et al., 2016). Similar to Pearson's correlation coefficient, positive assortativity indicates that nodes within the network possess high connectivity with similar structures; it is calculated through the following equation:

$$a = \frac{E^{-1} \sum_i j_i k_i - \left[E^{-1} \sum_i \frac{1}{2}(j_i k_i)\right]^2}{E^{-1} \sum_i \frac{1}{2}(j_i^2 + k_i^2) - \left[E^{-1} \sum_i \frac{1}{2}(j_i + k_i)\right]^2}$$

In the equation, E are the network edges, j_i and k_i are the degrees of the nodes linked by i-th edge, and $i = 1, \dots, E$ (Fornito et al., 2016).

Modularity

Modularity (Q) is a graph theory measure of how divided the nodes of a network are into modules, communities of strongly interconnected nodes, with high levels of modularity indicating that the nodes are highly connected to other nodes within their modules but weakly connected with nodes outside of their module (Fornito et al., 2016). Modularity of a network is determined through the following equation:

$$Q = \frac{1}{2E} \sum_{ij} (A_{ij} - e_{ij}) \, \delta(m_i, m_j)$$

In this equation, δ refers to the Kronecker delta function, which equals one if node i and node j belong to the same module ($m_i = m_j$) but zero otherwise (Fornito et al., 2016). Additionally, e_{ij} represents the total number of edges between node i and node j that occur due to chance, as calculated in the following equation:

$$e_{ij} = \frac{k_i k_j}{2E}$$

Global Efficiency

Global efficiency (E_{glob}) measures how efficiently the network communicates information by inferring how well the information is communicated through all node pairs in the network (Fornito et al., 2016). The global efficiency of a network is defined as the average of the inverse shortest path lengths between all pairs of nodes, which is calculated in the following equation:

$$E_{glob} = \frac{1}{L'} = \frac{1}{N(N-1)} \sum_{i \neq j} \frac{1}{d(j, i)}$$

2. Chapter 2: Materials & Methods

2.1. Participants and Scanning

      FTUS patients were recruited after having experienced an FTUS and undergoing ancillary testing that involved a 1.5T or 3T clinical MRI scan. Patients were not recruited if they possessed any significant medical comorbidities that could be contributing factors to the seizure occurrence or if the patient's ancillary testing led to a diagnosis of epilepsy due to the identification of epileptogenic lesions or by the patient's EEG scans possessing epileptiform discharges. Healthy controls were recruited from the local London, Ontario community, excluding all individuals who knowingly possessed a neurological disorder.

      After being recruited into the research project, participants were requested to visit the University of Western Ontario's Centre for Functional and Metabolic Mapping for a 7T MRI scan. FTUS patients were excluded from the research study if they experienced a second unprovoked seizure prior to undergoing the 7T MRI scan or if an epileptogenic lesion was identified in a participant's 7T MRI scan.

      Participant recruitment began in August 2016 and ended in September 2022, during which 32 participants were recruited for this research project: 16 FTUS patients (27.7 ± 12.1 years, nine males) and 16 age- and sex-matched healthy controls (29.8 ± 11.9 years, nine males). Of the 16 FTUS patients, six received a formal epilepsy diagnosis after their 7T MRI scan. 7T MRI scan data of 16 healthy participants age- and sex-matched to the FTUS patients was also collected; seven of these 16 healthy control participants were selected from the Khan Lab SNSX healthy control database (Table 2.1).

      All participants provided informed consent, and ethical approval was obtained from the Health Sciences Research Ethics Board of the University of Western Ontario and Lawson Health Research Institute (See Appendix B).

Table 2.1. Participant Demographic Data

Displays the demographic data of the First-Time Unprovoked Seizure patient group, the FTUS sub-group of patients confirmed as epileptic (CE) as well as the age- and sex-matched healthy controls (HC) of both, in which Female = F and Male = M.

Groups	FTUS (CE)		HC (CE-matching controls)	
	F FTUS **(F CE)**	**M FTUS** **(M CE)**	**F HC** **(F CE controls)**	**M HC** **(M CE controls)**
n	16 (6)		16 (6)	
	7 (3)	9 (3)	7 (3)	9 (3)
Age	27.7 (23.7)		29.8 (25.8)	
(years)	29.3 (19.7)	26.9 (27.7)	31.4 (22.3)	28.6 (29.3)

2.2. Imaging protocol

All participants were scanned with the Siemens MAGNETOM Terra 7T MRI at the University of Western Ontario's Centre for Functional and Metabolic Mapping. High-resolution 3D T1-weighted sagittal anatomical images were obtained using the 3D MP2RAGE sequence, with the parameters set to a 6000 millisecond (ms) TR, 2.73 ms TE, 4° flip angle, 240x240 millimetre (mm) field of view (FoV), 0.8 mm isotropic, and 208 contiguous slices.

After the MRI scans were taken, two resting-state fMRI sessions were acquired using an echoplanar imaging sequence (1250 ms TR, 20 ms TE, 208 mm FoV, 45° flip angle), 2 mm isotropic, 60 slices, 300 volumes, with multiband acceleration factor of 3, GRAPPA acceleration factor of 3 and 7/8 phase partial Fourier. During the fMRI scans, the participants were instructed to remain awake with their eyes closed for the resting state sequences. These fMRI scans were acquired for other research; we analysed them as ethically approved secondary analysis.

2.3. MRI Image Processing

The 7T MRI-generated images were processed in an anatomical pre-processing pipeline called anat_preproc that combined several processing pipelines (Figure 2.1). In this processing pipeline, the first thing done is to gradcorrect the brain scan images; gradcorrect is a Brain Imaging Data Structure application that corrects the gradient non-linearity image distortions of the T1w images (Khan & Haast, 2020). Afterwards, the 3dMPRAGEise processing script is used to remove unwanted background signals from UNI, using the Analysis of Functional NeuroImages (AFNI) toolbox and the two gradient echo images (INV1 and INV2) images generated by the MP2RAGE MRI sequence as a guideline in a process called denoising (Choi et al., 2018; Cox, 1996; Kashyap, 2021). Once denoised, the signals from non-brain tissue are identified and removed from the image using the deep learning program Synthstrip in a process called skull stripping (Hoopes et al., 2022). After skull stripping, the fMRIprep anatomical processing pipeline corrects the non-uniformity of MRI signal intensity in the images and employs the FreeSurfer recon-all processing pipeline on the corrected images (Dale et al., 1999; Esteban et al., 2018). In the recon-all processing pipeline, the 3D reference image is affine registered with the MNI305 atlas (Collins et al., 1994; Dale et al., 1999). This registration ensures that the MRI images possess seed points that can be read and used by the FreeSurfer algorithm (Dale et al., 1999). Once registered, the brain images were segmented based on brain matter type and hemispheres (Dale et al., 1999). Subsequently, white matter and pial surfaces were generated and outlined on the original T1-weighted image. These surfaces were then used to measure cortical parameters, such as cortical thickness, at each point along the cortex (Dale et al., 1999). The FreeSurfer recon-all output is then fed into the ciftify_recon_all processing pipeline, which converts the FreeSurfer recon-all produced files from a FreeSurfer format to a CIFTI format as well as implements MNI inter-subject anatomy-based registration and resampling (Dickie et al., 2019). The outputs of the ciftify_recon_all are then put into the ciftify_vis_recon_all pipeline to generate quality assurance visualisations, which were then reviewed by the researcher (Dickie et al., 2019).
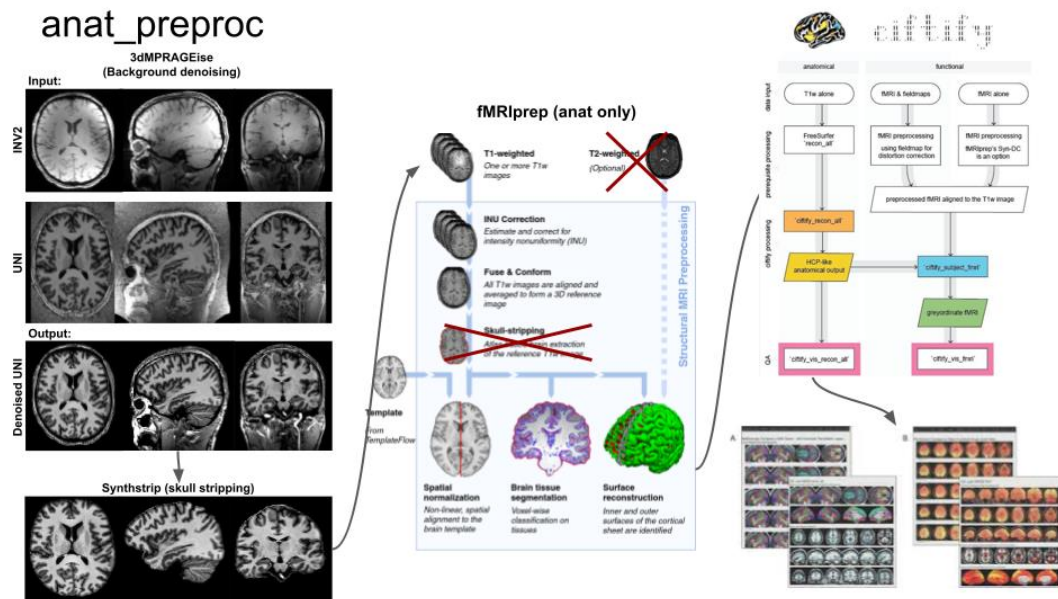
Figure 2.1 anat_preproc Processing Pipeline. The anat_preproc processing pipeline which utilises multiple programs and processing pipelines to process the 7T MRI scans of the FTUS and HC participants.

2.4. Data and Statistical Analysis

2.4.1. Group analysis

In this study, two sets of cortical thickness comparisons were conducted. The first set of analyses focused on the 16 FTUS patients and their 16 age- and sex-matched healthy controls, while the second set focused on the subset of six FTUS patients confirmed to be epileptic (CE) and their six age- and sex-matched healthy controls.

Both sets of cortical thickness analyses compared the average cortical thickness per brain region of the patient groups with those of their age- and sex-matched healthy controls. Afterwards, the patient group and their matched control group were separated based on sex, and the cortical thickness comparison process was repeated for each sex for a set of sex-based comparisons.

These comparisons were conducted once using the 17 network 200 parcel Schaefer 2018 atlas and again using the 17 network 100 parcel Schaefer 2018 atlas (Schaefer et al., 2017). Each cortical thickness comparison was conducted using the independent two-sample t-test, comparing the patient groups with their age- and sex-matched healthy controls with p-value significance adjusted using the false discovery rate (FDR) Benjamini-Hochberg procedure to control for type 1 statistical errors ($p \leq$ 0.05, FDR correction for multiple comparisons) (Benjamini & Hochberg, 1995).

2.4.2. Structural Covariance Analysis

Structural covariance analysis was used to evaluate and characterise any changes to the patterns of cortical thickness covariance between brain regions and the overall patterns of interrelatedness within the brain, using the Whitaker Labs structural covariance brain network analyses (SCONA) Python toolkit (Fornito et al., 2016; Whitaker & Staden, 2018). Within each participant group, the participant's cortical thicknesses, after accounting for the covariate variable of age, were used by the toolkit to generate a correlation matrix quantifying the inter-regional relationships within each group using Pearson correlation coefficients (Whitaker & Staden, 2018). The absolute of each Pearson correlation coefficient value in these correlation matrices were then used to generate weighted graphs (connectivity matrices) representing the cortical thickness correlations between brain regions (as shown in Figure 3.5) (Fornito et al., 2016; Whitaker & Staden, 2018).

The density-based thresholding method was then used to filter out the weakest edges of the matrices until the matrices' densities reached the threshold value (τ) of 15%, removing any superfluous connections within the matrices (Fornito et al., 2016; Whitaker & Staden, 2018). The threshold value of 15% was selected as it has been shown to be the minimal density at which all networks are fully connected based on the Bernhardt et al. (2011) and He et al. (2008) studies. SCONA thresholding is guided by a minimum spanning tree, which ensures that a path can be found between all of the remaining edges, minimising the potential of isolated nodes resulting from the density-based thresholding (Fornito et al., 2016; Whitaker & Staden, 2018). Once thresholded, the weighted graph was binarised into an adjacency (binary) graph with edges filtered out of the matrix represented as zeros and the remaining edges as ones (Fornito et al., 2016; Whitaker & Staden, 2018) (as shown in Figure 3.6). These adjacency graphs were then used to calculate the participant groups' nodal and global measures (Fornito et al., 2016; Whitaker & Staden, 2018). The nodal measures used in this study were betweenness centrality, shortest path length, clustering coefficient and participation coefficient, while the global measures used were assortativity, global efficiency, average clustering coefficient, and average shortest path length (Fornito et al., 2016; Whitaker & Staden, 2018).

Structural covariance global and nodal measures were compared in two sets of comparisons, with each set of comparisons using a non-parametric 1000 permutation test (Phipson & Smyth, 2010). For each permutation, the raw cortical thickness data of the participants were randomly assigned to one of the two groups, after which the nodal and global measures for each 'new' group were calculated using the SCONA toolkit. This was repeated 1000 times, with a new randomised assignment of cortical thickness measures in each repetition, to generate a null distribution of differences (Artzy-Randrup et al., 2004; Phipson & Smyth, 2010). This form of randomisation was used to ensure the data accurately represented the spatial distance between brain regions, as the proximity of two brain regions to each other has been shown to correlate positively with their cortical thickness covariance (Alexander-Bloch et al., 2013; Artzy-Randrup et al., 2004; Phipson & Smyth, 2010). This is important as should brain region proximities not be accounted for during randomisation there is a risk of any statistically significant differences between the subject data and the null distribution being due to the null distribution inaccurately representing the correlations and covariances of brain regions' cortical thicknesses (Alexander-Bloch et al., 2013; Artzy-Randrup et al., 2004; Phipson & Smyth, 2010).

The differences in nodal and global measures between the patient groups and their age- and sex-matched healthy controls were then placed in their corresponding null distributions to determine their percentile position in the distributions. This percentile position was used to determine the p-value significance level of the two-tailed group difference between the patient group and their age- and sex-matched healthy controls; based on past research, this significance was thresholded at a p-value of 0.05 (Bernhardt et al., 2011; He et al., 2008). These p-values were then adjusted using the FDR Benjamini-Hochberg procedure to control for false positive errors (Benjamini & Hochberg, 1995).

3. Chapter 3: Results

As stated earlier, the cortical thicknesses of the study's participants were parcellated on two levels: the 17 network 200 parcel Schaefer 2018 parcellation atlas and the 17 network 100 parcel Schaefer 2018 parcellation atlas. As parcellation maps with high levels of delineation, the Schaefer 2018 Parcellation maps possess multiple sub-divisions for each brain region.

Due to a data storage error, the data for three FTUS patients, two of whom were CE patients, was lost after analysing the 200 parcellation data but before the analysis of the 100 parcellation data. As such, the data of these three FTUS patients and their age- and sex-matched healthy controls are not included in the 100 parcellation map data analysis.

3.1. Cortical Thickness Comparisons

At each parcellation map, the cortical thicknesses of the FTUS patients were compared with those of their age- and sex-matched healthy controls; this comparison was then repeated for sex-dependent comparisons between the groups. These comparisons were repeated once more with only the CE patients.

3.1.1. 200 Parcellation Map Analysis

The cortical thicknesses of the mixed-sex FTUS patients showed no statistically significant differences from their age- and sex-matched healthy controls when multiple comparison correction p-value adjustments were made ($p \leq 0.05$, FDR correction for multiple comparisons). However, there were trends ($p \leq 0.05$ uncorrected) of cortical thickening in the mixed-sex FTUS patients' right extra-striatal, somatosensory/sensorimotor/sensorimotor, insular and mid-cingulate cortices as well as the dorsal- and lateral-prefrontal cortices (Fig. 3.1A). Similarly, when conducting sex-based comparisons, neither the male nor the female patients displayed statistically significant differences in cortical thickness once corrected for multiple comparisons. However, they did display trends ($p \leq 0.05$, uncorrected) of sex-dependent cortical thickening and thinning. The female FTUS patients showed a trend of cortical thinning in their left somatosensory/sensorimotor/sensorimotor cortex as well as their right somatosensory/sensorimotor/sensorimotor and striate-calcarine cortices (Fig. 3.1B).

The male FTUS patients showed a cortical thickening trend comparable to the sex-independent analysis (Fig. 3.1C).

Figure 3.1. Cortical Thickness Differences between FTUS patients and Healthy Controls on the 200 parcel Schaefer 2018 Atlas.

The differences in average cortical thickness between the FTUS participants and their age- and sex-matched healthy controls (HC) were statistically significant prior to multiple comparison correction (p-value < 0.05, uncorrected). A) Mixed-sex FTUS participants compared with HC. B) Female FTUS participants compared with HC. C) Male FTUS participants compared with HC.

When the cortical thicknesses of the mixed-sex CE patients were compared with those of their age- and sex-matched healthy controls, it was found that there were no statistically significant differences after applying the FDR Benjamini-Hochberg procedure ($p \leq 0.05$, FDR correction for multiple comparisons) (Benjamini & Hochberg, 1995). There were trends ($p \leq 0.05$, uncorrected) of cortical thinning in the left somatosensory/sensorimotor cortex (Fig. 3.2A). There were also trends ($p \leq 0.05$, uncorrected) of cortical thickening in the temporal and secondary somatosensory/sensorimotor cortices as well as the lateral and ventral lateral cortices (Fig. 3.2A). In the right hemisphere of the mixed-sex CE patients, there were trends ($p \leq 0.05$, uncorrected) of cortical thickening in the precuneus, precuneus posterior

cingulate, secondary somatosensory/sensorimotor, inferior parietal lobule, parietal operculum, temporal-parietal cortex, temporal pole and orbitofrontal cortices, as well as the ventral-, lateral-, medial posterior-prefrontal cortices (Fig. 3.2A).

When conducting sex-based comparisons, neither sex displayed statistically significant differences in cortical thickness once corrected for multiple comparisons. The female CE patients displayed trends ($p \leq 0.05$, uncorrected) of bilateral cortical thinning in the somatosensory/sensorimotor cortices as well as cortical thickening in the left temporal, secondary somatosensory/sensorimotor, extra-striate superior, dorsal- and lateral-prefrontal cortices (Fig. 3.2B). The male CE patients displayed trends ($p \leq 0.05$, uncorrected) of cortical thickening in the somatosensory/sensorimotor, temporal parietal, extrastriate, precuneus and dorsal lateral- and medial-prefrontal cortices (Fig. 3.2C).

Figure 3.2 Cortical Thickness Differences between CE patients and Healthy Controls on the 200 parcel Schaefer 2018 Atlas.

The differences in average cortical thickness between the FTUS participants and their age- and sex-matched healthy controls (HC) were statistically significant prior to multiple comparison correction (p-value < 0.05, uncorrected). **A)** Mixed-sex CE participants compared with HC. **B)** Female CE compared with HC. **C)** Male CE compared with HC.

3.1.2. 100 Parcellation Map Analysis

On the 100 parcellation map level of analysis, the cortical thicknesses of the mixed-sex FTUS patients showed no statistically significant differences from their age- and sex-matched healthy controls when multiple comparison correction p-value adjustments were made ($p \leq 0.05$, FDR correction for multiple comparisons). However, there were trends ($p \leq 0.05$ uncorrected) of cortical thickening in the mixed-sex FTUS patients' right medial- and lateral-prefrontal cortices (Fig. 3.3A).

Similarly, when conducting sex-based comparisons, neither the male nor female patients displayed statistically significant differences in cortical thickness once corrected for multiple comparisons. However, they did display trends ($p \leq 0.05$, uncorrected) of sex-dependent cortical thickening and thinning. The female FTUS patients displayed a trend of cortical thinning in the right somatosensory/sensorimotor and striate calcarine cortices (Fig. 3.3B). The male FTUS patients showed a trend of cortical thickening in the left intraparietal sulcus and extrastriate cortex, the right intraparietal sulcus, somatosensory/sensorimotor, precuneus posterior cingulate, temporal occipital cortices and the right dorsal-, lateral- and ventral-prefrontal cortices (Fig. 3.3C).

When the cortical thicknesses of the mixed-sex CE patients were compared with those of their age- and sex-matched healthy controls, it was found that there were no statistically significant differences after applying the FDR Benjamini-Hochberg procedure ($p \leq 0.05$, FDR correction for multiple comparisons), with trends ($p \leq 0.05$, uncorrected) of cortical thickening in the left secondary somatosensory/sensorimotor and lateral prefrontal cortices (Fig. 3.4A) (Benjamini & Hochberg, 1995). When conducting sex-based comparisons, neither sex displayed statistically significant differences in cortical thickness once corrected for multiple comparisons. The female CE patients displayed trends ($p \leq 0.05$, uncorrected) of cortical thinning in the somatosensory/sensorimotor cortex (Fig. 3.4B). They also displayed trends of cortical thickening in the cortices of the left extra-striate superior and insula and the right

inferior parietal lobule, post-central and medial posterior prefrontal cortices (Fig. 3.4B). The male CE patients displayed a single trend (p ≤ 0.05, uncorrected) of cortical thickening in the precuneus posterior cingulate cortex (Fig. 3.4C).
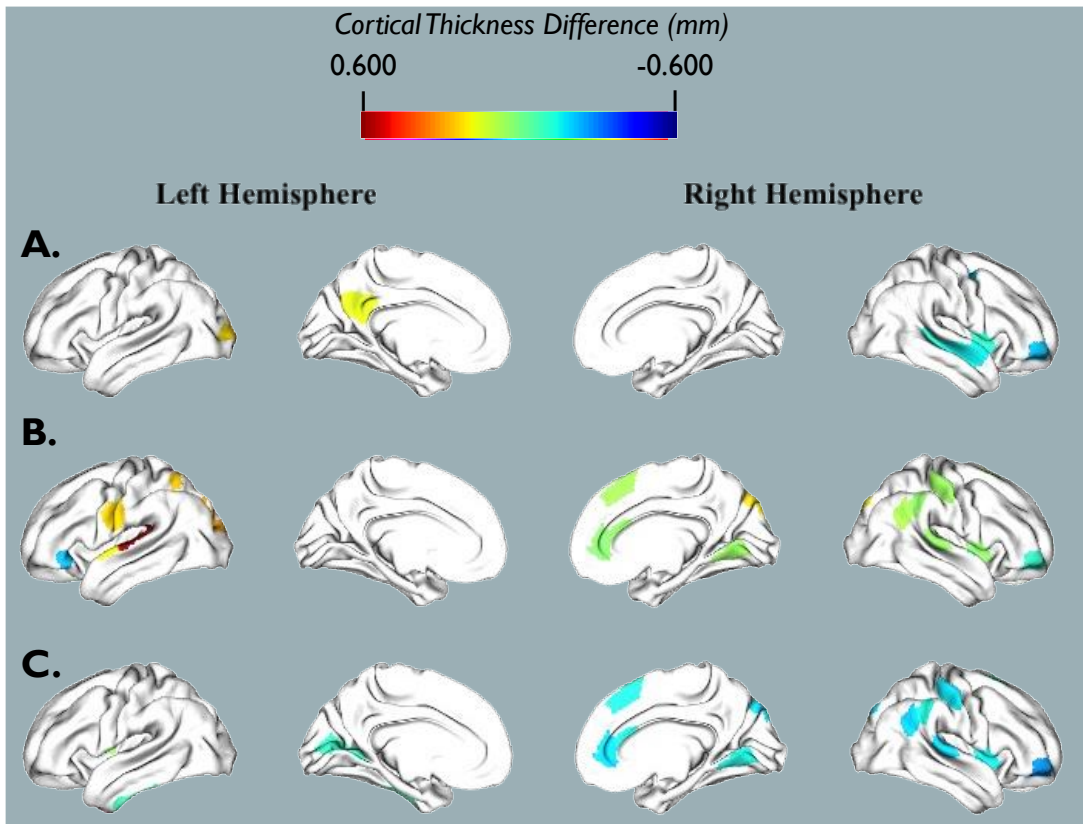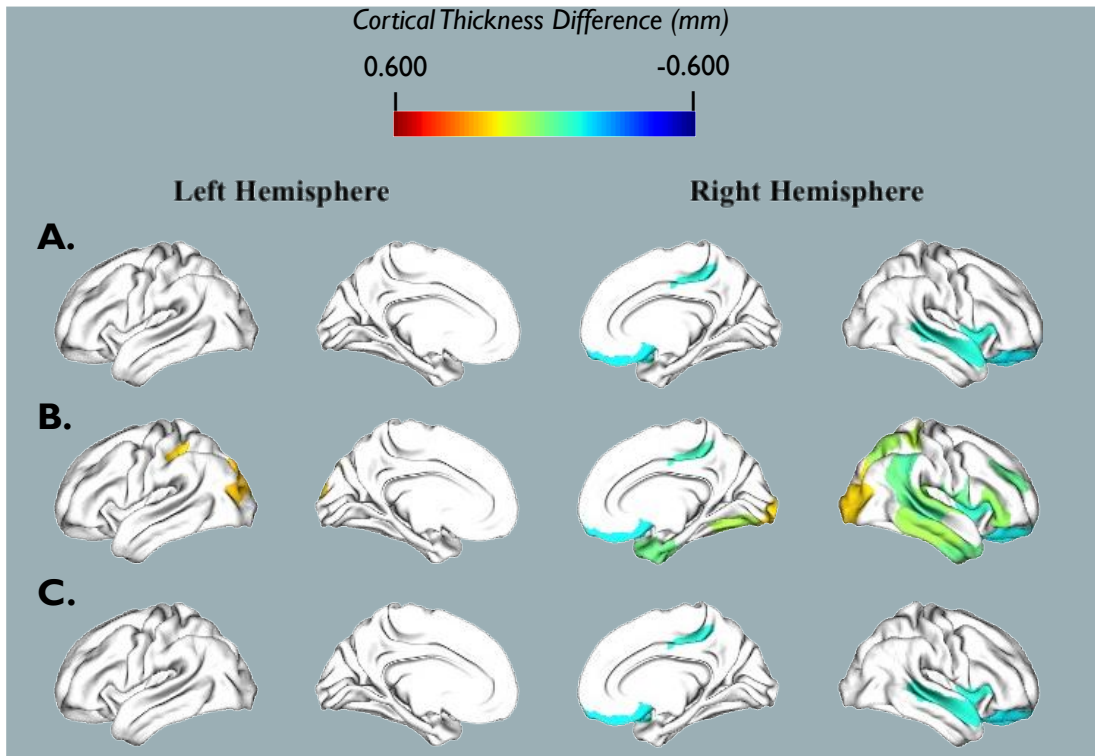

Figure 3.3 Thickness Differences between FTUS patients and Healthy Controls on the 100 parcel Schaefer 2018 Atlas

The differences in average cortical thickness between the FTUS participants and their age- and sex-matched HC were statistically significant prior to multiple comparison correction (p-value < 0.05, uncorrected). **A)** Mixed-sex FTUS participants compared with HC. **B)** Female FTUS participants compared with HC. **C)** Male FTUS participants compared with HC.
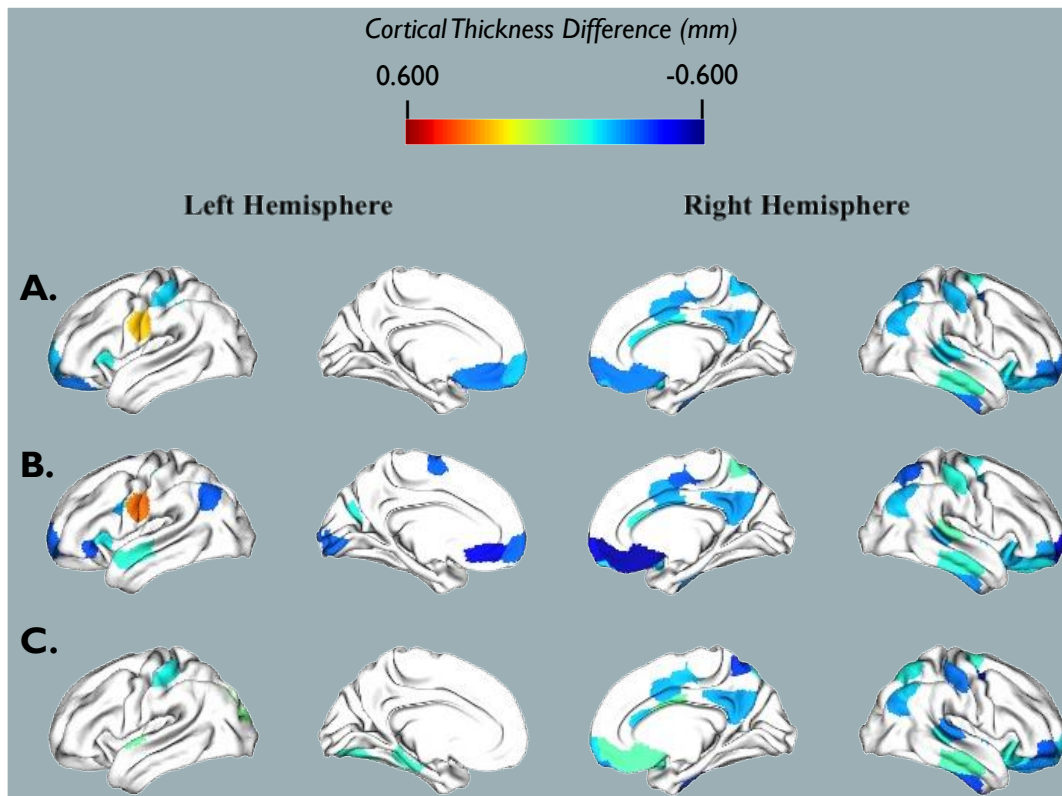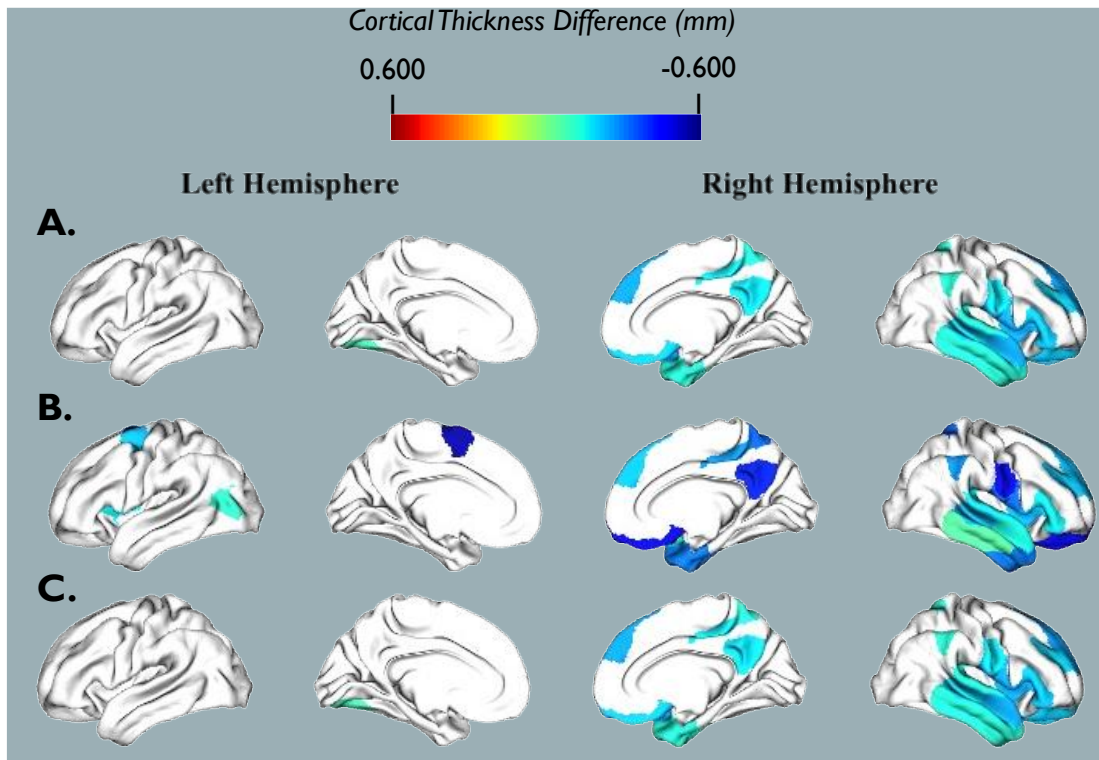
Figure 3.4 Cortical Thickness Differences between CE patients and Healthy Controls on the 100 parcel Schaefer 2018 Atlas.

The differences in average cortical thickness between the CE participants and their age- and sex-matched HC participants were statistically significant prior to multiple comparison correction (p-value < 0.05, uncorrected). **A)** Mixed-sex CE participants compared with HC. **B)** Female CE compared with HC. **C)** Male CE compared with HC.

3.2. Nodal Measures

As stated earlier, the structural covariance measures of the FTUS patients were compared with those of their age- and sex-matched healthy controls. These measures were calculated using the cortical thickness measurements' absolute correlations and adjacency matrices, as shown in Figure 3.5-3.6. This comparison was done using a non-parametric 1000 permutation test while using the FDR Benjamini-Hochberg procedure to adjust the p-values to correct for multiple comparisons. This method was repeated for the CE patients and their age- and sex-matched healthy controls.
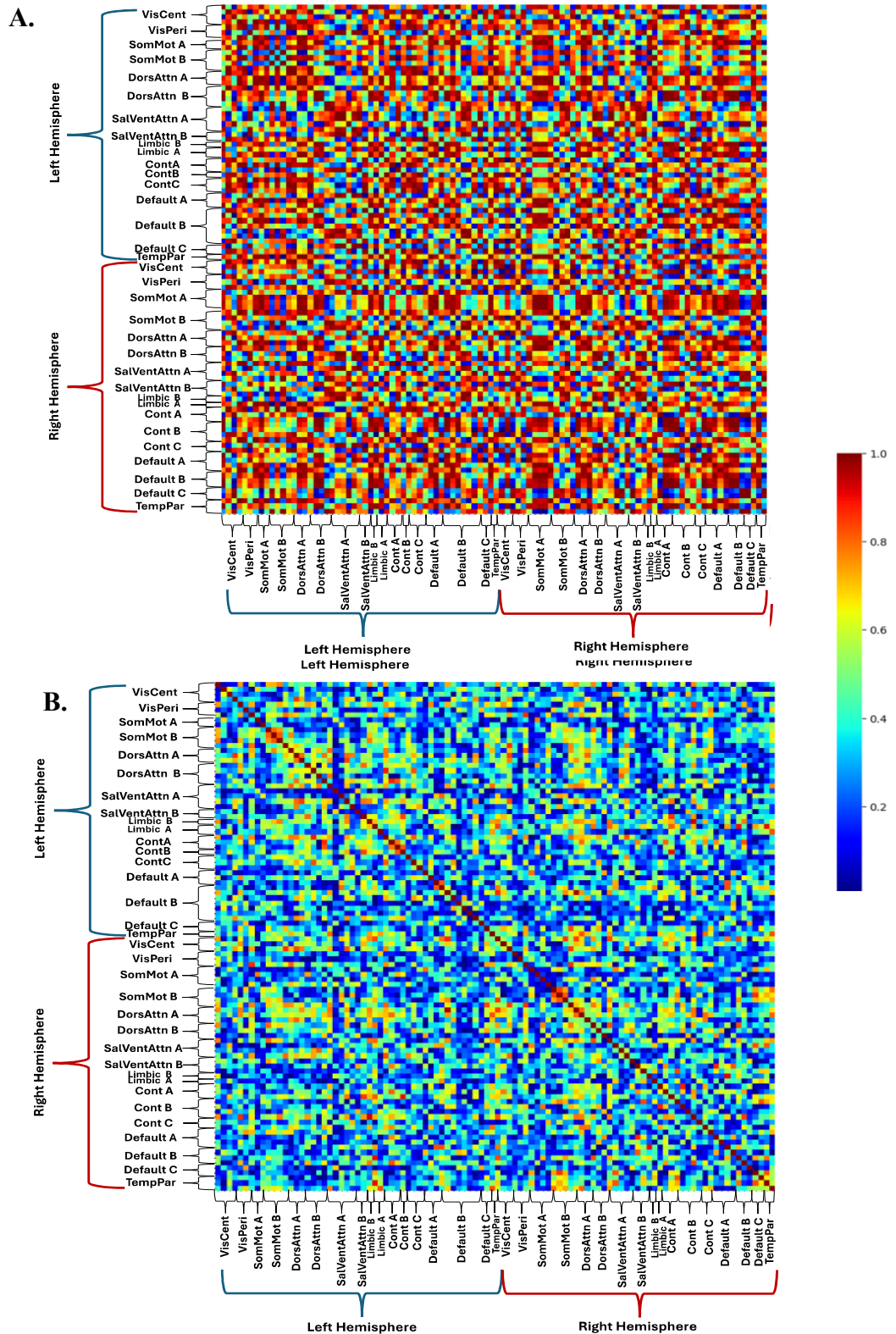
Figure 3.5 The Absolute Correlation Matrices of the FTUS and HC participants in the 100-parcel Schaefer 2018 parcellation map.

The absolute cortical thickness correlations of the participant groups, measured using the 100-parcel Schaefer 2018 parcellation map and labelled by network name: (A) The FTUS (B) Age- and sex-matched healthy controls.
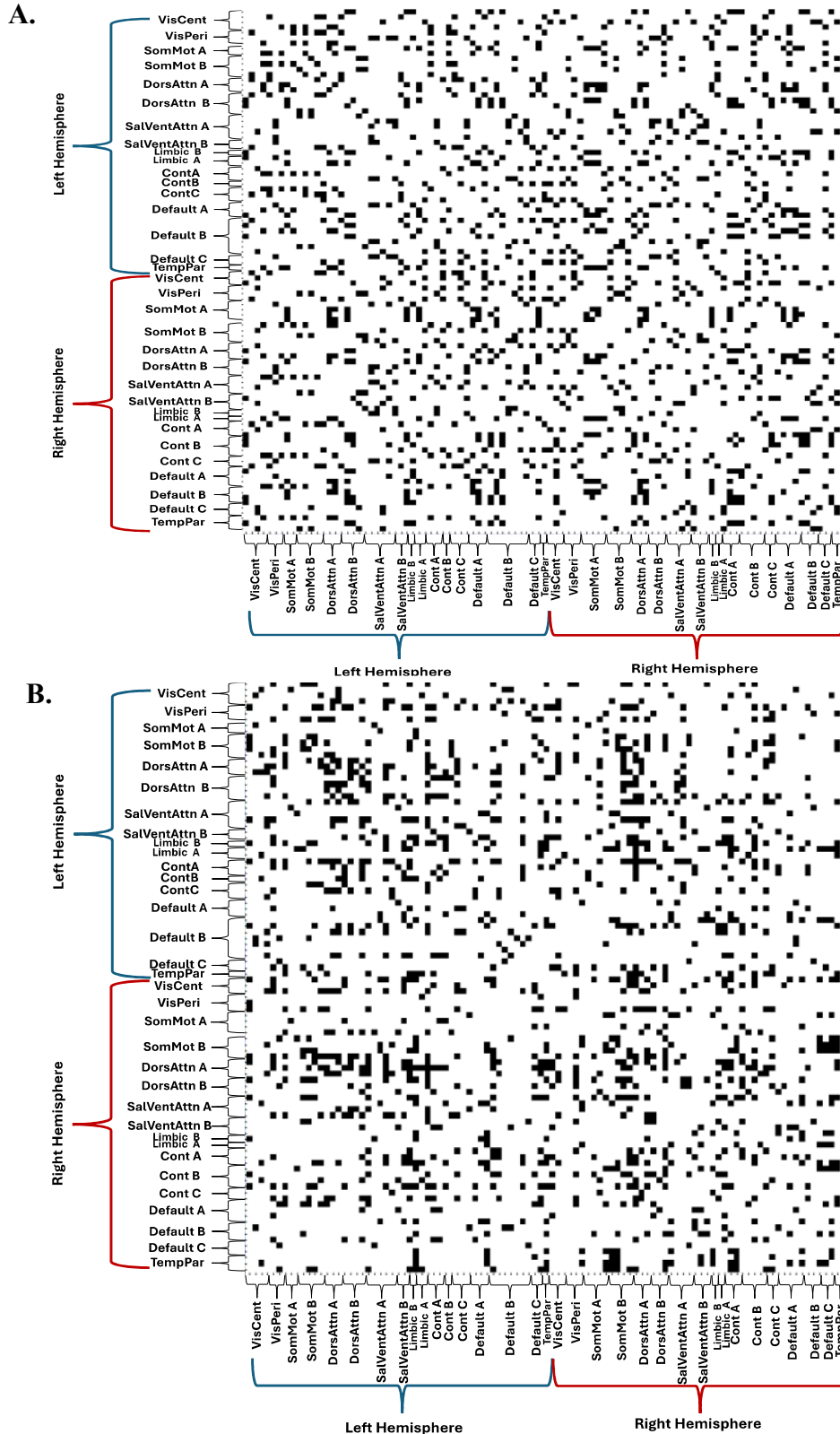
Figure 3.6. Adjacency Matrices of the FTUS participants and Healthy Controls

The thresholded (τ = 15%) and binarised adjacency matrices of FTUS and HC participants, measured using the 100-parcel Schaefer 2018 parcellation map and labelled by network name: **(A)** FTUS participants **(B)** Age- and sex-matched healthy controls.
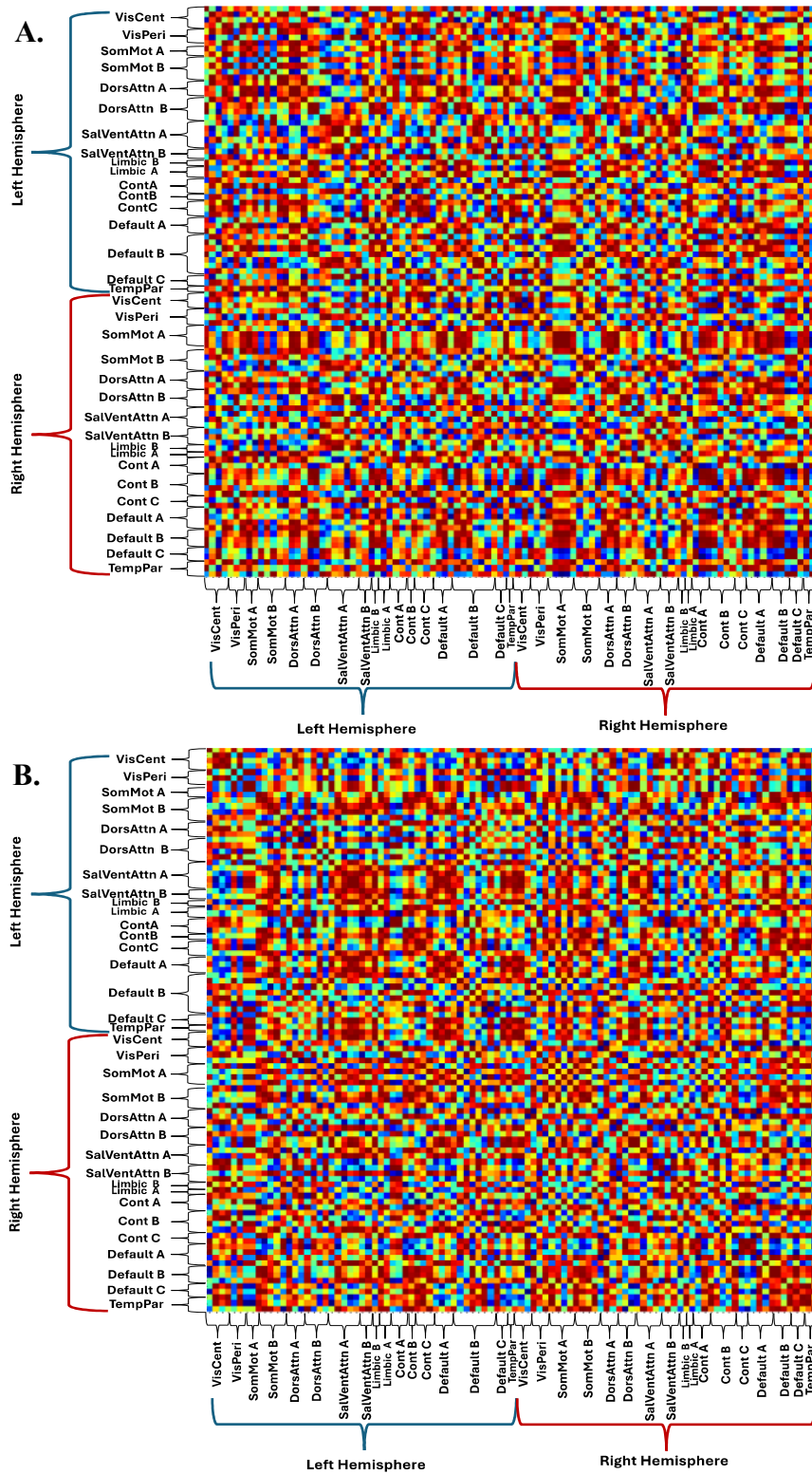
Figure 3.5 The Absolute Correlation Matrices of the CE and HC participants in the 100-parcel Schaefer 2018 parcellation map.

The absolute cortical thickness correlations of the participant groups, measured using the 100-parcel Schaefer 2018 parcellation map and labelled by network name: **(A)** CE participants **(B)** Age- and sex-matched healthy controls.

42
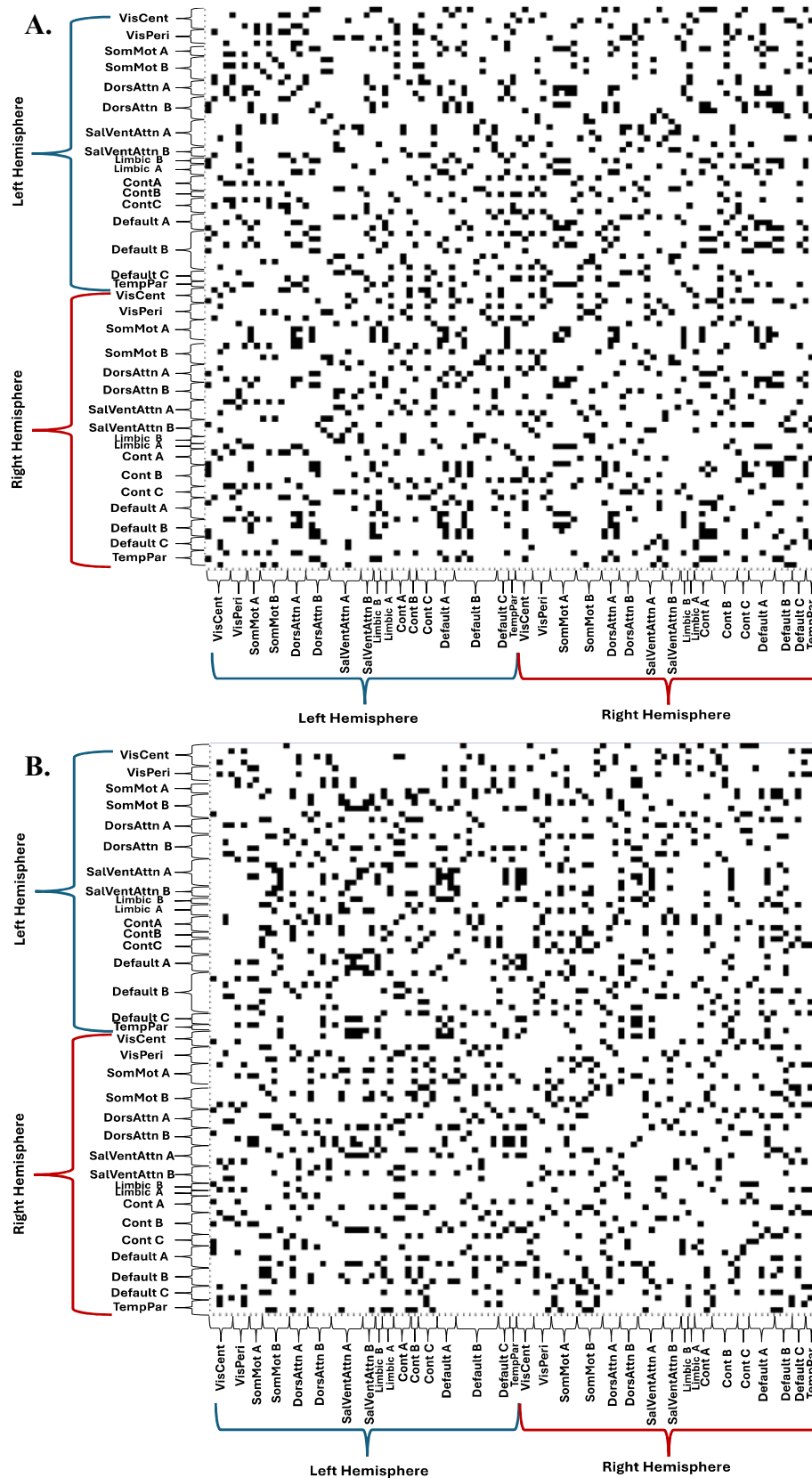
Figure 3.8. Adjacency Matrices of the CE participants and Healthy Controls

*The thresholded (τ = 15%) and binarised adjacency matrices of the participants, measured using the 100-parcel Schaefer 2018 parcellation map and labelled by network name: (**A**) CE participants (**B**) Age- and sex-matched healthy controls.*

3.2.1. 200 Parcellation Map Analysis

It was determined that at the 200-parcellation map level of analysis, statistically significant changes were only observed when looking at the betweenness centrality of the female CE patients and the male CE patients during sex-dependent analysis ($p \leq$ 0.05, FDR correction for multiple comparisons) (Fig. 3.7). There were no other statistically significant changes in the nodal measures of the FTUS patients and the CE patients once multiple comparison correction was conducted ($p \leq 0.05$, FDR correction for multiple comparisons). However, there were notable trends ($p \leq 0.05$, uncorrected) of differences in the nodal measures of all the FTUS and the CE subjects compared to their healthy control counterparts. All of these are further elaborated on below.

Betweenness Centrality

It should be noted that the female and male CE patients displayed statistically significant betweenness centrality changes. The female CE patients displayed bilateral increases in the somatomotor cortices, their left temporal, auditory and striate calcarine cortices, as well as their right frontal eye fields, dorsal- and lateral-prefrontal cortices (Fig. 3.7A). They also displayed decreases in their left temporal pole, precuneus posterior cingulate and ventral lateral prefrontal cortices, as well as their right insula and superior parietal lobule (Fig. 3.7A). The male CE patients displayed increases in the right superior parietal lobule and left precuneus posterior cingulate as well as decreases in their left midcingulate cortex and their right secondary somatosensory/sensorimotor, temporal, striate, extra-striate inferior, dorsal- and ventral prefrontal cortices (Fig. 3.7B).

While the FTUS and mixed-sex CE patients did not display any statistically significant changes in betweenness centrality once correcting for multiple comparisons, there were trends of changes when uncorrected. The mixed-sex FTUS patients displayed trends of betweenness centrality increases in the right anterior temporal cortex as well as the left extrastriate, medial- and dorsal-prefrontal cortices and a decrease in the right orbitofrontal cortex. The female FTUS patients displayed trends of increases in the left intraparietal sulcus and the cortices of the left temporal and right precuneus posterior cingulate. The male FTUS patients displayed only a decrease in their orbitofrontal cortex. Similarly, the mixed-sex CE patients displayed a trend of

decreases in their right post-central cortex, right inferior parietal lobule and right intraparietal sulcus.
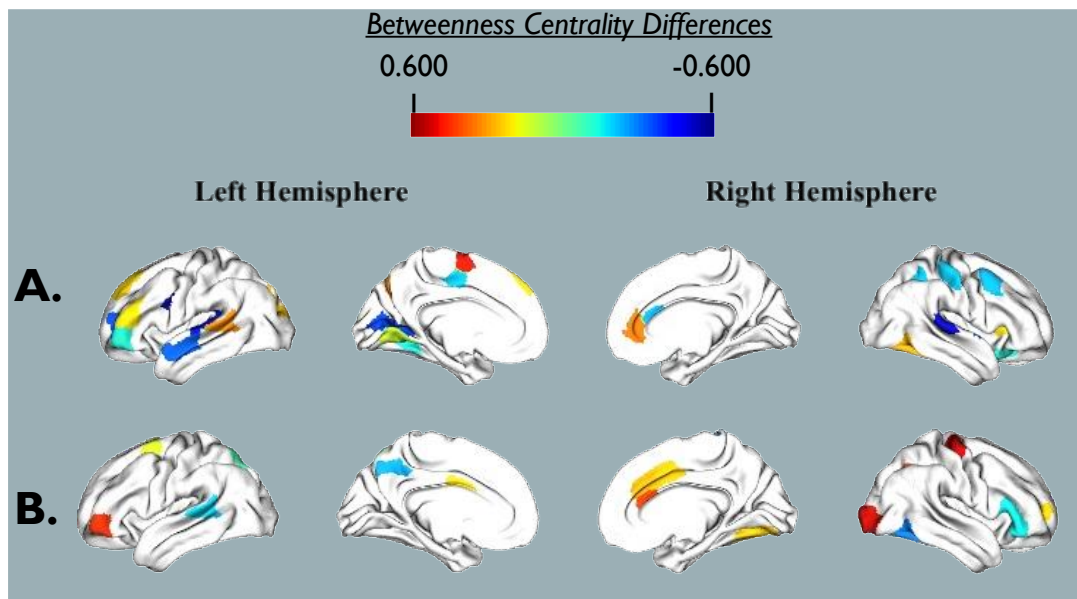
Figure 3.9. Statistically significant betweenness centrality differences between CE patients and Healthy Controls on the 200 parcel Schaefer 2018 Atlas.

The statistically significant (p-value < 0.05, FDR corrected) differences betweenness centrality measures of the CE participants and their age- and sex-matched healthy controls (HC) once corrected for multiple comparisons. A) Differences between Female CE and HC participants. B) Differences between Male CE and HC participants.

Clustering Coefficient

The patterns of clustering coefficient changes in the FTUS patients and CE patients were not statistically significant once corrected for multiple comparisons, but there were trends of changes when uncorrected.

The mixed-sex FTUS patients displayed clustering coefficient increases in the left insula, right somatosensory/sensorimotor cortex and right intraparietal sulcus, as well as decreases in the left extrastriate cortex and right medial prefrontal cortex. The female FTUS patients displayed bilateral increases in their temporal pole cortices, their left somatomotor cortex, along with the right insula, post-central and medial posterior prefrontal cortices. The male FTUS patients displayed decreases in the right ventral prefrontal cortex and their left secondary somatosensory/sensorimotor cortex, precuneus and ventrolateral prefrontal cortices. The mixed-sex CE patients displayed

an increase in the clustering coefficient of their left parahippocampal cortex. However, this difference did not persist when comparing the CE patients based on sex.

Participation Coefficient

None of the observed patterns of participation coefficient changes were statistically significant once corrected for multiple comparisons, but there were several trends of changes when uncorrected.

The mixed-sex FTUS patients displayed trends of participation coefficient increases in the left lateral prefrontal cortex. They also displayed decreases in the right somatosensory/sensorimotor cortex and intraparietal sulcus as well as the left insula, orbitofrontal cortices and precuneus posterior cingulate cortices. The female FTUS patients displayed decreases in the left striate cortex and the right somatosensory/sensorimotor and post-central cortices. The female FTUS patients also displayed bilateral increases in their precuneus, right insula, and right temporal occipital cortex. The male FTUS patients displayed decreases in their left temporal pole and ventral prefrontal cortex as well as bilateral increases in their somatosensory/sensorimotor cortex and their right mid-cingulate cortex.

The mixed-sex CE patients displayed bilateral increases in their somatosensory/sensorimotor and dorsal-prefrontal cortices. They also displayed increases in their left orbitofrontal, temporal pole, and dorsal prefrontal cortices, as well as their right central and extra-striate cortices. In comparison, the female CE patients displayed a decrease in their right temporal occipital cortex and an increase in their left post-central cortex. The CE male patients displayed no trends of differences in their participation coefficient.

Shortest Path Length

The observed patterns of shortest path length changes were not statistically significant once corrected for multiple comparisons in either group, but there were several trends of changes when uncorrected.

The mixed-sex FTUS patients displayed increases in the shortest path lengths of the left superior extrastriate and left precuneus posterior cingulate cortices and a decrease in the right anterior temporal lobe. The female FTUS patients displayed bilateral decreases in their precuneus posterior cingulate cortex and left extra-striate. The male FTUS patients displayed an increase in their right inferior parietal lobule and

a decrease in their right inferior parietal lobule and somatosensory/sensorimotor cortex. None of the CE patients displayed trends of differences in their shortest path lengths.

3.2.2. 100 Parcellation Map Analysis

When analysing the nodal measures of the participants at the 100-parcellation map level of analysis, it was found that both the female and male CE patients displayed statistically significant differences from their healthy control counterparts in the betweenness centrality nodal measure ($p \leq 0.05$, FDR correction for multiple comparisons) (Fig. 3.8). Additionally, the female CE patients displayed statistically significant differences in the participation coefficient measure and clustering coefficient measures, while the males displayed statistically significant differences in shortest path lengths ($p \leq 0.05$, FDR correction for multiple comparisons) (Fig. 3.9 – 3.10 & Fig. 3.11). Beyond the statistically significant differences in nodal measures, there were trends ($p \leq 0.05$, uncorrected) of nodal measure differences between the patient groups and their age- and sex-matched healthy controls. All of the statistically significant differences ($p \leq 0.05$, FDR correction for multiple comparisons) and trends ($p \leq 0.05$, uncorrected) are further elaborated on below.

Betweenness Centrality

The female and male CE patients displayed statistically significant ($p \leq 0.05$, FDR correction for multiple comparisons) changes in their betweenness centrality. The Female CE patients displayed decreases in the left precuneus and striate as well as the right temporal-parietal, temporal pole, orbitofrontal, and lateral prefrontal cortices (Fig. 3.8A). They also displayed statistically significant ($p \leq 0.05$, FDR correction for multiple comparisons) increases in the left central, frontal medial, inferior extrastriate, temporal and ventral prefrontal cortices as well as the right insula, parietal occipital and secondary somatosensory/sensorimotor cortices (Fig. 3.8A). The male CE patients displayed statistically significant ($p \leq 0.05$, FDR correction for multiple comparisons) bilateral decreases in the insula, the left secondary somatosensory/sensorimotor cortex, as well as the right somatosensory/sensorimotor and lateral prefrontal cortices (Fig. 3.8B). They also displayed statistically significant ($p \leq 0.05$, FDR correction for multiple comparisons) bilateral increases in the inferior parietal lobule and lateral

prefrontal cortex as well as the left posterior cingulate and precuneus cortices and the right parietal medial, dorsolateral- and medial-prefrontal cortices (Fig. 3.8B).

All the FTUS patients and mixed-sex CE patients did not display statistically significant differences once corrected for multiple comparisons, but there were trends of changes when uncorrected. The mixed-sex FTUS patients displayed betweenness centrality increases in their left precuneus, extrastriate, and medial prefrontal cortices. The female FTUS patients displayed increases in the left retrosplenial, extrastriate and inferior extra-striate cortices. Similarly, the mixed-sex CE patients displayed a non-statistically significant decrease in the left inferior extrastriate.
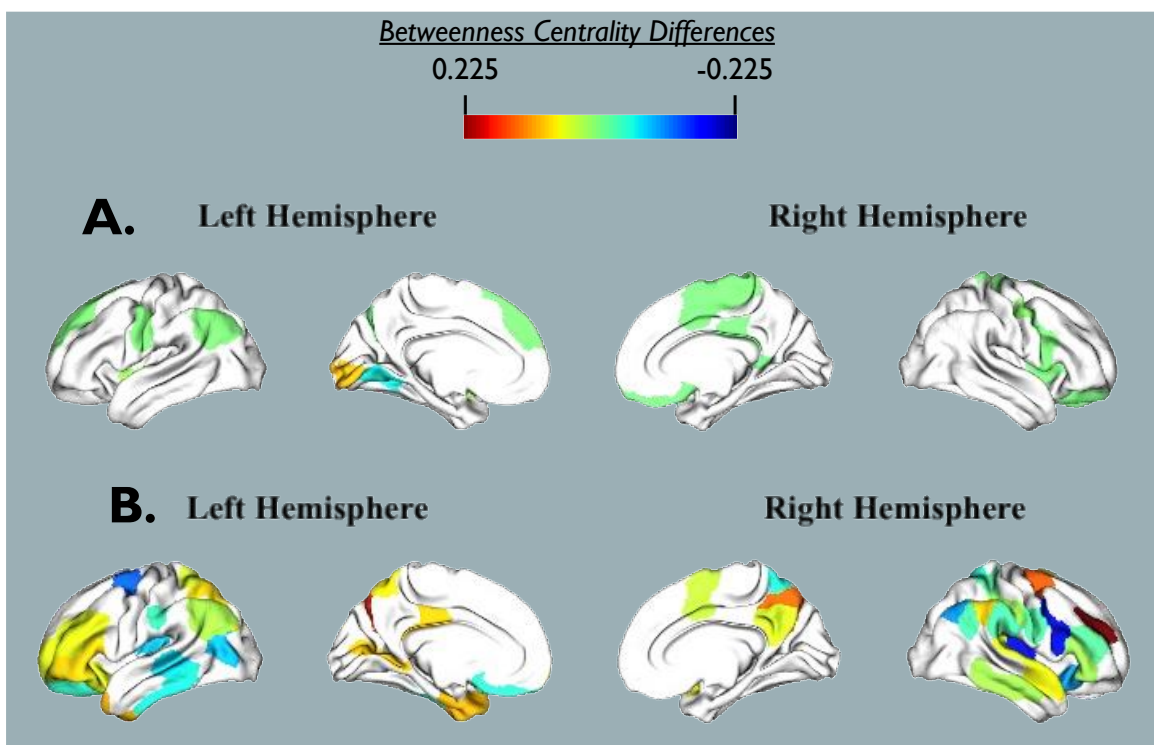
Figure 3.10. Statistically significant Betweenness Centrality differences between the CE patients and Healthy Controls on the 100 parcel Schaefer 2018 Atlas.

*The statistically significant (p-value < 0.05, FDR corrected) differences in nodal measures of the CE participants and their age- and sex-matched healthy controls (HC) once corrected for multiple comparisons. **A)** Betweenness centrality differences between Female CE participants and with HC. **B)** Betweenness centrality differences between Male CE participants and HC.*

Clustering Coefficient

Only the female CE patients displayed statistically significant ($p \leq 0.05$, FDR correction for multiple comparisons) changes in their clustering coefficient measures. The female CE patients displayed decreases in the left secondary

somatosensory/sensorimotor, extra-striate and striate calcarine, as well as the right parietal medial and ventral prefrontal cortices (Fig. 3.9). They also displayed statistically significant (p ≤ 0.05, FDR correction for multiple comparisons) increases in the left striate, precuneus and precuneus posterior cingulate cortices as well as the right temporal-parietal and dorsal prefrontal cortices (Fig. 3.9).

None of the patterns of clustering coefficient changes in all the FTUS patients, the mixed-sex CE patients and male CE patients were statistically significant once corrected for multiple comparisons, but there were trends of changes when uncorrected.

The mixed-sex FTUS patients displayed a decrease in the clustering coefficient of the right ventral prefrontal cortex. The female FTUS patients displayed bilateral increases in the precuneus posterior cingulate cortex, the left precuneus, and the right parietal operculum. The male FTUS patients displayed a decrease in the right temporal pole cortex as well as increases bilaterally in the temporal parietal, the right superior parietal lobule, and the extra-striate cortex. The mixed-sex CE patients displayed no trends of clustering coefficient changes. The male CE patients also displayed trends of decreases in the left dorsal prefrontal cortex as well as the right orbitofrontal and somatosensory/sensorimotor cortices.
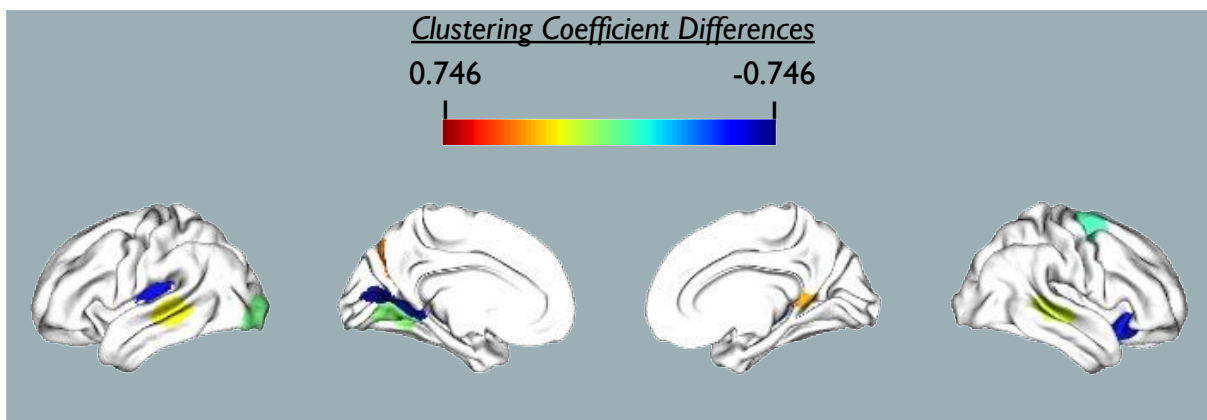
Figure 3.11. Statistically significant Clustering coefficient differences between the Female CE patients and Healthy Controls on the 100 parcel Schaefer 2018 Atlas.

The statistically significant differences (p-value < 0.05, FDR corrected) in the Clustering coefficient measures of the female CE participants and their age- and sex-matched healthy controls (HC) once corrected for multiple comparisons.

Participation Coefficient

Similar to the clustering coefficient, only the female CE patients displayed statistically significant ($p \leq 0.05$, FDR correction for multiple comparisons) changes in their participation coefficient measures. The female CE patients displayed bilateral decreases in the superior extra-striate cortices and the right precuneus posterior cingulate cortex as well as the left insula, medial parietal and lateral prefrontal cortices (Fig. 3.10). The female CE patients also displayed increases in the right somatosensory/sensorimotor and central cortices (Fig. 3.10).

None of the patterns of participation coefficient changes in all the FTUS patients, mixed-sex CE patients and male CE patients were statistically significant once corrected for multiple comparisons, but there were trends of changes when uncorrected. The mixed-sex FTUS patients displayed an increase in the participation coefficient of the dorsal prefrontal cortex as well as decreases in the striate, superior extra-striate, parahippocampal and ventrolateral prefrontal cortices. The female FTUS patients displayed a decrease in the left extra-striate, precuneus posterior cingulate and orbitofrontal cortices, as well as the right parietal operculum and dorsolateral prefrontal cortex. The male FTUS patients displayed decreases in the left frontal medial, extra-striate, dorsal- and lateral-prefrontal cortices as well as the right post-central cortex.

The mixed-sex CE patients displayed a decrease in the left inferior extra-striate and right inferior parietal lobule. Additionally, they displayed bilateral increases in the lateral prefrontal cortices, the left extra-striate, the right insula, auditory, secondary somatosensory/sensorimotor, orbitofrontal, and lateral prefrontal cortices.
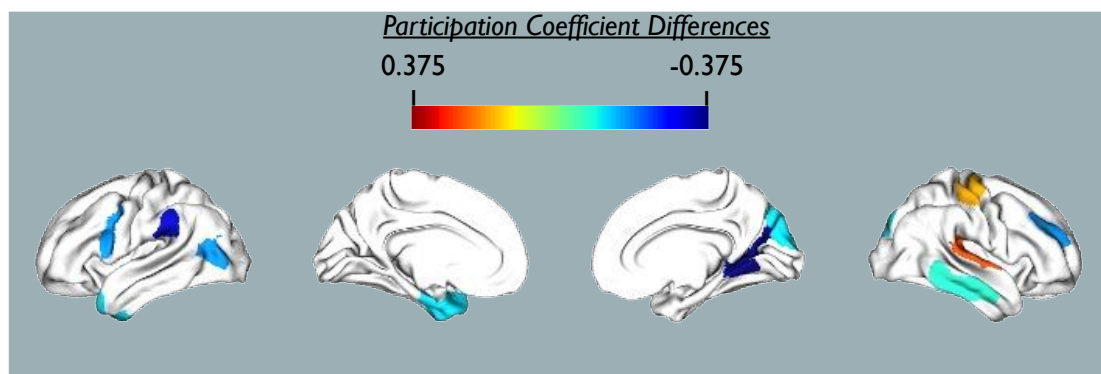
Figure 3.12. Statistically significant Participation coefficient differences between the Female CE patients and Healthy Controls on the 100 parcel Schaefer 2018 Atlas.

The statistically significant differences (p-value < 0.05, FDR corrected) in the Participation coefficient measures of the female CE participants and their age- and sex-matched healthy controls (HC) once corrected for multiple comparisons.

Shortest Path Length

Only the male CE patients displayed trends (p ≤ 0.05, uncorrected) of shortest path length as well as statistically significant differences (p ≤ 0.05, FDR correction for multiple comparisons); these large-scale patterns of differences can be seen in Fig. 3.11.

The FTUS patients displayed non-statistically significant (p ≤ 0.05, uncorrected) change trends, but neither the mixed-sex nor the female CE patients displayed any trends. The mixed-sex FTUS patients displayed an increase in the shortest path length of the right inferior parietal lobule. The female FTUS patients displayed increases in the cortices of the left insula and parietal operculum as well as the left extra-striate superior and post-central cortices. The male FTUS patients displayed a decrease in the right temporal and occipital cortex, as well as increases in the left insula and bilaterally in the somatosensory/sensorimotor and dorsal prefrontal cortices.
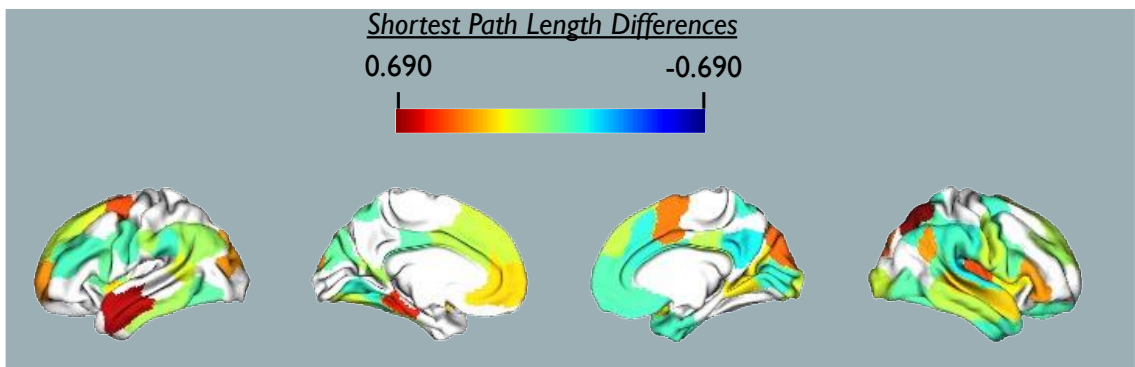
Figure 3.13. Statistically significant Shortest path length differences between the Male CE patients and Healthy Controls on the 100 parcel Schaefer 2018 Atlas.

The statistically significant differences (p-value < 0.05, FDR corrected) in the Shortest path length measures of the male CE participants and their age- and sex-matched healthy controls (HC) once corrected for multiple comparisons.

3.3. Global Measures

The patient groups, FTUS patients and CE patients, displayed no statistically significant differences (p ≤ 0.05, FDR correction for multiple comparisons) in their global measures compared to their age- and sex-matched healthy controls. This lack of statistical significance persisted regardless of parcellation level, both 100 parcellation maps and 200 parcellation maps, and sex. No trends of differences trends (p ≤ 0.05, uncorrected) were identified either.

4. Chapter 4: Discussion

4.1. Overview

This case-control study investigated cortical thickness changes in FTUS patients by comparing their cortical thicknesses with those of age- and sex-matched healthy controls based on the comparison methods used in past epilepsy research (Bernhardt et al., 2009; Bernhardt et al., 2010; Galovic et al., 2019; Jber et al., 2020; Kemmotsu et al., 2011; Ogren et al., 2018). Based on past research, higher cortical thickness levels in patients relative to healthy controls would be interpreted as cortical thickening, and lower cortical thicknesses would indicate cortical thinning. The measured cortical thicknesses were used to conduct a structural covariance analysis to identify any neural network disruptions occurring in the patient groups (Bernhardt et al., 2011; Liu et al., 2023). These comparisons were conducted twice, employing two distinct levels of the 17-network Schaefer 2018 atlas: the 200-parcel atlas and the 100-parcel atlas (Schaefer et al., 2017).

4.1.1. Cortical Thickness

In both the 200-parcel and 100-parcel atlases, there were no statistically significant patterns of cortical thickness changes after adjusting for multiple comparisons using the FDR Benjamini–Hochberg method (Benjamini & Hochberg, 1995)

4.1.2. Structural Covariance Analysis Nodal Measures

In both the 200-parcel and 100-parcel atlases, the CE patients displayed statistically significant betweenness centrality changes but only when conducting sex-dependent analyses. At the 200-parcel level, the female CE patients displayed bilateral betweenness centrality decreases in the frontal and temporal cortices, indicating that these regions are becoming less important to information transference in the network, while the increases in the parietal cortices indicating they are becoming more important (Fornito et al., 2016). The opposite occurred for the male CE patients as they displayed

increases in the prefrontal, occipital, temporal and parietal cortices, indicating such regions are becoming connection hubs networks (Fornito et al., 2016).

At the 100-parcel level, these betweenness centrality changes shift as the female CE patients exhibited intriguing fluctuations. The female CE patients displayed both increases and decreases within the frontal, temporal and occipital cortices rather than solely an increase or decrease, with contrasting changes occurring within the contralateral brain region, showing an opposite change. Similar patterns of change occurred in the male CE patients in the prefrontal, frontal and parietal cortices, with slightly more increases occurring than decreases. Overall, these patterns of change indicate a disruption of inter-regional communication (Fornito et al., 2016).

Additional sex-dependent statistically significant differences were present in the nodal measures of the CE patients at the 100-parcel level; the females exhibited clustering coefficient and participant coefficient changes, while the males displayed shortest path length changes. The female CE patients exhibited decreases in participant coefficients across the prefrontal, motor, occipital, parietal, and insula cortices, alongside an increase in the motor and central cortices of the frontal lobe. These alterations collectively suggest a reduction in the diverse structural connectivities within these regions, reinforcing the possibility of ongoing structural reorganisation (Fornito et al., 2016). The female CE patients' clustering coefficients increased and decreased within the frontal, parietal and occipital cortices rather than solely increasing or decreasing, except for the parietal temporal cortex, which displayed a distinct increase. Such changes indicate complex structural connectivity reorganisation within these regions (Fornito et al., 2016). The male CE patients showed widespread changes in their shortest path lengths. Specifically, their frontal lobes displayed decreased structural connectivity and efficiency as their shortest path lengths increased. In contrast, their parietal and temporal cortices displayed shortest path length decreases, indicating increased structural connectivity and efficiency (Fornito et al., 2016).

4.1.3. Structural Covariance Analysis Global Measures

Despite statistically significant nodal measure differences observed in the CE patients at both parcellation levels, neither of the patient groups displayed any statistically significant differences in global measures, even when conducting sex-dependent analyses.

4.2. Significance

Cortical thinning and overall grey matter atrophy is a well-documented structural phenomenon in PWE, with several studies showing that PWE experience progressive widespread cortical thinning (Bernhardt et al., 2009; Bernhardt et al., 2010; Bernasconi et al., 2004; Coan et al., 2014; Galovic et al., 2019; Jber et al., 2020). The progressive nature of this cortical thinning, especially that it is most prominent in the first five years following seizure onset, was the basis for this research study as it suggests the possibility of such changes being detectable as early as the first seizure onset (Bernasconi et al., 2004; Coan et al., 2014; Galovic et al., 2019; Jber et al., 2020). Further structural covariance analysis was conducted on the FTUS patients to investigate whether there were observable changes to the patients' structural covariance brain networks (SCN), as past epilepsy research has determined that epilepsy is a network disorder (Bernasconi et al., 2004; Bernhardt et al., 2011; Larivière et al., 2022; Wang et al., 2023). In the Bernasconi et al. (2004) study, it was proposed that the observed patterns of grey matter volume atrophy in TLE were the product of decreasing the white matter projections in the TLE patients' temporal and frontal lobes, disrupting their frontotemporal networks and resulting in their becoming epileptic. While the cause of epilepsy cortical thinning and network disruptions remain uncertain, there is increasing support for the explanation proposed in the Bernasconi et al. (2004) study. Several studies have provided evidence indicating that the network disruptions occurring in PWE are associated with a decline in neuronal-axonal connections and white matter fibre tracts, which in turn cause cortical thinning (Bernasconi et al., 2004; Bernhardt et al., 2011; Bernhardt et al., 2013; Bernhardt et al., 2009; Liu et al., 2017; Liu et al., 2023; Yasuda et al., 2015; Wang et al., 2023).

This study revealed various sex-dependent patterns of SCN changes among the CE patients throughout the cortex. However, despite such changes, there was no statistically significant cortical thinning or thickening after FDR multiple comparison corrections. This indicates that the SCN alterations associated with epilepsy occur before statistically significant cortical thickness changes occur, supporting the notion that epilepsy-related cortical thinning is affected by network disruptions, as proposed by Bernasconi et al. (2004). In summary, the extensive changes in the nodal measures of the CE patients' SCNs suggest that their small-world networks are significantly disrupted and reorganised.

As stated in the Introduction, past studies have documented patterns of brain network changes, determined via structural covariance analysis, occurring in patterns dependent on the type of epilepsy the patient is experiencing (Bernhardt et al., 2011; Bernhardt et al., 2013; Bernhardt et al., 2009; Larivière et al., 2022; Liu et al., 2023; van Diessen et al., 2013; Wang et al., 2023; Yasuda et al., 2015). Individuals with TLE exhibit disruptions to their small-world networks as their node hubs go from being evenly distributed to being predominantly concentrated in the limbic and temporal cortices, with these regions increasing in local connectivity while decreasing in global efficiency (Bernhardt et al., 2011; Bernhardt et al., 2013; Larivière et al., 2022; van Diessen et al., 2013; Yasuda et al., 2015). Such changes occur in a lateralised manner as the increases in connectivity occur ipsilateral to the seizure focus, TLE type, while the decreases occur contralateral to it (Bernhardt et al., 2011; Larivière et al., 2022; Wang et al., 2023; Yasuda et al., 2015). In comparison, those with FLE display overall reductions in their small-world network nodal measures, with the network hubs shifting towards the parietal lobes (Liu et al., 2023). Similarly, IGE cases, PWE displayed significant small-world network disruption as the nodal measures throughout the temporal, frontal and parietal cortices show a notable decrease (Larivière et al., 2022). While this study observed network changes in FTUS patients, the primary similarity between these changes and the patterns identified in previous research predominantly lies in their occurrence rather than in the specific patterns in which they occur. Such dissimilarity in this study's findings from past research could be due to several factors, including, but not limited to, the fact that the data collection and analysis was focused on FTUS patients while past research was predominantly focused on diagnosed PWE. As such, the patients in this study and past research are at very different stages of epilepsy progression, an important factor as the aforementioned patterns of epilepsy-type dependent brain network changes have been shown to be progressive and influenced by factors such as epilepsy duration, seizure frequency and AED/ASM load (Drenthen et al., 2018; Larivière et al., 2022; van Diessen et al., 2013). This suggests a possibility that the patterns of epilepsy-type dependent brain network changes become more evident and in line with expectations over time, possibly explaining the discrepancy between the patterns observed in this study and the patterns observed in past studies (Drenthen et al., 2018; Larivière et al., 2022; van Diessen et al., 2013). However, as there is no known cause behind the cortical thickness and SCN changes

observed in PWE, it is currently not possible to state definitively why such patterns of SCN changes are occurring in the CE patients.

4.3. Limitations and Future Research

This study noted that the CE patients displayed patterns of SCN changes distinct from any SCN patterns previously detected in PWE. While these patterns of SCN changes could be attributed to the early stage of epilepsy, an alternative explanation for the observed changes could be the study's parcellation maps, the current sample size, especially that of the CE participant group, as well as the technical and statistical issues regarding the processing and analysis of the MRI data.

4.3.1. Parcellation Maps

In this study, two parcellation maps were used: the 100-parcel and 200-parcel Schaefer 2018 parcellation maps, which could potentially contribute to the unique patterns of SCN changes observed (Fürtjes et al., 2023; Schaefer et al., 2018). Although more finely segmented, the Schaefer 2018 parcellation map is less commonly employed in epilepsy research. Many epilepsy studies prefer coarser parcellation maps, such as the 68 Desikan-Killiany atlas, risking more subtle SCN changes in PWE being overlooked (Fürtjes et al., 2023; Larivière et al., 2022). As a result, the distinctiveness of the SCN changes observed in this study could be attributed to such changes being overlooked in past research (Fürtjes et al., 2023). Furthermore, it is worth noting that differences in the layout of parcellation maps can impact the quantification of SCNs as they vary in their distribution and assignment of cortical regions, which, in turn, can affect the calculated cortical correlations as well as the global and nodal measurements (Fürtjes et al., 2023; Yao et al., 2015). Such variations were observed in the Pegg et al. (2020) IGE meta-analysis in which, of the 13 studies compiled and analysed, the only two that used different parcellation maps were also the only ones that displayed variations in their nodal measures. Currently, there is no definitive parcellation map that can be used for epilepsy research. However, future studies may benefit from employing multiple commonly used parcellation maps, akin to the approach adopted in this study. Such an approach would enable their findings to be compared to past and future research, enhancing the continuity and comparability of results.

4.3.2. Sample Size Issues

The sample of this study was relatively small, with an initial sample of 16 individuals who experienced an FTUS; of these individuals, six were diagnosed with epilepsy after undergoing a 7T MRI scan. As an incredibly heterogeneous neurological disorder, cases of epilepsy vary in how the seizures manifest and their site origin (Fisher et al., 2017; Scheffer et al., 2017). Due to the stage at which the CE patients were diagnosed with epilepsy, several lacked identified seizure-onset sites; this, combined with the already small sample of CE patients, led to this variable not being accounted for during the statistical analysis. Consequently, the cortical thickness and SCN analyses were performed on a group of CE patients that could hypothetically consist of various epilepsy types. This could be a contributing factor to the pattern of observed results, as several studies have shown that in PWE, the lateralisation of seizure onset influences the observed patterns of cortical thickness and SCN changes (Bernhardt et al., 2011; Drenthen et al., 2018; Larivière et al., 2022; van Diessen et al., 2013). Thus, the SCN changes observed could be due to the data representing a mixture of epileptic conditions.

This is one of many issues regarding the patient group sample size, as the overall FTUS sample size is small, which limits sensitivity to differences between the FTUS patients and the healthy controls. The issue of small sample sizes in such epilepsy research is best illustrated in the study conducted by Dickey et al. (2022). Their analysis of 69 epilepsy surgery studies conducted from 1980 to 2020 revealed a median sample size of 39 subjects with a notably low statistical power of .24 (Dickey et al., 2022). Similarly, in the Bernhardt et al. (2010) and Carmon et al. (2020) studies, it was estimated that for a statistically significant difference to be identified between participant groups with a meaningful amount of statistical power, a considerably larger sample size would be required. However, the suggested sample size varied between the two studies, as the power analysis conducted by Bernhardt et al. (2010) suggested a sample size of 160 participants, while Carmon et al. (2020) suggested a minimum of 30 participants. The challenge of small sample sizes is exacerbated in the case of the six CE patients in this study, especially when conducting sex-based group analyses. These analyses further reduced the sample size from six participants to three and

subsequently down to two when conducting the analyses using the 100-parcel 17-network Schaefer 2018 atlas due to a data issue.

Future 7T MRI research regarding cortical thickness changes of individuals experiencing a first-time unprovoked seizure should aim to use a larger sample size, ideally one closer to 160 patients, as estimated by Bernhardt et al. (2010) or at minimum 30 patients, as indicated in Carmon et al. (2020). Moreover, for enhanced patient classification of FTUS patients as possessing epilepsy, future research should consider implementing a two-year minimum wait period after FTUS occurrence before analysing participant data. This timeframe allows multiple EEGs to be conducted, facilitating more reliable epileptiform abnormality detection (Baldin et al., 2014). Additionally, the likelihood of a second seizure and subsequent epilepsy diagnosis decreases significantly after two years, warranting this suggested waiting period (Berg, 2008).

4.3.3. Technical Considerations

Several additional weaknesses of this study were due to the use of the relatively novel 7T MRI neuroimaging for structural data acquisition. The superior strength of the 7T MRI magnets allows for the generation of T1w images with higher SNR and, thus, better spatial resolution. However, the positives of these stronger magnets do not come without negatives, as 7T MRIs are much more likely to experience B1+ transmit field inhomogeneities and geometric artefacts than MRIs of lower strength (Collin et al., 1998; Haast et al., 2018; Karamat et al., 2016; Lau et al., 2018; Vaughan et al., 2001). While the gradient non-linearities were corrected for in the anat_preproc pipeline through the use of the gradcorrect application, there is no guarantee that the geometric artefacts present in the MRI images were not fully corrected (Khan & Haast, 2020; Lau et al., 2018). Future research would benefit from also implementing the field map correction methodology used by the Human Connectome Project (Glasser et al., 2013; Lau et al., 2018).

B_1^+ transmit field inhomogeneities manifest when the B_1 field fails to be homogenous throughout the scanner, theses inhomogeneities have been noted to be more likely to occur in 7T MRI scans than in those of lower magnetic field strengths, such as 4T MRIs, due to their smaller RF transmit field wavelengths (Collin et al., 1998; Karamat et al., 2016; Vaughan et al., 2001). These B_1^+ inhomogeneities cause MRI

image distortions, which can hinder brain tissue differentiation and the measurement of neuroimaging metrics, including cortical thickness measurements (Haast et al., 2018). Past 7T MRI research indicates that the ideal way to circumvent B_1^+ inhomogeneity would be the use of the saturation-prepared with 2 rapid Gradient Echoes (SA2RAGE) sequence for post-hoc B_1^+ inhomogeneity correction (Eggenschwiler et al., 2012; Haast et al., 2018; Marques & Gruetter, 2013). On the other hand, the MP2RAGE sequence parameters of the University of Western Ontario have been shown to produce T1w images with B_1^+ inhomogeneity levels comparable to those of T1w images generated by Maastricht University's MP2RAGE sequence with SA2RAGE post-hoc B_1^+ inhomogeneity correction (Haast et al., 2021). However, it should be noted that these comparable levels of B_1^+ inhomogeneity reduction without post-hoc correction were attained at the sacrifice of sub-cortical region contrast (Haast et al., 2021). As such, using the Maastricht sequence with SA2RAGE post-hoc B1+ inhomogeneity correction might be a better path for future research. Doing so would allow for accurate investigation of sub-cortical regions, such as the hippocampus, after an FTUS as several past epilepsy studies have indicated several sub-cortical regions undergo epilepsy-linked volume reductions and network changes in PWE (Alvim et al., 2016; Bernasconi et al., 2004; Bernhardt et al., 2010; He et al., 2020; Lee et al., 1998; Larivière et al., 2022).

Moreover, even when corrected for B_1^+ inhomogeneities, MRI T1w images have been shown to have reduced tissue contrast in low B_1^+ regions, predominantly the frontal and temporal lobes (Haast et al., 2021). This allows potential mismeasurements of cortical thickness as B_1^+ inhomogeneities have been shown to result in cortical thickness measurements being overestimated by approximately 70% around the frontal and temporal cortices (Haast et al., 2018; Haast et al., 2021). This could be a potential explanation for the lack of statistically significant cortical thickness changes observed in the FTUS patients of this study, especially considering past epilepsy research has indicated that the frontal and temporal cortices display significant epilepsy-linked cortical thickness and SCN changes (Bernasconi et al., 1999; Bernasconi et al., 2004; Bernhardt et al., 2010; Bernhardt et al., 2011; Galovic et al., 2019; Larivière et al., 2022; Lee et al., 1998; Ogren et al., 2018; van Diessen et al., 2013).

An additional potential issue within this study pertains to the visual quality assurance methods used. While researcher-driven visual quality assurance could theoretically be efficiently implemented to mitigate any MRI image artefacts

influencing the research data and outcomes, it poses certain flaws. Relying solely on such a method with a single researcher lacking MRI image processing experience can risk observer error and bias. Future research using the anat_preproc processing pipeline would benefit from visual quality assurance being conducted by multiple researchers, with an emphasis on those with experience in epilepsy.

4.3.4. Heterogeneity of Epilepsy and Associated Challenges

As stated earlier, epilepsy is an incredibly heterogeneous neurological disorder that can manifest in a multitude of different ways, with each manifestation being accompanied by varying structural changes that reflect the underlying neural network changes (Bartolomei et al., 2017; Fisher et al., 2017; Lehnertz et al., 2023; Sinha et al., 2022; Spencer, 2002; Van Diessen et al., 2013). Consequently, in a study focused on FTUS patients, there is a notable risk of the participants with epilepsy, both confirmed and potentially confirmed in the future, possessing different forms of epilepsy and thus displaying a multitude of epilepsy-type dependent structural changes (Bernhardt et al., 2011; Drenthen et al., 2018; Larivière et al., 2022; van Diessen et al., 2013). These variations in structural changes can conceal each other as the structural changes present in one FTUS participant with a specific epilepsy-type may be concealed by the absence of such changes in other FTUS subjects with different forms of epilepsy that lack such changes (Bartolomei et al., 2017; Fisher et al., 2017; Lehnertz et al., 2023; Sinha et al., 2022; Spencer, 2002; Van Diessen et al., 2013).

Several issues in this study contributed to the possibility of these structural changes being undetected, one of which was the utilisation of density-based thresholding instead of weight-based thresholding. Density-based thresholding was used to prevent over-filtering of low-connectivity matrices; however, by doing so, there is a risk of more evident changes in connectivity, such as one subject group having more connectivities than the other, being overlooked (Fornito et al., 2016).

Additionally, this study utilised group-based covariance analysis instead of an individual-based analysis, further underscoring the possibility of overlooking structural changes during data analysis. The heterogeneity of epilepsy-type-dependent structural changes can mask one another, as changes occurring in one epilepsy-type may be absent in another, compensating for each other in group-level analyses (Bartolomei et al., 2017; Fisher et al., 2017; Lehnertz et al., 2023; Sinha et al., 2022; Spencer, 2002; Van Diessen

et al., 2013). Consequently, when conducting a group-level analysis, there is a notable risk of epilepsy-type-specific changes being overlooked. This risk could be circumnavigated by conducting individual-based morphometric similarity analysis (King & Wood, 2020; Li et al., 2017; Seidlitz et al., 2018). Morphometric similarity analysis is a form of graph theory that, like structural covariance analysis, utilises morphometric features to reconstruct and quantify brain networks (King & Wood, 2020; Li et al., 2017; Seidlitz et al., 2018). However, unlike structural covariance analysis, morphometric similarity brain networks are generated using morphometric similarity mapping, in which inter-regional correlation matrices are generated using either five or ten micro-structural and macro-structural features measured via MRI scans (King & Wood, 2020; Li et al., 2017; Seidlitz et al., 2018; Zhang et al., 2021). These morphometric similarity correlation matrices can then be thresholded, binarised and used to calculate the nodal and global measures of the morphometric similarity network (King & Wood, 2020; Li et al., 2017; Seidlitz et al., 2018; Zhang et al., 2021).

The morphometric similarity analysis method allows for both individual-based analysis, by using solely the morphometric measures of a single individual, and group-based analysis, by using the average measures of each morphometric measure per group (King & Wood, 2020; Li et al., 2017; Seidlitz et al., 2018; Zhang et al., 2021). This flexibility in analysis levels would allow FTUS research to be utilised on two fronts. Individual-based analysis can be used to identify epilepsy-type specific structural changes better and make the results of future studies more applicable for epilepsy diagnosis. Meanwhile, group-based morphometric similarity analysis could ensure that whatever observed changes are not limited to the individual FTUS participants and allow for the development of a broader understanding of the general pathology of epilepsy after an FTUS. Future FTUS research would benefit from utilising morphometric similarity analysis over structural covariance analysis.

4.3.5. Non-parametric Permutation Test Null Distribution Issues

In addition to the issues linked to the graph theory analysis level and method, this study has an additional issue regarding the statistical analysis method. This is because while the intergroup randomisation utilised for the 1000-parametric permutation test preserves the impact of regional proximity on brain region structural covariances; it does not ensure consistent network degree distributions between each randomisation (Fornito et al., 2016; Rubinov & Sporns, 2010).

Degree distribution is a fundamental topological feature of networks in graph theory, akin to the number of edges and nodes, that represents the spread of nodal degrees within a network and is considered an indicator of network development and resilience (Bethlehem et al., 2017; Fornito et al., 2016; Rubinov & Sporns, 2010; Wang et al., 2021). Past research has shown that in humans, and several other biological networks, degree distribution typically presents in a scale-free network configuration (Fornito et al., 2016; Milo et al., 2002; Rubinov & Sporns, 2010). In such configurations, the array of degree distribution follows a power law in which the majority of nodes have low degrees, possessing few connections, while a minority of nodes are degree hubs, possessing high degrees and high amounts of connections (Fornito et al., 2016; Milo et al., 2002; Rubinov & Sporns, 2010). As nodal degrees are the measure of edges connected to a node, indicating the importance and connectivity of a node within the network, degree distribution changes can influence several nodal and global measures both directly and indirectly (Fornito et al., 2016; Milo et al., 2002; Rubinov & Sporns, 2010). Thus, there is a risk that during the randomisation process for permutation tests, the observed differences in nodal and global measures are due to the intergroup randomisations producing new data sets with degree distributions different from the original data sets and the expected scale-free network configuration, resulting in type I errors (Fornito et al., 2016; Milo et al., 2002; Rubinov & Sporns, 2010).

Using the randomisation method of Milo et al. (2002), degree distribution can be controlled during non-parametric permutation tests by randomly shuffling pairs of edges in the correlation matrices instead of randomly re-assigning participants' raw data prior to correlation matrix generation (Artzy-Randrup et al., 2004; Fornito et al., 2016; Milo et al., 2002). This randomisation process ensures no degree distribution changes as the edges are shuffled rather than re-calculated (Artzy-Randrup et al., 2004; Fornito et al., 2016; Milo et al., 2002). However, as stated in Artzy-Randrup et al. (2004), this method preserves degree distribution by ensuring that the edges of the randomised correlation matrices are entirely independent of the spatial distance between nodes, running contrary to the current scientific consensus that the structural covariance of brain regions positively correlate with spatial proximity (Alexander-Bloch et al., 2013; Fornito et al., 2016; Phipson & Smyth, 2010).

Currently, there is no definitive randomisation method for non-parametric permutation tests that controls degree distribution and accounts for the impact of spatial proximity on structural covariance (Artzy-Randrup et al., 2004). Future research on the structural

covariance of FTUS patients could benefit from utilising both the spatial proximity-preserving permutation tests, randomising subject groups, and the degree distribution-preserving permutation test to identify changes that persist in both such tests.

4.4. Conclusion

The results of this study provide evidence that there are no statistically significant differences in cortical thickness in individuals who have experienced an FTUS, even in cases later diagnosed with epilepsy. This implies that the observed patterns of cortical thickening and thinning in PWE are not a causal factor for their experienced seizures, supporting the notion of epilepsy as a progressive condition. However, due to this study's small sample size, this cannot be stated definitively, and future research with larger samples is needed. Despite this, the data did indicate that FTUS patients later diagnosed with epilepsy do experience sex-dependent changes in their brain networks. While these brain network changes are not consistent with any pattern of network changes seen in past epilepsy research, their presence as early as the FTUS in PWE supports the Bernasconi et al. (2004) theory that the observed patterns of cortical thinning are a product of network connectivity changes occurring as a result of epilepsy.

References

Abbasi, B., & Goldenholz, D. M. (2019). Machine learning applications in epilepsy. Epilepsia, 60(10), 2037–2047. https://doi.org/10.1111/epi.16333

Abdennadher, M., Saxena, A., & Pavlova, M. K. (2021). Evaluation and Management of First-Time Seizure in Adults. Seminars in Neurology, 41(05), 477–482. https://doi.org/10.1055/s-0041-1735143

Adamczyk, B., Węgrzyn, K., Wilczyński, T., Maciarz, J., Morawiec, N., & Adamczyk-Sowa, M. (2021). The Most Common Lesions Detected by Neuroimaging as Causes of Epilepsy. Medicina, 57(3), 294. https://doi.org/10.3390/medicina57030294

Ahmed, R., Rubinger, L., Go, C., Drake, J. M., Rutka, J. T., Carter Snead, O., & Widjaja, E. (2018). Utility of additional dedicated high-resolution 3T MRI in children with medically refractory focal epilepsy. Epilepsy Research, 143, 113–119. https://doi.org/10.1016/j.eplepsyres.2018.01.002

Alexander-Bloch, A., Giedd, J. N., & Bullmore, E. (2013). Imaging structural co-variance between human brain regions. Nature Reviews Neuroscience, 14(5), 322–336. https://doi.org/10.1038/nrn3465

Alvim, M. K. M., Coan, A. C., Campos, B. M., Yasuda, C. L., Oliveira, M. C., Morita, M. E., & Cendes, F. (2016). Progression of gray matter atrophy in seizure-free patients with temporal lobe epilepsy. Epilepsia, 57(4), 621–629. https://doi.org/10.1111/epi.13334

Amin, U., & Benbadis, S. R. (2019). The Role of EEG in the Erroneous Diagnosis of Epilepsy. Journal of Clinical Neurophysiology, 36(4), 294–297. https://doi.org/10.1097/WNP.0000000000000572

Arora, S., & Majumdar, A. (2022). Machine learning and soft computing applications in textile and clothing supply chain: Bibliometric and network analyses to delineate future research agenda. Expert Systems with Applications, 200, 117000. https://doi.org/10.1016/j.eswa.2022.117000

Artzy-Randrup, Y., Fleishman, S. J., Ben-Tal, N., & Stone, L. (2004). Comment on 'Network Motifs: Simple Building Blocks of Complex Networks' and 'Superfamilies of Evolved and Designed Networks'. Science, 305(5687), 1107–1107. https://doi.org/10.1126/science.1099334

Asadi-Pooya, A. A., Zeraatpisheh, Z., Barzegar, Z., Jafari, A., Hashemi, E., Sadeghi, A., Setayesh, A. S., Tahmasbi, Z., & Zahadatpour, Z. (2022). Driving restrictions in patients with seizures; a review of the regulations from the English-speaking nations. Epilepsy & Behavior, 135, 108888. https://doi.org/10.1016/j.yebeh.2022.108888

Ashburner, J., & Friston, K. J. (2000). Voxel-Based Morphometry—The Methods. NeuroImage, 11(6), 805–821. https://doi.org/10.1006/nimg.2000.0582

Baldin, E., Hauser, W. A., Buchhalter, J. R., Hesdorffer, D. C., & Ottman, R. (2014). Yield of epileptiform electroencephalogram abnormalities in incident unprovoked seizures: A population-based study. Epilepsia, 55(9), 1389–1398. https://doi.org/10.1111/epi.12720

Banerjee, J., Chandra, S., Kurwale, N., & Tripathi, M. (2014). Epileptogenic networks and drug-resistant epilepsy: Present and future perspectives of epilepsy research-Utility for the epileptologist and the epilepsy surgeon. Annals of Indian Academy of Neurology, 17(5), 134. https://doi.org/10.4103/0972-2327.128688

Barisano, G., Sepehrband, F., Ma, S., Jann, K., Cabeen, R., Wang, D. J., Toga, A. W., & Law, M. (2019). Clinical 7 T MRI: Are we there yet? A review about magnetic resonance imaging at ultra-high field. The British Journal of Radiology, 92(1094), 20180492. https://doi.org/10.1259/bjr.20180492

Bartolomei, F., Lagarde, S., Wendling, F., McGonigal, A., Jirsa, V., Guye, M., & Bénar, C. (2017). Defining epileptogenic networks: Contribution of SEEG and signal analysis. Epilepsia, 58(7), 1131–1147. https://doi.org/10.1111/epi.13791

Bassett, D. S., & Sporns, O. (2017). Network neuroscience. Nature Neuroscience, 20(3), 353–364. https://doi.org/10.1038/nn.4502

Beghi, E. (2020). The Epidemiology of Epilepsy. Neuroepidemiology, 54(2), 185–191. https://doi.org/10.1159/000503831

Behr, C., Goltzene, M. A., Kosmalski, G., Hirsch, E., & Ryvlin, P. (2016). Epidemiology of epilepsy. Revue Neurologique, 172(1), 27–36. https://doi.org/10.1016/j.neurol.2015.11.003

Ben-Ari, Y., & Dudek, F. E. (2010). Primary and Secondary Mechanisms of Epileptogenesis in the Temporal Lobe: There is a before and an After. Epilepsy Currents, 10(5), 118–125. https://doi.org/10.1111/j.1535-7511.2010.01376.x

Benbadis, S. R. (2007). Errors in EEGs and the misdiagnosis of epilepsy: Importance, causes, consequences, and proposed remedies. Epilepsy & Behavior, 11(3), 257–262. https://doi.org/10.1016/j.yebeh.2007.05.013

Benbadis, S. R., & Tatum, W. O. (2003). Overintepretation of EEGs and Misdiagnosis of Epilepsy: Journal of Clinical Neurophysiology, 20(1), 42–44. https://doi.org/10.1097/00004691-200302000-00005

Benjamini, Y., & Hochberg, Y. (1995). Controlling the False Discovery Rate: A Practical and Powerful Approach to Multiple Testing. Journal of the Royal Statistical Society. Series B (Methodological), 57(1), 289–300. JSTOR.

Berg, A. T. (2008). Risk of recurrence after a first unprovoked seizure. Epilepsia, 49(s1), 13–18. https://doi.org/10.1111/j.1528-1167.2008.01444.x

Berger, A. (2002). How does it work?: Magnetic resonance imaging. BMJ, 324(7328), 35–35. https://doi.org/10.1136/bmj.324.7328.35

Bernasconi, A., Cendes, F., Theodore, W. H., Gill, R. S., Koepp, M. J., Hogan, R. E., Jackson, G. D., Federico, P., Labate, A., Vaudano, A. E., Blümcke, I., Ryvlin, P., & Bernasconi, N. (2019). Recommendations for the use of structural magnetic resonance imaging in the care of patients with epilepsy: A consensus report from the International League Against Epilepsy Neuroimaging Task Force. Epilepsia, 60(6), 1054–1068. https://doi.org/10.1111/epi.15612

Bernasconi, N., Bernasconi, A., Andermann, F., Dubeau, F., Feindel, W., & Reutens, D. C. (1999). Entorhinal cortex in temporal lobe epilepsy: A quantitative MRI study. Neurology, 52(9), 1870–1870. https://doi.org/10.1212/WNL.52.9.1870

Bernasconi, N., Duchesne, S., Janke, A., Lerch, J., Collins, D. L., & Bernasconi, A. (2004). Whole-brain voxel-based statistical analysis of gray matter and white matter in temporal lobe epilepsy. NeuroImage, 23(2), 717–723. https://doi.org/10.1016/j.neuroimage.2004.06.015

Bernhardt, B. C., Bernasconi, N., Concha, L., & Bernasconi, A. (2010). Cortical thickness analysis in temporal lobe epilepsy: Reproducibility and relation to outcome. Neurology, 74(22), 1776–1784. https://doi.org/10.1212/WNL.0b013e3181e0f80a

Bernhardt, B. C., Chen, Z., He, Y., Evans, A. C., & Bernasconi, N. (2011). Graph-Theoretical Analysis Reveals Disrupted Small-World Organization of Cortical Thickness Correlation Networks in Temporal Lobe Epilepsy. Cerebral Cortex, 21(9), 2147–2157. https://doi.org/10.1093/cercor/bhq291

Bernhardt, B. C., Hong, S., Bernasconi, A., & Bernasconi, N. (2013). Imaging structural and functional brain networks in temporal lobe epilepsy. Frontiers in Human Neuroscience, 7. https://doi.org/10.3389/fnhum.2013.00624

Bernhardt, B. C., Rozen, D. A., Worsley, K. J., Evans, A. C., Bernasconi, N., & Bernasconi, A. (2009). Thalamo–cortical network pathology in idiopathic generalized epilepsy: Insights from MRI-based morphometric correlation analysis. NeuroImage, 46(2), 373–381. https://doi.org/10.1016/j.neuroimage.2009.01.055

Bethlehem, R. A. I., Romero-Garcia, R., Mak, E., Bullmore, E. T., & Baron-Cohen, S. (2017). Structural Covariance Networks in Children with Autism or ADHD. Cerebral Cortex, 27(8), 4267–4276. https://doi.org/10.1093/cercor/bhx135

Bhattacharya, S., Sinha, S., Dey, P., Saha, A., Chowdhury, C., & Roy, S. (2023). Online social-network sensing models. In Computational Intelligence Applications for Text and Sentiment Data Analysis (pp. 113–140). Elsevier. https://doi.org/10.1016/B978-0-32-390535-0.00010-0

Bonilha, L., Rorden, C., Halford, J. J., Eckert, M., Appenzeller, S., Cendes, F., & Li, L. M. (2006). Asymmetrical extra-hippocampal grey matter loss related to hippocampal atrophy in patients with medial temporal lobe epilepsy. Journal of Neurology, Neurosurgery & Psychiatry, 78(3), 286–294. https://doi.org/10.1136/jnnp.2006.103994

Britton, J. W., Frey, L. C., Hopp, J. L., Korb, P., Koubeissi, M. Z., Lievens, W. E., Pestana-Knight, E. M., & St. Louis, E. K. (2016). Electroencephalography (EEG): An Introductory Text and Atlas of Normal and Abnormal Findings in Adults, Children, and Infants (E. K. St. Louis & L. C. Frey, Eds.). American Epilepsy Society. http://www.ncbi.nlm.nih.gov/books/NBK390354/

Bullmore, E., & Sporns, O. (2009). Complex brain networks: Graph theoretical analysis of structural and functional systems. Nature Reviews Neuroscience, 10(3), 186–198. https://doi.org/10.1038/nrn2575

Carmon, J., Heege, J., Necus, J. H., Owen, T. W., Pipa, G., Kaiser, M., Taylor, P. N., & Wang, Y. (2020). Reliability and comparability of human brain structural covariance networks. NeuroImage, 220, 117104. https://doi.org/10.1016/j.neuroimage.2020.117104

Choi, U.-S., Kawaguchi, H., Matsuoka, Y., Kober, T., & Kida, I. (2018). Brain tissue segmentation based on MP2RAGE multi-contrast images in 7 T MRI. https://doi.org/10.1101/455576

Coan, A. C., Appenzeller, S., Bonilha, L., Li, L. M., & Cendes, F. (2009). Seizure frequency and lateralization affect progression of atrophy in temporal lobe epilepsy. Neurology, 73(11), 834–842. https://doi.org/10.1212/WNL.0b013e3181b783dd

Coan, A. C., Campos, B. M., Yasuda, C. L., Kubota, B. Y., Bergo, F. Pg., Guerreiro, C. Am., & Cendes, F. (2014). Frequent Seizures Are Associated with a Network of Gray Matter Atrophy in Temporal Lobe Epilepsy with or without Hippocampal Sclerosis. PLoS ONE, 9(1), e85843. https://doi.org/10.1371/journal.pone.0085843

Collins, C. M., Li, S., & Smith, M. B. (1998). SAR and B 1 field distributions in a heterogeneous human head model within a birdcage coil. Magnetic Resonance in Medicine, 40(6), 847–856. https://doi.org/10.1002/mrm.1910400610

Collins, D. L., Neelin, P., Peters, T. M., & Evans, A. C. (1994). Automatic 3D Intersubject Registration of MR Volumetric Data in Standardized Talairach Space: Journal of Computer Assisted Tomography, 18(2), 192–205. https://doi.org/10.1097/00004728-199403000-00005

Connectivity Matrices and Brain Graphs. (2016). In Fundamentals of Brain Network Analysis (pp. 89–113). Elsevier. https://doi.org/10.1016/B978-0-12-407908-3.00003-0

Cox, R. W. (1996). AFNI: Software for Analysis and Visualization of Functional Magnetic Resonance Neuroimages. Computers and Biomedical Research, 29(3), 162–173. https://doi.org/10.1006/cbmr.1996.0014

Dale, A. M., Fischl, B., & Sereno, M. I. (1999). Cortical Surface-Based Analysis. NeuroImage, 9(2), 179–194. https://doi.org/10.1006/nimg.1998.0395

Desikan, R. S., & Barkovich, A. J. (2016). Malformations of cortical development. Annals of Neurology, 80(6), 797–810. https://doi.org/10.1002/ana.24793

Desikan, R. S., Ségonne, F., Fischl, B., Quinn, B. T., Dickerson, B. C., Blacker, D., Buckner, R. L., Dale, A. M., Maguire, R. P., Hyman, B. T., Albert, M. S., & Killiany, R. J. (2006). An automated labeling system for subdividing the human cerebral cortex on MRI scans into gyral based regions of interest. NeuroImage, 31(3), 968–980. https://doi.org/10.1016/j.neuroimage.2006.01.021

Dickey, A. S., Krafty, R. T., & Pedersen, N. P. (2022). Empowering Research on Epilepsy Surgery Outcomes. https://doi.org/10.1101/2022.05.11.22274965

Dickie, E. W., Anticevic, A., Smith, D. E., Coalson, T. S., Manogaran, M., Calarco, N., Viviano, J. D., Glasser, M. F., Van Essen, D. C., & Voineskos, A. N. (2019). Ciftify: A framework for surface-based analysis of legacy MR acquisitions. NeuroImage, 197, 818–826. https://doi.org/10.1016/j.neuroimage.2019.04.078

Dreifuss, F., Martinez-Lage, M., & Johns, R. (1985). Proposal for Classification of Epilepsies and Epileptic Syndromes. Epilepsia, 26(3), 268–278. https://doi.org/10.1111/j.1528-1157.1985.tb05417.x

Drenthen, G. S., Backes, W. H., Rouhl, R. P. W., Vlooswijk, M. C. G., Majoie, M. H. J. M., Hofman, P. A. M., Aldenkamp, A. P., & Jansen, J. F. A. (2018). Structural covariance networks relate to the severity of epilepsy with focal-onset seizures. NeuroImage: Clinical, 20, 861–867. https://doi.org/10.1016/j.nicl.2018.09.023

Duan, D., & Wen, D. (2023). MRI-based structural covariance network in early human brain development. Frontiers in Neuroscience, 17, 1302069. https://doi.org/10.3389/fnins.2023.1302069

Egesa, I. J., Newton, C. R. J. C., & Kariuki, S. M. (2022). Evaluation of the International League Against Epilepsy 1981, 1989, and 2017 classifications of seizure semiology and etiology in a population-based cohort of children and adults with epilepsy. Epilepsia Open, 7(1), 98–109. https://doi.org/10.1002/epi4.12562

Eggenschwiler, F., Kober, T., Magill, A. W., Gruetter, R., & Marques, J. P. (2012). SA2RAGE: A new sequence for fast B 1 + -mapping. Magnetic Resonance in Medicine, 67(6), 1609–1619. https://doi.org/10.1002/mrm.23145

Eickhoff, S. B., Yeo, B. T. T., & Genon, S. (2018). Imaging-based parcellations of the human brain. Nature Reviews Neuroscience, 19(11), 672–686. https://doi.org/10.1038/s41583-018-0071-7

Emerton, B. C., Jerram, M., Deckersbach, T., Dougherty, D. D., Fulwiler, C., & Gansler, D. A. (2009). A Comparison of Voxel-Based Morphometry and Volumetry Methods in the Context of the Neural Basis of Aggression. Brain Imaging and Behavior, 3(4), 332–341. https://doi.org/10.1007/s11682-009-9075-2

Engel, J., Jr., Thompson, P. M., Stern, J. M., Staba, R. J., Bragin, A., & Mody, I. (2013). Connectomics and epilepsy: Current Opinion in Neurology, 26(2), 186–194. https://doi.org/10.1097/WCO.0b013e32835ee5b8

Esteban, O., Markiewicz, C. J., Blair, R. W., Moodie, C. A., Isik, A. I., Erramuzpe, A., Kent, J. D., Goncalves, M., DuPre, E., Snyder, M., Oya, H., Ghosh, S. S., Wright, J., Durnez, J., Poldrack, R. A., & Gorgolewski, K. J. (2019). fMRIPrep: A robust

preprocessing pipeline for functional MRI. Nature Methods, 16(1), 111–116. https://doi.org/10.1038/s41592-018-0235-4

Fattorusso, A., Matricardi, S., Mencaroni, E., Dell'Isola, G. B., Di Cara, G., Striano, P., & Verrotti, A. (2021). The Pharmacoresistant Epilepsy: An Overview on Existant and New Emerging Therapies. Frontiers in Neurology, 12, 674483. https://doi.org/10.3389/fneur.2021.674483

Fiest, K. M., Sauro, K. M., Wiebe, S., Patten, S. B., Kwon, C.-S., Dykeman, J., Pringsheim, T., Lorenzetti, D. L., & Jetté, N. (2017). Prevalence and incidence of epilepsy: A systematic review and meta-analysis of international studies. Neurology, 88(3), 296–303. https://doi.org/10.1212/WNL.0000000000003509

Fischl, B. (2004). Automatically Parcellating the Human Cerebral Cortex. Cerebral Cortex, 14(1), 11–22. https://doi.org/10.1093/cercor/bhg087

Fischl, B. (2012). FreeSurfer. NeuroImage, 62(2), 774–781. https://doi.org/10.1016/j.neuroimage.2012.01.021

Fischl, B., & Dale, A. M. (2000). Measuring the thickness of the human cerebral cortex from magnetic resonance images. Proceedings of the National Academy of Sciences, 97(20), 11050–11055. https://doi.org/10.1073/pnas.200033797

Fisher, R. S., Acevedo, C., Arzimanoglou, A., Bogacz, A., Cross, J. H., Elger, C. E., Engel, J., Forsgren, L., French, J. A., Glynn, M., Hesdorffer, D. C., Lee, B. I., Mathern, G. W., Moshé, S. L., Perucca, E., Scheffer, I. E., Tomson, T., Watanabe, M., & Wiebe, S. (2014). ILAE Official Report: A practical clinical definition of epilepsy. Epilepsia, 55(4), 475–482. https://doi.org/10.1111/epi.12550

Fisher, R. S., Boas, W. V. E., Blume, W., Elger, C., Genton, P., Lee, P., & Engel, J. (2005). Epileptic Seizures and Epilepsy: Definitions Proposed by the International League Against Epilepsy (ILAE) and the International Bureau for Epilepsy (IBE). Epilepsia, 46(4), 470–472. https://doi.org/10.1111/j.0013-9580.2005.66104.x

Fisher, R. S., Cross, J. H., D'Souza, C., French, J. A., Haut, S. R., Higurashi, N., Hirsch, E., Jansen, F. E., Lagae, L., Moshé, S. L., Peltola, J., Roulet Perez, E., Scheffer, I. E., Schulze-Bonhage, A., Somerville, E., Sperling, M., Yacubian, E. M., & Zuberi, S. M. (2017). Instruction manual for the ILAE 2017 operational classification of seizure types. Epilepsia, 58(4), 531–542. https://doi.org/10.1111/epi.13671

Fornito, A., Zalesky, A., & Bullmore, E. T. (Eds.). (2016). Connectivity Matrices and Brain Graphs. In Fundamentals of Brain Network Analysis (pp. 89–113). Elsevier. https://doi.org/10.1016/B978-0-12-407908-3.00003-0

Foster, E., Carney, P., Liew, D., Ademi, Z., O'Brien, T., & Kwan, P. (2019). First seizure presentations in adults: Beyond assessment and treatment. Journal of Neurology, Neurosurgery & Psychiatry, 90(9), 1039–1045. https://doi.org/10.1136/jnnp-2018-320215

Fürtjes, A. E., Cole, J. H., Couvy-Duchesne, B., & Ritchie, S. J. (2023). A quantified comparison of cortical atlases on the basis of trait morphometricity. Cortex, 158, 110–126. https://doi.org/10.1016/j.cortex.2022.11.001

Galizia, E. C., & Faulkner, H. J. (2018). Seizures and epilepsy in the acute medical setting: Presentation and management. Clinical Medicine (London, England), 18(5), 409–413. https://doi.org/10.7861/clinmedicine.18-5-409

Galovic, M., Van Dooren, V. Q. H., Postma, T. S., Vos, S. B., Caciagli, L., Borzì, G., Cueva Rosillo, J., Vuong, K. A., De Tisi, J., Nachev, P., Duncan, J. S., & Koepp, M. J. (2019). Progressive Cortical Thinning in Patients With Focal Epilepsy. JAMA Neurology, 76(10), 1230. https://doi.org/10.1001/jamaneurol.2019.1708

Glasser, M. F., Coalson, T. S., Robinson, E. C., Hacker, C. D., Harwell, J., Yacoub, E., Ugurbil, K., Andersson, J., Beckmann, C. F., Jenkinson, M., Smith, S. M., & Van Essen, D. C. (2016). A multi-modal parcellation of human cerebral cortex. Nature, 536(7615), 171–178. https://doi.org/10.1038/nature18933

Glasser, M. F., Sotiropoulos, S. N., Wilson, J. A., Coalson, T. S., Fischl, B., Andersson, J. L., Xu, J., Jbabdi, S., Webster, M., Polimeni, J. R., Van Essen, D. C., & Jenkinson, M. (2013). The minimal preprocessing pipelines for the Human Connectome Project. NeuroImage, 80, 105–124. https://doi.org/10.1016/j.neuroimage.2013.04.127

Gruber, B., Froeling, M., Leiner, T., & Klomp, D. W. J. (2018). RF coils: A practical guide for nonphysicists. Journal of Magnetic Resonance Imaging, 48(3), 590–604. https://doi.org/10.1002/jmri.26187

Guery, D., & Rheims, S. (2021). Clinical Management of Drug Resistant Epilepsy: A Review on Current Strategies. Neuropsychiatric Disease and Treatment, Volume 17, 2229–2242. https://doi.org/10.2147/NDT.S256699

Gugger, J. J., Walter, A. E., Diaz-Arrastia, R., Huang, J., Jack, C. R., Reid, R., Kucharska-Newton, A. M., Gottesman, R. F., Schneider, A. L. C., & Johnson, E. L. (2024). Association between structural brain MRI abnormalities and epilepsy in older adults. Annals of Clinical and Translational Neurology, 11(2), 342–354. https://doi.org/10.1002/acn3.51955

Haast, R. A. M., Ivanov, D., & Uludağ, K. (2018). The impact of correction on MP2RAGE cortical T 1 and apparent cortical thickness at 7 T. Human Brain Mapping, 39(6), 2412–2425. https://doi.org/10.1002/hbm.24011

Haast, R. A. M., Lau, J. C., Ivanov, D., Menon, R. S., Uludağ, K., & Khan, A. R. (2021). Effects of MP2RAGE B1+ sensitivity on inter-site T1 reproducibility and hippocampal morphometry at 7T. NeuroImage, 224, 117373. https://doi.org/10.1016/j.neuroimage.2020.117373

Hauser, W. A., Rich, S. S., Lee, J. R.-J., Annegers, J. F., & Anderson, V. E. (1998). Risk of Recurrent Seizures after Two Unprovoked Seizures. New England Journal of Medicine, 338(7), 429–434. https://doi.org/10.1056/NEJM199802123380704

He, X., Chaitanya, G., Asma, B., Caciagli, L., Bassett, D. S., Tracy, J. I., & Sperling, M. R. (2020). Disrupted basal ganglia–thalamocortical loops in focal to bilateral tonic-clonic seizures. Brain, 143(1), 175–190. https://doi.org/10.1093/brain/awz361

He, Y., Chen, Z., & Evans, A. (2008). Structural Insights into Aberrant Topological Patterns of Large-Scale Cortical Networks in Alzheimer's Disease. The Journal of Neuroscience, 28(18), 4756–4766. https://doi.org/10.1523/JNEUROSCI.0141-08.2008

Hirsch, E., French, J., Scheffer, I. E., Bogacz, A., Alsaadi, T., Sperling, M. R., Abdulla, F., Zuberi, S. M., Trinka, E., Specchio, N., Somerville, E., Samia, P., Riney, K., Nabbout, R., Jain, S., Wilmshurst, J. M., Auvin, S., Wiebe, S., Perucca, E., … Wirrell, E. C. (2022). ILAE definition of the Idiopathic Generalized Epilepsy Syndromes: Position statement by the ILAE Task Force on Nosology and Definitions. Epilepsia, 63(6), 1475–1499. https://doi.org/10.1111/epi.17236

Hoopes, A., Mora, J. S., Dalca, A. V., Fischl, B., & Hoffmann, M. (2022). SynthStrip: Skull-stripping for any brain image. NeuroImage, 260, 119474. https://doi.org/10.1016/j.neuroimage.2022.119474

Hutton, C., De Vita, E., Ashburner, J., Deichmann, R., & Turner, R. (2008). Voxel-based cortical thickness measurements in MRI. NeuroImage, 40(4), 1701–1710. https://doi.org/10.1016/j.neuroimage.2008.01.027

Hutton, C., Draganski, B., Ashburner, J., & Weiskopf, N. (2009). A comparison between voxel-based cortical thickness and voxel-based morphometry in normal aging. NeuroImage, 48(2), 371–380. https://doi.org/10.1016/j.neuroimage.2009.06.043

Isaacs, B. R., Mulder, M. J., Groot, J. M., Van Berendonk, N., Lute, N., Bazin, P.-L., Forstmann, B. U., & Alkemade, A. (2020). 3 versus 7 Tesla magnetic resonance imaging for parcellations of subcortical brain structures in clinical settings. PLOS ONE, 15(11), e0236208. https://doi.org/10.1371/journal.pone.0236208

Jacoby, A., Gamble, C., Doughty, J., Marson, A., & Chadwick, D. (2007). Quality of life outcomes of immediate or delayed treatment of early epilepsy and single seizures. Neurology, 68(15), 1188–1196. https://doi.org/10.1212/01.wnl.0000259411.78423.50

Jber, M., Habibabadi, J. M., Sharifpour, R., Marzbani, H., Hassanpour, M., Seyfi, M., Mobarakeh, N. M., Keihani, A., Hashemi-Fesharaki, S. S., Ay, M., & Nazem-Zadeh, M.-R. (2021). Temporal and extratemporal atrophic manifestation of temporal lobe epilepsy using voxel-based morphometry and corticometry: Clinical application in lateralization of epileptogenic zone. Neurological Sciences, 42(8), 3305–3325. https://doi.org/10.1007/s10072-020-05003-2

Karamat, M. I., Darvish-Molla, S., & Santos-Diaz, A. (2016). Opportunities and Challenges of 7 Tesla Magnetic Resonance Imaging: A Review. Critical Reviews in Biomedical Engineering, 44(1–02), 73–89. https://doi.org/10.1615/CritRevBiomedEng.2016016365

Kashyap, S. (2021). srikash/3dMPRAGEise: Ondu (1.0) [Computer software]. [object Object]. https://doi.org/10.5281/ZENODO.4626825

Kawahara, D., & Nagata, Y. (2021). T1-weighted and T2-weighted MRI image synthesis with convolutional generative adversarial networks. Reports of Practical Oncology and Radiotherapy, 26(1), 35–42. https://doi.org/10.5603/RPOR.a2021.0005

Kemmotsu, N., Girard, H. M., Bernhardt, B. C., Bonilha, L., Lin, J. J., Tecoma, E. S., Iragui, V. J., Hagler, D. J., Halgren, E., & McDonald, C. R. (2011). MRI analysis in temporal lobe epilepsy: Cortical thinning and white matter disruptions are related to side of seizure onset. Epilepsia, 52(12), 2257–2266. https://doi.org/10.1111/j.1528-1167.2011.03278.x

Khan, A., & Haast, R. (2020). Gradcorrect [Computer software]. https://github.com/khanlab/gradcorrect

Kim, L. G., Johnson, T. L., Marson, A. G., & Chadwick, D. W. (2006). Prediction of risk of seizure recurrence after a single seizure and early epilepsy: Further results

from the MESS trial. *The Lancet Neurology*, 5(4), 317–322. https://doi.org/10.1016/S1474-4422(06)70383-0

King, D. J., & Wood, A. G. (2020). Clinically feasible brain morphometric similarity network construction approaches with restricted magnetic resonance imaging acquisitions. *Network Neuroscience*, 4(1), 274–291. https://doi.org/10.1162/netn_a_00123

Kobau, R., & DiIorio, C. (2003). Epilepsy self-management: A comparison of self-efficacy and outcome expectancy for medication adherence and lifestyle behaviors among people with epilepsy. *Epilepsy & Behavior*, 4(3), 217–225. https://doi.org/10.1016/S1525-5050(03)00057-X

Kong, X., Shi, Y., Yu, S., Liu, J., & Xia, F. (2019). Academic social networks: Modeling, analysis, mining and applications. *Journal of Network and Computer Applications*, 132, 86–103. https://doi.org/10.1016/j.jnca.2019.01.029

Kramer, M. A., & Cash, S. S. (2012). Epilepsy as a Disorder of Cortical Network Organization. *The Neuroscientist*, 18(4), 360–372. https://doi.org/10.1177/1073858411422754

Krumholz, A., Wiebe, S., Gronseth, G. S., Gloss, D. S., Sanchez, A. M., Kabir, A. A., Liferidge, A. T., Martello, J. P., Kanner, A. M., Shinnar, S., Hopp, J. L., & French, J. A. (2015). Evidence-based guideline: Management of an unprovoked first seizure in adults: Report of the Guideline Development Subcommittee of the American Academy of Neurology and the American Epilepsy Society. *Neurology*, 84(16), 1705–1713. https://doi.org/10.1212/WNL.0000000000001487

Kwan, P., & Brodie, M. J. (2006). Combination Therapy in Epilepsy: When and What to Use. *Drugs*, 66(14), 1817–1829. https://doi.org/10.2165/00003495-200666140-00004

Labate, A., Cerasa, A., Aguglia, U., Mumoli, L., Quattrone, A., & Gambardella, A. (2010). Voxel-based morphometry of sporadic epileptic patients with mesiotemporal sclerosis. *Epilepsia*, 51(4), 506–510. https://doi.org/10.1111/j.1528-1167.2009.02310.x

Larivière, S., Royer, J., Rodríguez-Cruces, R., Paquola, C., Caligiuri, M. E., Gambardella, A., Concha, L., Keller, S. S., Cendes, F., Yasuda, C. L., Bonilha, L., Gleichgerrcht, E., Focke, N. K., Domin, M., Von Podewills, F., Langner, S., Rummel, C., Wiest, R., Martin, P., … Bernhardt, B. C. (2022). Structural network alterations in focal and generalized epilepsy assessed in a worldwide ENIGMA

study follow axes of epilepsy risk gene expression. Nature Communications, 13(1), 4320. https://doi.org/10.1038/s41467-022-31730-5

Lee, J. W., Andermann, F., Dubeau, F., Bernasconi, A., MacDonald, D., Evans, A., & Reutens, D. C. (1998). Morphometric Analysis of the Temporal Lobe in Temporal Lobe Epilepsy. Epilepsia, 39(7), 727–736. https://doi.org/10.1111/j.1528-1157.1998.tb01158.x

Lehnertz, K., Bröhl, T., & Wrede, R. V. (2023). Epileptic-network-based prediction and control of seizures in humans. Neurobiology of Disease, 181, 106098. https://doi.org/10.1016/j.nbd.2023.106098

Li, W., Yang, C., Shi, F., Wu, S., Wang, Q., Nie, Y., & Zhang, X. (2017). Construction of Individual Morphological Brain Networks with Multiple Morphometric Features. Frontiers in Neuroanatomy, 11, 34. https://doi.org/10.3389/fnana.2017.00034

Liu, G., Slater, N., & Perkins, A. (2017). Epilepsy: Treatment Options. American Academy of Family Physicians, 96(2), 87–96.

Liu, Y., Li, Q., Yi, D., Duan, J., Zhang, Q., Huang, Y., He, H., Liao, Y., Song, Z., Deng, L., Wang, W., & Liu, D. (2023). Topological abnormality of structural covariance network in MRI-negative frontal lobe epilepsy. Frontiers in Neuroscience, 17, 1136110. https://doi.org/10.3389/fnins.2023.1136110

López-Rivera, J. A., Smuk, V., Leu, C., Nasr, G., Vegh, D., Stefanski, A., Pérez-Palma, E., Busch, R., Jehi, L., Najm, I., Blümcke, I., & Lal, D. (2022). Incidence and prevalence of major epilepsy-associated brain lesions. Epilepsy & Behavior Reports, 18, 100527. https://doi.org/10.1016/j.ebr.2022.100527

Marques, J. P., & Gruetter, R. (2013). New Developments and Applications of the MP2RAGE Sequence—Focusing the Contrast and High Spatial Resolution R1 Mapping. PLoS ONE, 8(7), e69294. https://doi.org/10.1371/journal.pone.0069294

Marques, J. P., Kober, T., Krueger, G., Van Der Zwaag, W., Van De Moortele, P.-F., & Gruetter, R. (2010). MP2RAGE, a self bias-field corrected sequence for improved segmentation and T1-mapping at high field. NeuroImage, 49(2), 1271–1281. https://doi.org/10.1016/j.neuroimage.2009.10.002

Marson, A., Jacoby, A., Johnson, A., Kim, L., Gamble, C., & Chadwick, D. (2005). Immediate versus deferred antiepileptic drug treatment for early epilepsy and

single seizures: A randomised controlled trial. The Lancet, 365(9476), 2007–2013. https://doi.org/10.1016/S0140-6736(05)66694-9

McRobbie, D. W., Moore, E. A., Graves, M. J., & Prince, M. R. (2017). MRI from Picture to Proton (3rd ed.). Cambridge University Press. https://doi.org/10.1017/9781107706958

Mesraoua, B., Abou-Khalil, B., Hosni Khodair, R., Melikyan, G., Al Hail, H., & Asadi-Pooya, A. A. (2021). Seizure clusters. Journal of Drug Assessment, 10(1), 86–90. https://doi.org/10.1080/21556660.2021.1962671

Mesraoua, B., Deleu, D., Hassan, A. H., Gayane, M., Lubna, A., Ali, M. A., Tomson, T., Khalil, B. A., Cross, J. H., & Asadi-Pooya, A. A. (2020). Dramatic outcomes in epilepsy: Depression, suicide, injuries, and mortality. Current Medical Research and Opinion, 36(9), 1473–1480. https://doi.org/10.1080/03007995.2020.1776234

Metere, R., Kober, T., Möller, H. E., & Schäfer, A. (2017). Simultaneous Quantitative MRI Mapping of T1, T2* and Magnetic Susceptibility with Multi-Echo MP2RAGE. PLOS ONE, 12(1), e0169265. https://doi.org/10.1371/journal.pone.0169265

Milo, R., Shen-Orr, S., Itzkovitz, S., Kashtan, N., Chklovskii, D., & Alon, U. (2002). Network Motifs: Simple Building Blocks of Complex Networks. Science, 298(5594), 824–827. https://doi.org/10.1126/science.298.5594.824

Mugler, J. P., & Brookeman, J. R. (1991). Rapid three-dimensional T1-weighted MR imaging with the MP-RAGE sequence. Journal of Magnetic Resonance Imaging, 1(5), 561–567. https://doi.org/10.1002/jmri.1880010509

Nashef, L., So, E. L., Ryvlin, P., & Tomson, T. (2012). Unifying the definitions of sudden unexpected death in epilepsy. Epilepsia, 53(2), 227–233. https://doi.org/10.1111/j.1528-1167.2011.03358.x

Neligan, A., Adan, G., Nevitt, S. J., Pullen, A., Sander, J. W., Bonnett, L., & Marson, A. G. (2023). Prognosis of adults and children following a first unprovoked seizure. Cochrane Database of Systematic Reviews, 2023(1). https://doi.org/10.1002/14651858.CD013847.pub2

Neligan, A., Bell, G. S., Johnson, A. L., Goodridge, D. M., Shorvon, S. D., & Sander, J. W. (2011). The long-term risk of premature mortality in people with epilepsy. Brain, 134(2), 388–395. https://doi.org/10.1093/brain/awq378

Ogren, J. A., Tripathi, R., Macey, P. M., Kumar, R., Stern, J. M., Eliashiv, D. S., Allen, L. A., Diehl, B., Engel, J., Rani, M. R. S., Lhatoo, S. D., & Harper, R. M. (2018).

Regional cortical thickness changes accompanying generalized tonic-clonic seizures. NeuroImage: Clinical, 20, 205–215. https://doi.org/10.1016/j.nicl.2018.07.015

Oliveira, Í. A. F., Roos, T., Dumoulin, S. O., Siero, J. C. W., & Van Der Zwaag, W. (2021). Can 7T MPRAGE match MP2RAGE for gray-white matter contrast? NeuroImage, 240, 118384. https://doi.org/10.1016/j.neuroimage.2021.118384

Ono, T., & Galanopoulou, A. S. (2012). Epilepsy and Epileptic Syndrome. In S. I. Ahmad (Ed.), Neurodegenerative Diseases (Vol. 724, pp. 99–113). Springer US. https://doi.org/10.1007/978-1-4614-0653-2_8

Panayiotopoulos, C. P. (2005). The Epilepsies: Seizures, Syndromes and Management. Bladon Medical Publishing. http://www.ncbi.nlm.nih.gov/books/NBK2606/

Pegg, E. J., Taylor, J. R., Keller, S. S., & Mohanraj, R. (2020). Interictal structural and functional connectivity in idiopathic generalized epilepsy: A systematic review of graph theoretical studies. Epilepsy & Behavior, 106, 107013. https://doi.org/10.1016/j.yebeh.2020.107013

Phal, P. M., Usmanov, A., Nesbit, G. M., Anderson, J. C., Spencer, D., Wang, P., Helwig, J. A., Roberts, C., & Hamilton, B. E. (2008). Qualitative Comparison of 3-T and 1.5-T MRI in the Evaluation of Epilepsy. American Journal of Roentgenology, 191(3), 890–895. https://doi.org/10.2214/AJR.07.3933

Phipson, B., & Smyth, G. K. (2010). Permutation P-values Should Never Be Zero: Calculating Exact P-values When Permutations Are Randomly Drawn. Statistical Applications in Genetics and Molecular Biology, 9(1). https://doi.org/10.2202/1544-6115.1585

Pitkänen, A., Lukasiuk, K., Dudek, F. E., & Staley, K. J. (2015). Epileptogenesis. Cold Spring Harbor Perspectives in Medicine, 5(10), a022822. https://doi.org/10.1101/cshperspect.a022822

Pittau, F., Grouiller, F., Spinelli, L., Seeck, M., Michel, C. M., & Vulliemoz, S. (2014). The Role of Functional Neuroimaging in Pre-Surgical Epilepsy Evaluation. Frontiers in Neurology, 5. https://doi.org/10.3389/fneur.2014.00031

Pohlmann-Eden, B., Beghi, E., Camfield, C., & Camfield, P. (2006). The first seizure and its management in adults and children. BMJ, 332(7537), 339–342. https://doi.org/10.1136/bmj.332.7537.339

Pohmann, R., Speck, O., & Scheffler, K. (2016). Signal-to-noise ratio and MR tissue parameters in human brain imaging at 3, 7, and 9.4 tesla using current receive coil

arrays. Magnetic Resonance in Medicine, 75(2), 801–809. https://doi.org/10.1002/mrm.25677

Ponnatapura, J., Vemanna, S., Ballal, S., & Singla, A. (2018). Utility of Magnetic Resonance Imaging Brain Epilepsy Protocol in New-Onset Seizures: How is it Different in Developing Countries? Journal of Clinical Imaging Science, 8, 43. https://doi.org/10.4103/jcis.JCIS_38_18

Redpath, T. W. (1998). Signal-to-noise ratio in MRI. The British Journal of Radiology, 71(847), 704–707. https://doi.org/10.1259/bjr.71.847.9771379

Riney, K., Bogacz, A., Somerville, E., Hirsch, E., Nabbout, R., Scheffer, I. E., Zuberi, S. M., Alsaadi, T., Jain, S., French, J., Specchio, N., Trinka, E., Wiebe, S., Auvin, S., Cabral-Lim, L., Naidoo, A., Perucca, E., Moshé, S. L., Wirrell, E. C., & Tinuper, P. (2022). International League Against Epilepsy classification and definition of epilepsy syndromes with onset at a variable age: Position statement by the ILAE Task Force on Nosology and Definitions. Epilepsia, 63(6), 1443–1474. https://doi.org/10.1111/epi.17240

Rizvi, S., Ladino, L. D., Hernandez-Ronquillo, L., & Téllez-Zenteno, J. F. (2017). Epidemiology of early stages of epilepsy: Risk of seizure recurrence after a first seizure. Seizure, 49, 46–53. https://doi.org/10.1016/j.seizure.2017.02.006

Robitaille, P.-M., & Berliner, L. (2006). Ultra High Field Magnetic Resonance Imaging (Vol. 26). Springer US. https://doi.org/10.1007/978-0-387-49648-1

Royer, J., Bernhardt, B. C., Larivière, S., Gleichgerrcht, E., Vorderwülbecke, B. J., Vulliémoz, S., & Bonilha, L. (2022). Epilepsy and brain network hubs. Epilepsia, 63(3), 537–550. https://doi.org/10.1111/epi.17171

Rubinov, M., & Sporns, O. (2010). Complex network measures of brain connectivity: Uses and interpretations. NeuroImage, 52(3), 1059–1069. https://doi.org/10.1016/j.neuroimage.2009.10.003

Schaefer, A., Kong, R., Gordon, E. M., Laumann, T. O., Zuo, X.-N., Holmes, A. J., Eickhoff, S. B., & Yeo, B. T. T. (2018). Local-Global Parcellation of the Human Cerebral Cortex from Intrinsic Functional Connectivity MRI. Cerebral Cortex, 28(9), 3095–3114. https://doi.org/10.1093/cercor/bhx179

Scharfman, H. E. (2007). The neurobiology of epilepsy. Current Neurology and Neuroscience Reports, 7(4), 348–354. https://doi.org/10.1007/s11910-007-0053-z

Scheffer, I. E., Berkovic, S., Capovilla, G., Connolly, M. B., French, J., Guilhoto, L., Hirsch, E., Jain, S., Mathern, G. W., Moshé, S. L., Nordli, D. R., Perucca, E.,

Tomson, T., Wiebe, S., Zhang, Y., & Zuberi, S. M. (2017). ILAE classification of the epilepsies: Position paper of the ILAE Commission for Classification and Terminology. Epilepsia, 58(4), 512–521. https://doi.org/10.1111/epi.13709

Schulze-Bonhage, A., Richardson, M. P., Brandt, A., Zabler, N., Dümpelmann, M., & San Antonio-Arce, V. (2023). Cyclical underreporting of seizures in patient-based seizure documentation. Annals of Clinical and Translational Neurology, 10(10), 1863–1872. https://doi.org/10.1002/acn3.51880

Seidlitz, J., Váša, F., Shinn, M., Romero-Garcia, R., Whitaker, K. J., Vértes, P. E., Wagstyl, K., Kirkpatrick Reardon, P., Clasen, L., Liu, S., Messinger, A., Leopold, D. A., Fonagy, P., Dolan, R. J., Jones, P. B., Goodyer, I. M., Raznahan, A., & Bullmore, E. T. (2018). Morphometric Similarity Networks Detect Microscale Cortical Organization and Predict Inter-Individual Cognitive Variation. Neuron, 97(1), 231-247.e7. https://doi.org/10.1016/j.neuron.2017.11.039

Seiger, R., Hahn, A., Hummer, A., Kranz, G. S., Ganger, S., Küblböck, M., Kraus, C., Sladky, R., Kasper, S., Windischberger, C., & Lanzenberger, R. (2015). Voxel-based morphometry at ultra-high fields. A comparison of 7T and 3T MRI data. NeuroImage, 113, 207–216. https://doi.org/10.1016/j.neuroimage.2015.03.019

Shaffer, J. J., Mani, M., Schmitz, S. L., Xu, J., Owusu, N., Wu, D., Magnotta, V. A., & Wemmie, J. A. (2020). Proton Exchange Magnetic Resonance Imaging: Current and Future Applications in Psychiatric Research. Frontiers in Psychiatry, 11, 532606. https://doi.org/10.3389/fpsyt.2020.532606

Shinnar, S., Berg, A. T., Moshé, S. L., Petix, M., Maytal, J., Kang, H., Goldensohn, E. S., & Hauser, W. A. (1990). Risk of Seizure Recurrence Following a First Unprovoked Seizure in Childhood: A Prospective Study. Pediatrics, 85(6), 1076–1085. https://doi.org/10.1542/peds.85.6.1076

Siebenbrodt, K., Willems, L. M., Von Podewils, F., Mross, P. M., Strüber, M., Langenbruch, L., Bierhansl, L., Gorny, I., Schulz, J., Gaida, B., Conradi, N., Süß, A., Rosenow, F., & Strzelczyk, A. (2023). Determinants of quality of life in adults with epilepsy: A multicenter, cross-sectional study from Germany. Neurological Research and Practice, 5(1), 41. https://doi.org/10.1186/s42466-023-00265-5

Sinha, N., Joshi, R. B., Sandhu, M. R. S., Netoff, T. I., Zaveri, H. P., & Lehnertz, K. (2022). Perspectives on Understanding Aberrant Brain Networks in Epilepsy. Frontiers in Network Physiology, 2, 868092. https://doi.org/10.3389/fnetp.2022.868092

Smith, S. J. M. (2005). EEG in the diagnosis, classification, and management of patients with epilepsy. Journal of Neurology, Neurosurgery & Psychiatry, 76(suppl_2), ii2–ii7. https://doi.org/10.1136/jnnp.2005.069245

Spencer, D. (2014). MRI (Minimum Recommended Imaging) in Epilepsy: Proposal for a Magnetic Resonance Imaging Protocol. Epilepsy Currents, 14(5), 261–263. https://doi.org/10.5698/1535-7597-14.5.261

Spencer, S. S. (2002). Neural Networks in Human Epilepsy: Evidence of and Implications for Treatment. Epilepsia, 43(3), 219–227. https://doi.org/10.1046/j.1528-1157.2002.26901.x

Sporns, O. (2018). Graph theory methods: Applications in brain networks. Dialogues in Clinical Neuroscience, 20(2), 111–121. https://doi.org/10.31887/DCNS.2018.20.2/osporns

Springer, E., Dymerska, B., Cardoso, P. L., Robinson, S. D., Weisstanner, C., Wiest, R., Schmitt, B., & Trattnig, S. (2016). Comparison of Routine Brain Imaging at 3 T and 7 T. Investigative Radiology, 51(8), 469–482. https://doi.org/10.1097/RLI.0000000000000256

Stafstrom, C. E. (2014). Recognizing Seizures and Epilepsy: Insights from Pathophysiology. In J. W. Miller & H. P. Goodkin (Eds.), Epilepsy (1st ed., pp. 1–9). Wiley. https://doi.org/10.1002/9781118456989.ch1

Stafstrom, C. E., & Carmant, L. (2015). Seizures and Epilepsy: An Overview for Neuroscientists. Cold Spring Harbor Perspectives in Medicine, 5(6), a022426–a022426. https://doi.org/10.1101/cshperspect.a022426

Suárez, L. E., Markello, R. D., Betzel, R. F., & Misic, B. (2020). Linking Structure and Function in Macroscale Brain Networks. Trends in Cognitive Sciences, 24(4), 302–315. https://doi.org/10.1016/j.tics.2020.01.008

Thom, M. (2014). Review: Hippocampal sclerosis in epilepsy: a neuropathology review. Neuropathology and Applied Neurobiology, 40(5), 520–543. https://doi.org/10.1111/nan.12150

Tomson, T., Battino, D., Bromley, R., Kochen, S., Meador, K. J., Pennell, P. B., & Thomas, S. V. (2022). Breastfeeding while on treatment with antiseizure medications: A systematic review from the ILAE Women Task Force. Epileptic Disorders, 24(6), 1020–1032. https://doi.org/10.1684/epd.2022.1492

Vaidya, M. V., Collins, C. M., Sodickson, D. K., Brown, R., Wiggins, G. C., & Lattanzi, R. (2016). Dependence of and field patterns of surface coils on the electrical

properties of the sample and the MR operating frequency. Concepts in Magnetic Resonance Part B: Magnetic Resonance Engineering, 46(1), 25–40. https://doi.org/10.1002/cmr.b.21319

Van Diessen, E., Diederen, S. J. H., Braun, K. P. J., Jansen, F. E., & Stam, C. J. (2013). Functional and structural brain networks in epilepsy: What have we learned? Epilepsia, 54(11), 1855–1865. https://doi.org/10.1111/epi.12350

Vaughan, J. T., Garwood, M., Collins, C. M., Liu, W., DelaBarre, L., Adriany, G., Andersen, P., Merkle, H., Goebel, R., Smith, M. B., & Ugurbil, K. (2001). 7T vs. 4T: RF power, homogeneity, and signal-to-noise comparison in head images. Magnetic Resonance in Medicine, 46(1), 24–30. https://doi.org/10.1002/mrm.1156

Velissaris, S. L., Wilson, S. J., Saling, M. M., Newton, M. R., & Berkovic, S. F. (2007). The psychological impact of a newly diagnosed seizure: Losing and restoring perceived control. Epilepsy & Behavior, 10(2), 223–233. https://doi.org/10.1016/j.yebeh.2006.12.008

Vergara López, S., Ramos-Jiménez, C., Adrián De La Cruz Reyes, L., Kevin Galindo Ruiz, A., Armando Baigts Arriola, L., Manuel Moncayo Olivares, J., Gabriela Aguirre Galindo, E., Fabricio Pérez Pedroza, I., & San-Juan, D. (2021). Epilepsy diagnosis based on one unprovoked seizure and ≥60% risk. A systematic review of the etiologies. Epilepsy & Behavior, 125, 108392. https://doi.org/10.1016/j.yebeh.2021.108392

Viessmann, O., & Polimeni, J. R. (2021). High-resolution fMRI at 7 Tesla: Challenges, promises and recent developments for individual-focused fMRI studies. Current Opinion in Behavioral Sciences, 40, 96–104. https://doi.org/10.1016/j.cobeha.2021.01.011

Von Oertzen, J. (2002). Standard magnetic resonance imaging is inadequate for patients with refractory focal epilepsy. Journal of Neurology, Neurosurgery & Psychiatry, 73(6), 643–647. https://doi.org/10.1136/jnnp.73.6.643

Wang, E., Jia, Y., Ya, Y., Xu, J., Mao, C., Luo, W., Fan, G., & Jiang, Z. (2021). Abnormal Topological Organization of Sulcal Depth-Based Structural Covariance Networks in Parkinson's Disease. Frontiers in Aging Neuroscience, 12, 575672. https://doi.org/10.3389/fnagi.2020.575672

Wang, I., Bernasconi, A., Bernhardt, B., Blumenfeld, H., Cendes, F., Chinvarun, Y., Jackson, G., Morgan, V., Rampp, S., Vaudano, A. E., & Federico, P. (2020). MRI

essentials in epileptology: A review from the ILAE Imaging Taskforce. Epileptic Disorders, 22(4), 421–437. https://doi.org/10.1684/epd.2020.1174

Wang, I., Oh, S., Blümcke, I., Coras, R., Krishnan, B., Kim, S., McBride, A., Grinenko, O., Lin, Y., Overmyer, M., Aung, T. T., Lowe, M., Larvie, M., Alexopoulos, A. V., Bingaman, W., Gonzalez-Martinez, J. A., Najm, I., & Jones, S. E. (2020). Value of 7T MRI and post-processing in patients with nonlesional 3T MRI undergoing epilepsy presurgical evaluation. Epilepsia, 61(11), 2509–2520. https://doi.org/10.1111/epi.16682

Wang, M., Cheng, X., Shi, Q., Xu, B., Hou, X., Zhao, H., Gui, Q., Wu, G., Dong, X., Xu, Q., Shen, M., Cheng, Q., Xue, S., Feng, H., & Ding, Z. (2023). Brain diffusion tensor imaging reveals altered connections and networks in epilepsy patients. Frontiers in Human Neuroscience, 17, 1142408. https://doi.org/10.3389/fnhum.2023.1142408

Whelan, C. D., Altmann, A., Botía, J. A., Jahanshad, N., Hibar, D. P., Absil, J., Alhusaini, S., Alvim, M. K. M., Auvinen, P., Bartolini, E., Bergo, F. P. G., Bernardes, T., Blackmon, K., Braga, B., Caligiuri, M. E., Calvo, A., Carr, S. J., Chen, J., Chen, S., … Sisodiya, S. M. (2018). Structural brain abnormalities in the common epilepsies assessed in a worldwide ENIGMA study. Brain, 141(2), 391–408. https://doi.org/10.1093/brain/awx341

Whitaker, K., & Staden, I. (2018). SCONA: Structural Covariance Network Analysis [Github]. https://whitakerlab.github.io/scona/

Winkler, A. M., Kochunov, P., Blangero, J., Almasy, L., Zilles, K., Fox, P. T., Duggirala, R., & Glahn, D. C. (2010). Cortical thickness or grey matter volume? The importance of selecting the phenotype for imaging genetics studies. NeuroImage, 53(3), 1135–1146. https://doi.org/10.1016/j.neuroimage.2009.12.028

Woermann, F. G., Free, S. L., Koepp, M. J., Ashburner, J., & Duncan, J. S. (1999). Voxel-by-Voxel Comparison of Automatically Segmented Cerebral Gray Matter—A Rater-Independent Comparison of Structural MRI in Patients with Epilepsy. NeuroImage, 10(4), 373–384. https://doi.org/10.1006/nimg.1999.0481

World Health Organization. (2019). Epilepsy: A public health imperative. World Health Organization. https://iris.who.int/handle/10665/325293

Yao, Z., Hu, B., Xie, Y., Moore, P., & Zheng, J. (2015). A review of structural and functional brain networks: Small world and atlas. Brain Informatics, 2(1), 45–52. https://doi.org/10.1007/s40708-015-0009-z

Yasuda, C. L., Chen, Z., Beltramini, G. C., Coan, A. C., Morita, M. E., Kubota, B., Bergo, F., Beaulieu, C., Cendes, F., & Gross, D. W. (2015). Aberrant topological patterns of brain structural network in temporal lobe epilepsy. Epilepsia, 56(12), 1992–2002. https://doi.org/10.1111/epi.13225

Yeo, B. T. T., Krienen, F. M., Sepulcre, J., Sabuncu, M. R., Lashkari, D., Hollinshead, M., Roffman, J. L., Smoller, J. W., Zöllei, L., Polimeni, J. R., Fischl, B., Liu, H., & Buckner, R. L. (2011). The organization of the human cerebral cortex estimated by intrinsic functional connectivity. Journal of Neurophysiology, 106(3), 1125–1165. https://doi.org/10.1152/jn.00338.2011

Zhang, Y., Ma, M., Xie, Z., Wu, H., Zhang, N., & Shen, J. (2021). Bridging the Gap Between Morphometric Similarity Mapping and Gene Transcription in Alzheimer's Disease. Frontiers in Neuroscience, 15, 731292. https://doi.org/10.3389/fnins.2021.731292

Appendix A

4.5. A.1. Schaefer 2018 200 Parcellation Label Glossary

Network Name	Parcellation Label Name	Full Region Name
	Left Hemisphere	
1) Central Visual Network	17Networks_LH_VisCent_ExStr_1	Extrastriate cortex
	17Networks_LH_VisCent_ExStr_2	Extrastriate cortex
	17Networks_LH_VisCent_Striate_1	Striate cortex
	17Networks_LH_VisCent_ExStr_3	Extrastriate cortex
	17Networks_LH_VisCent_ExStr_4	Extrastriate cortex
	17Networks_LH_VisCent_ExStr_5	Extrastriate cortex
2) Peripheral Visual Network	17Networks_LH_VisPeri_ExStrInf_1	Inferior extrastriate cortex
	17Networks_LH_VisPeri_ExStrInf_2	Inferior extrastriate cortex
	17Networks_LH_VisPeri_ExStrInf_3	Inferior extrastriate cortex
	17Networks_LH_VisPeri_StriCal_1	Striate Calcarine cortex
	17Networks_LH_VisPeri_ExStrSup_1	Superior Extrastriate
	17Networks_LH_VisPeri_ExStrSup_2	Superior Extrastriate
3) Somatomotor A Network	17Networks_LH_SomMotA_1	Somatomotor cortex
	17Networks_LH_SomMotA_2	Somatomotor cortex
	17Networks_LH_SomMotA_3	Somatomotor cortex
	17Networks_LH_SomMotA_4	Somatomotor cortex
	17Networks_LH_SomMotA_5	Somatomotor cortex
	17Networks_LH_SomMotA_6	Somatomotor cortex
	17Networks_LH_SomMotA_7	Somatomotor cortex
	17Networks_LH_SomMotA_8	Somatomotor cortex
	17Networks_LH_SomMotB_Aud_1	Auditory Cortex
	17Networks_LH_SomMotB_Aud_2	Auditory Cortex

	17Networks_LH_SomMotB_S2_1	Secondary somatosensory cortex
4) Somatomotor B Network	17Networks_LH_SomMotB_S2_2	Secondary somatosensory cortex
	17Networks_LH_SomMotB_Aud_3	Auditory Cortex
	17Networks_LH_SomMotB_S2_3	Secondary somatosensory cortex
	17Networks_LH_SomMotB_Cent_1	Central sulcus cortex
	17Networks_LH_SomMotB_Cent_2	Central sulcus cortex
5) Dorsal Attention A Network	17Networks_LH_DorsAttnA_TempOcc_1	Temporal Occipital cortex
	17Networks_LH_DorsAttnA_TempOcc_2	Temporal Occipital cortex
	17Networks_LH_DorsAttnA_ParOcc_1	Parietal occipital cortex
	17Networks_LH_DorsAttnA_SPL_1	Superior parietal lobule
	17Networks_LH_DorsAttnA_SPL_2	Superior parietal lobule
	17Networks_LH_DorsAttnA_SPL_3	Superior parietal lobule
6) Dorsal Attention B Network	17Networks_LH_DorsAttnB_PostC_1	Post-central cortex
	17Networks_LH_DorsAttnB_PostC_2	Post-central cortex
	17Networks_LH_DorsAttnB_PostC_3	Post-central cortex
	17Networks_LH_DorsAttnB_PostC_4	Post-central cortex
	17Networks_LH_DorsAttnB_FEF_1	Frontal eye-fields
	17Networks_LH_SalVentAttnA_ParOper_1	Parietal occipital cortex

7) **Salience/Ventr** **al Attention A**	17Networks_LH_SalVentAttnA_Ins _1	Insula
	17Networks_LH_SalVentAttnA_Fr Oper_1	Frontal Operculum
	17Networks_LH_SalVentAttnA_Fr Oper_2	Frontal Operculum
	17Networks_LH_SalVentAttnA_Par Med_1	Parietal medial cortex
	17Networks_LH_SalVentAttnA_Fr Med_1	Frontal medial cortex
	17Networks_LH_SalVentAttnA_Fr Med_2	Frontal medial cortex
8) **Salience/Ventr** **al Network**	17Networks_LH_SalVentAttnB_IPL _1	Inferior parietal lobule
	17Networks_LH_SalVentAttnB_PF Cl_1	Lateral prefrontal cortex
	17Networks_LH_SalVentAttnB_Ins _1	Insula
	17Networks_LH_SalVentAttnB_PF Cmp_1	Medial posterier prefrontal cortex
9) Limbic B **Network**	17Networks_LH_LimbicB_OFC_1	Orbito frontal cortex
	17Networks_LH_LimbicB_OFC_2	Orbito frontal cortex
10) Limbic A **Network**	17Networks_LH_LimbicA_TempPo le_1	Temporal Pole
	17Networks_LH_LimbicA_TempPo le_2	Temporal Pole
	17Networks_LH_LimbicA_TempPo le_3	Temporal Pole
	17Networks_LH_LimbicA_TempPo le_4	Temporal Pole
11) Control A **Network**	17Networks_LH_ContA_Temp_1	Temporal cortex
	17Networks_LH_ContA_IPS_1	Intraparietal sulcus
	17Networks_LH_ContA_IPS_2	Intraparietal sulcus

	17Networks_LH_ContA_IPS_3	Intraparietal sulcus
	17Networks_LH_ContA_PFCd_1	Dorsal prefrontal cortex
	17Networks_LH_ContA_PFClv_1	Ventrolateral prefrontal cortex
	17Networks_LH_ContA_PFCl_1	Lateral prefrontal cortex
	17Networks_LH_ContA_PFCl_2	Lateral prefrontal cortex
	17Networks_LH_ContA_PFCl_3	Lateral prefrontal cortex
	17Networks_LH_ContA_Cingm_1	Mid-cingulate cortex
12) Control B Network	17Networks_LH_ContB_Temp_1	Temporal cortex
	17Networks_LH_ContB_IPL_1	Intraparietal sulcus
	17Networks_LH_ContB_PFCl_1	Lateral prefrontal cortex
	17Networks_LH_ContB_PFClv_1	Ventrolateral prefrontal cortex
	17Networks_LH_ContB_PFClv_2	Ventrolateral prefrontal cortex
13) Control C Network	17Networks_LH_ContC_pCun_1	Precuneus
	17Networks_LH_ContC_pCun_2	Precuneus
	17Networks_LH_ContC_Cingp_1	Posterior cingulate
14) Default A Network	17Networks_LH_DefaultA_IPL_1	Intraparietal sulcus
	17Networks_LH_DefaultA_PFCd_1	Dorsal prefrontal cortex
	17Networks_LH_DefaultA_pCunPCC_1	Precuneus posterior cingulate cortex
	17Networks_LH_DefaultA_pCunPCC_2	Precuneus posterior cingulate cortex
	17Networks_LH_DefaultA_pCunPCC_3	Precuneus posterior cingulate cortex
	17Networks_LH_DefaultA_PFCm_1	Medial posterier prefrontal cortex
	17Networks_LH_DefaultA_PFCm_2	Medial posterier prefrontal cortex
	17Networks_LH_DefaultA_PFCm_3	Medial posterier prefrontal cortex
	17Networks_LH_DefaultB_Temp_1	Temporal cortex

	17Networks_LH_DefaultB_Temp_2	Temporal cortex
	17Networks_LH_DefaultB_Temp_3	Temporal cortex
	17Networks_LH_DefaultB_Temp_4	Temporal cortex
	17Networks_LH_DefaultB_IPL_1	Inferior parietal lobule
	17Networks_LH_DefaultB_PFCd_1	Dorsal prefrontal cortex
15) Default B	17Networks_LH_DefaultB_PFCd_2	Dorsal prefrontal cortex
Network	17Networks_LH_DefaultB_PFCd_3	Dorsal prefrontal cortex
	17Networks_LH_DefaultB_PFCd_4	Dorsal prefrontal cortex
	17Networks_LH_DefaultB_PFCv_1	Ventral prefrontal cortex
	17Networks_LH_DefaultB_PFCv_2	Ventral prefrontal cortex
	17Networks_LH_DefaultB_PFCv_3	Ventral prefrontal cortex
	17Networks_LH_DefaultB_PFCv_4	Ventral prefrontal cortex
16) Default C	17Networks_LH_DefaultC_IPL_1	Inferior parietal lobule
Network	17Networks_LH_DefaultC_Rsp_1	Retrosplenial cortex
	17Networks_LH_DefaultC_PHC_1	Parahippocampal cortex
17) Temporal	17Networks_LH_TempPar_1	Temporal parietal cortex
Parietal **Network**	17Networks_LH_TempPar_2	Temporal parietal cortex
Right Hemisphere		
	17Networks_RH_VisCent_ExStr_1	Extrastriate cortex
	17Networks_RH_VisCent_ExStr_2	Extrastriate cortex
1) Central	17Networks_RH_VisCent_Striate_1	Striate cortex
Visual	17Networks_RH_VisCent_ExStr_3	Extrastriate cortex
Network	17Networks_RH_VisCent_ExStr_4	Extrastriate cortex
	17Networks_RH_VisCent_ExStr_5	Extrastriate cortex
	17Networks_RH_VisPeri_ExStrInf_1	Inferior extrastriate cortex
2) Peripheral	17Networks_RH_VisPeri_ExStrInf_2	Inferior extrastriate cortex
Visual	17Networks_RH_VisPeri_StriCal_1	Striate Calcarine cortex
Network	17Networks_RH_VisPeri_ExStrSup_1	Superior Extrastriate

	17Networks_RH_VisPeri_ExStrSup _2	Superior Extrastriate
	17Networks_RH_VisPeri_ExStrSup _3	Superior Extrastriate
3) Somatomotor A Network	17Networks_RH_SomMotA_1	Somatomotor cortex
	17Networks_RH_SomMotA_2	Somatomotor cortex
	17Networks_RH_SomMotA_3	Somatomotor cortex
	17Networks_RH_SomMotA_4	Somatomotor cortex
	17Networks_RH_SomMotA_5	Somatomotor cortex
	17Networks_RH_SomMotA_6	Somatomotor cortex
	17Networks_RH_SomMotA_7	Somatomotor cortex
	17Networks_RH_SomMotA_8	Somatomotor cortex
	17Networks_RH_SomMotA_9	Somatomotor cortex
	17Networks_RH_SomMotA_10	Somatomotor cortex
	17Networks_RH_SomMotA_11	Somatomotor cortex
4) Somatomotor B Network	17Networks_RH_SomMotB_Aud_1	Auditory Cortex
	17Networks_RH_SomMotB_Aud_2	Auditory Cortex
	17Networks_RH_SomMotB_S2_1	Secondary somatosensory cortex
	17Networks_RH_SomMotB_S2_2	Secondary somatosensory cortex
	17Networks_RH_SomMotB_S2_3	Secondary somatosensory cortex
	17Networks_RH_SomMotB_S2_4	Secondary somatosensory cortex
	17Networks_RH_SomMotB_Cent_1	Central sulcus cortex
5) Dorsal Attention A Network	17Networks_RH_DorsAttnA_Temp Occ_1	Temporal Occipital cortex
	17Networks_RH_DorsAttnA_ParOc c_1	Parietal occipital cortex
	17Networks_RH_DorsAttnA_SPL_ 1	Superior parietal lobule

	17Networks_RH_DorsAttnA_SPL_2	Superior parietal lobule
	17Networks_RH_DorsAttnA_SPL_3	Superior parietal lobule
	17Networks_RH_DorsAttnA_SPL_4	Superior parietal lobule
6) Dorsal Attention B Network	17Networks_RH_DorsAttnB_PostC_1	Post-central cortex
	17Networks_RH_DorsAttnB_PostC_2	Post-central cortex
	17Networks_RH_DorsAttnB_PostC_3	Post-central cortex
	17Networks_RH_DorsAttnB_PostC_4	Post-central cortex
	17Networks_RH_DorsAttnB_FEF_1	Frontal eye-fields
7) Salience/Ventral Attention A	17Networks_RH_SalVentAttnA_ParOper_1	Parietal operculum
	17Networks_RH_SalVentAttnA_PrC_1	Precuneus
	17Networks_RH_SalVentAttnA_Ins_1	Insula
	17Networks_RH_SalVentAttnA_Ins_2	Insula
	17Networks_RH_SalVentAttnA_FrOper_1	Frontal Operculum
	17Networks_RH_SalVentAttnA_FrMed_1	Frontal medial cortex
	17Networks_RH_SalVentAttnA_ParMed_1	Parietal medial cortex
	17Networks_RH_SalVentAttnA_ParMed_2	Parietal medial cortex

	17Networks_RH_SalVentAttnA_Fr Med_2	Frontal medial cortex
8) Salience/Ventr al Attention B Network	17Networks_RH_SalVentAttnB_IPL _1	Inferior parietal lobule
	17Networks_RH_SalVentAttnB_PF Clv_1	Ventrolateral prefrontal cortex
	17Networks_RH_SalVentAttnB_PF Cl_1	Lateral prefrontal cortex
	17Networks_RH_SalVentAttnB_Ins _1	Insula
	17Networks_RH_SalVentAttnB_Ins _2	Insula
	17Networks_RH_SalVentAttnB_PF Cmp_1	Medial posterier prefrontal cortex
9) Limbic B Network	17Networks_RH_LimbicB_OFC_1	Orbito frontal cortex
	17Networks_RH_LimbicB_OFC_2	Orbito frontal cortex
	17Networks_RH_LimbicB_OFC_3	Orbito frontal cortex
	17Networks_RH_LimbicB_OFC_4	Orbito frontal cortex
10) Limbic A Network	17Networks_RH_LimbicA_TempPo le_1	Temporal pole
	17Networks_RH_LimbicA_TempPo le_2	Temporal pole
	17Networks_RH_LimbicA_TempPo le_3	Temporal pole
	17Networks_RH_LimbicA_TempPo le_4	Temporal pole
11) Control A Network	17Networks_RH_ContA_IPS_1	Intraparietal sulcus
	17Networks_RH_ContA_IPS_2	Intraparietal sulcus
	17Networks_RH_ContA_PFCd_1	Dorsal prefrontal cortex
	17Networks_RH_ContA_PFCl_1	Lateral prefrontal cortex
	17Networks_RH_ContA_PFCl_2	Lateral prefrontal cortex
	17Networks_RH_ContA_Cingm_1	Mid-cingulate cortex
	17Networks_RH_ContB_Temp_1	Temporal cortex

	17Networks_RH_ContB_Temp_2	Temporal cortex
	17Networks_RH_ContB_IPL_1	Inferior parietal lobule
	17Networks_RH_ContB_IPL_2	Inferior parietal lobule
	17Networks_RH_ContB_PFCld_1	Dorsal prefrontal cortex
	17Networks_RH_ContB_PFCld_2	Dorsal prefrontal cortex
12) Control B Network	17Networks_RH_ContB_PFClv_1	Ventrolateral prefrontal cortex
	17Networks_RH_ContB_PFClv_2	Ventrolateral prefrontal cortex
	17Networks_RH_ContB_PFCmp_1	Medial posterier prefrontal cortex
	17Networks_RH_ContB_PFCld_3	Dorsolateral prefrontal cortex
13) Control C Network	17Networks_RH_ContC_pCun_1	Precuneus
	17Networks_RH_ContC_pCun_2	Precuneus
	17Networks_RH_ContC_Cingp_1	Posterior cingulate
	17Networks_RH_DefaultA_IPL_1	Inferior parietal lobule
	17Networks_RH_DefaultA_PFCd_1	Dorsal prefrontal cortex
	17Networks_RH_DefaultA_pCunPCC_1	Precuneus posterior cingulate cortex
14) Default A Network	17Networks_RH_DefaultA_PFCm_1	Medial prefrontal cortex
	17Networks_RH_DefaultA_PFCm_2	Medial prefrontal cortex
	17Networks_RH_DefaultA_PFCm_3	Medial prefrontal cortex
	17Networks_RH_DefaultB_Temp_1	Temporal cortex
15) Default B Network	17Networks_RH_DefaultB_AntTemp_1	Anterior Temporal cortex
	17Networks_RH_DefaultB_PFCd_1	Dorsal prefrontal cortex
	17Networks_RH_DefaultB_PFCv_1	Ventral prefrontal cortex
16) Default C Network	17Networks_RH_DefaultC_IPL_1	Inferior parietal lobule
	17Networks_RH_DefaultC_Rsp_1	Retrosplenial cortex

	17Networks_RH_DefaultC_PHC_1	Parahippocampal cortex
17) Temporal Parietal Network	17Networks_RH_TempPar_1	Temporal parietal cortex
	17Networks_RH_TempPar_2	Temporal parietal cortex
	17Networks_RH_TempPar_3	Temporal parietal cortex
	17Networks_RH_TempPar_4	Temporal parietal cortex

4.6. A.2. Schaefer 2018 100 Parcellation Label Glossary

Network Name	Parcellation Label Name	Full Region Name
Left Hemisphere		
1) Central Visual Network	17Networks_LH_VisCent_ExStr_1	Extrastriate cortex
	17Networks_LH_VisCent_ExStr_2	Extrastriate cortex
	17Networks_LH_VisCent_Striate_1	Striate cortex
	17Networks_LH_VisCent_ExStr_3	Extrastriate cortex
2) Peripheral Visual Network	17Networks_LH_VisPeri_ExStrInf_1	Inferior extrastriate cortex
	17Networks_LH_VisPeri_StriCal_1	Striate Calcarine cortex
	17Networks_LH_VisPeri_ExStrSup_1	Superior Extrastriate cortex
3) Somatomotor A Network	17Networks_LH_SomMotA_1	Somatomotor cortex
	17Networks_LH_SomMotA_2	Somatomotor cortex
4) Somatomotor B Network	17Networks_LH_SomMotB_Aud_1	Auditory cortex
	17Networks_LH_SomMotB_S2_1	Secondary somatosensory cortex
	17Networks_LH_SomMotB_S2_2	Secondary somatosensory cortex
	17Networks_LH_SomMotB_Cent_1	Central sulcus cortex
5) Dorsal Attention A Network	17Networks_LH_DorsAttnA_TempOcc_1	Temporal Occipital cortex
	17Networks_LH_DorsAttnA_ParOcc_1	Parietal occipital cortex
	17Networks_LH_DorsAttnA_SPL_1	Superior parietal lobule
6) Dorsal Attention B Network	17Networks_LH_DorsAttnB_PostC_1	Post-central cortex
	17Networks_LH_DorsAttnB_PostC_2	Post-central cortex
	17Networks_LH_DorsAttnB_PostC_3	Post-central cortex

	17Networks_LH_DorsAttnB_FEF_1	Frontal eye-fields
7) Salience / Ventral Attention A Network	17Networks_LH_SalVentAttnA_ParOper_1	Parietal operculum
	17Networks_LH_SalVentAttnA_Ins_1	Insula
	17Networks_LH_SalVentAttnA_Ins_2	Insula
	17Networks_LH_SalVentAttnA_ParMed_1	Parietal medial cortex
	17Networks_LH_SalVentAttnA_FrMed_1	Frontal medial cortex
8) Salience / Ventral Attention B Network	17Networks_LH_SalVentAttnB_PFCl_1	Lateral prefrontal cortex
	17Networks_LH_SalVentAttnB_PFCmp_1	Medial posterier prefrontal cortex
9) Limbic B Network	17Networks_LH_LimbicB_OFC_1	Orbito frontal cortex
10) Limbic A Network	17Networks_LH_LimbicA_TempPole_1	Temporal pole
	17Networks_LH_LimbicA_TempPole_2	Temporal pole
11) Control A Network	17Networks_LH_ContA_IPS_1	Intraparietal sulcus
	17Networks_LH_ContA_PFCl_1	Lateral prefrontal cortex
	17Networks_LH_ContA_PFCl_2	Lateral prefrontal cortex
12) Control B Network	17Networks_LH_ContB_PFClv_1	Ventrolateral prefrontal cortex
13) Control C Network	17Networks_LH_ContC_pCun_1	Precuneus
	17Networks_LH_ContC_pCun_2	Precuneus
	17Networks_LH_ContC_Cingp_1	Posterior cingulate
14) Default A Network	17Networks_LH_DefaultA_PFCd_1	Dorsal prefrontal cortex
	17Networks_LH_DefaultA_pCunPCC_1	Precuneus posterior cingulate cortex

	17Networks_LH_DefaultA_PFCm_1	Medial prefrontal cortex
15) Default B Network	17Networks_LH_DefaultB_Temp_1	Temporal cortex
	17Networks_LH_DefaultB_Temp_2	Temporal cortex
	17Networks_LH_DefaultB_IPL_1	Inferior parietal lobule
	17Networks_LH_DefaultB_PFCd_1	Dorsal prefrontal cortex
	17Networks_LH_DefaultB_PFCl_1	Lateral prefrontal cortex
	17Networks_LH_DefaultB_PFCv_1	Ventrolateral prefrontal cortex
	17Networks_LH_DefaultB_PFCv_2	Ventrolateral prefrontal cortex
16) Default C Network	17Networks_LH_DefaultC_Rsp_1	Retrosplenial cortex
	17Networks_LH_DefaultC_PHC_1	Parahippocampal cortex
17) Temporal Parietal Network	17Networks_LH_TempPar_1	Temporal parietal cortex
Right Hemisphere		
1) Central Visual Network	17Networks_RH_VisCent_ExStr_1	Extrastriate cortex
	17Networks_RH_VisCent_ExStr_2	Extrastriate cortex
	17Networks_RH_VisCent_ExStr_3	Extrastriate cortex
2) Peripheral Visual Network	17Networks_RH_VisPeri_StriCal_1	Striate Calcarine cortex
	17Networks_RH_VisPeri_ExStrInf_1	Inferior extrastriate cortex
	17Networks_RH_VisPeri_ExStrSup_1	Superior Extrastriate cortex
3) Somatomotor A Network	17Networks_RH_SomMotA_1	Somatomotor cortex
	17Networks_RH_SomMotA_2	Somatomotor cortex
	17Networks_RH_SomMotA_3	Somatomotor cortex
	17Networks_RH_SomMotA_4	Somatomotor cortex
4) Somatomotor B Network	17Networks_RH_SomMotB_Aud_1	Auditory cortex
	17Networks_RH_SomMotB_S2_1	Secondary somatosensory cortex

	17Networks_RH_SomMotB_S2_2	Secondary somatosensory cortex
	17Networks_RH_SomMotB_Cent_1	Central sulcus cortex
5) Dorsal Attention A Network	17Networks_RH_DorsAttnA_TempOcc_1	Temporal Occipital cortex
	17Networks_RH_DorsAttnA_ParOcc_1	Parietal occipital cortex
	17Networks_RH_DorsAttnA_SPL_1	Superior parietal lobule
6) Dorsal Attention B Network	17Networks_RH_DorsAttnB_PostC_1	Posterior cingulate
	17Networks_RH_DorsAttnB_PostC_2	Posterior cingulate
	17Networks_RH_DorsAttnB_FEF_1	Frontal eye-fields
7) Salience / Ventral Attention A Network	17Networks_RH_SalVentAttnA_ParOper_1	Parietal operculum
	17Networks_RH_SalVentAttnA_Ins_1	Insula
	17Networks_RH_SalVentAttnA_ParMed_1	Parietal medial cortex
	17Networks_RH_SalVentAttnA_FrMed_1	Frontal medial cortex
8) Salience / Ventral Attention B Network	17Networks_RH_SalVentAttnB_IPL_1	Inferior parietal lobule
	17Networks_RH_SalVentAttnB_PFCl_1	Lateral prefrontal cortex
	17Networks_RH_SalVentAttnB_PFCmp_1	Medial posterier prefrontal cortex
9) Limbic B Network	17Networks_RH_LimbicB_OFC_1	Orbito frontal cortex

	17Networks_RH_LimbicA_TempPole_1	Temporal pole
10) Limbic A Network	17Networks_RH_LimbicA_TempPole_1	Temporal pole
11) Control A Network	17Networks_RH_ContA_IPS_1	Intraparietal sulcus
	17Networks_RH_ContA_PFCl_1	Lateral prefrontal cortex
	17Networks_RH_ContA_PFCl_2	Lateral prefrontal cortex
12) Control B Network	17Networks_RH_ContB_Temp_1	Temporal cortex
	17Networks_RH_ContB_IPL_1	Inferior parietal lobule
	17Networks_RH_ContB_PFCld_1	Dorsal prefrontal cortex
	17Networks_RH_ContB_PFClv_1	Ventrolateral prefrontal cortex
13) Control C Network	17Networks_RH_ContC_Cingp_1	Posterior cingulate
	17Networks_RH_ContC_pCun_1	Precuneus
14) Default A Network	17Networks_RH_DefaultA_IPL_1	Inferior parietal lobule
	17Networks_RH_DefaultA_PFCd_1	Dorsal prefrontal cortex
	17Networks_RH_DefaultA_pCunPCC_1	Precuneus posterior cingulate cortex
	17Networks_RH_DefaultA_PFCm_1	Medial prefrontal cortex
15) Default B Network	17Networks_RH_DefaultB_PFCd_1	Dorsal prefrontal cortex
	17Networks_RH_DefaultB_PFCv_1	Ventrolateral prefrontal cortex
	17Networks_RH_DefaultB_PFCv_2	Ventrolateral prefrontal cortex
16) Default C Network	17Networks_RH_DefaultC_Rsp_1	Retrosplenial cortex
	17Networks_RH_DefaultC_PHC_1	Parahippocampal cortex
17) Temporal Parietal Network	17Networks_RH_TempPar_1	Temporal parietal cortex
	17Networks_RH_TempPar_2	Temporal parietal cortex
	17Networks_RH_TempPar_3	Temporal parietal cortex

Appendix B

4.7. B.1. Ethical Approval from the Health Sciences Research Ethics Board of the University of Western Ontario

Western Research

Date: 16 September 2022

To: Dr. Seyed Mirsattari

Project ID: 107246

Review Reference: 2022-107246-70938

Study Title: Changes in network connectivity after an unprovoked first seizure and status epilepticus using resting state functional magnetic resonance imaging.

Application Type: HSREB Amendment Form

Review Type: Delegated

Meeting Date / Full Board Reporting Date: 27/Sept/2022

Date Approval Issued: 16/Sep/2022 08:53

REB Approval Expiry Date: 17/Feb/2023

Dear Dr. Seyed Mirsattari ,

The Western University Health Sciences Research Ethics Board (HSREB) has reviewed and approved the WREM application form for the amendment, as of the date noted above.

Documents Approved:

Document Name	Document Type	Document Date	Document Version
REBApplication_FirstSz_SE New members Sep 2022	Protocol	13/Sep/2022	1

Documents Acknowledged:

Document Name	Document Type	Document Date	Document Version
Summary of Changes_First Sz Keza and Gaby	Summary of Changes	12/Sep/2022	1

REB members involved in the research project do not participate in the review, discussion or decision.

The Western University HSREB operates in compliance with, and is constituted in accordance with, the requirements of the TriCouncil Policy Statement: Ethical Conduct for Research Involving Humans (TCPS 2); the International Conference on Harmonisation Good Clinical Practice Consolidated Guideline (ICH GCP); Part C, Division 5 of the Food and Drug Regulations; Part 4 of the Natural Health Products Regulations; Part 3 of the Medical Devices Regulations and the provisions of the Ontario Personal Health Information Protection Act (PHIPA 2004) and its applicable regulations. The HSREB is registered with the U.S. Department of Health & Human Services under the IRB registration number IRB 00000940.

Please do not hesitate to contact us if you have any questions.

Electronically signed by:

Patricia Sargeant, Ethics Officer ~~█████████~~ n behalf of Dr. Philip Jones, HSREB Chair, 16/Sep/2022 08:53

Reason: I am approving this document.

Note: This correspondence includes an electronic signature (validation and approval via an online system that is compliant with all regulations).

4.8. Curriculum Vitae

Name	Keza Thuso Motlana	
Education:	**Master of Neuroscience (candidate),** University of Western Ontario, London, ON, Canada **Supervisors:** Dr Ali Khan & Dr Seyed Mirsattari **Thesis:** Cortical Thickness Changes as a Potential Biomarker for Epilepsy in People with First-Time Unprovoked Seizure	**2022 – 2024**
	Honours Bachelor of Science, University of Toronto, Mississauga, ON, Canada	**2016 - 2021**
Honours and Awards:	**Western Graduate Research Scholarship (WGRS),** The University of Western Ontario	**2022 – 2024**
Related Work Experience:	**Graduate Teaching Assistant in Biology,** The University of Western Ontario	**2022 – 2024**
Academic Papers:	Abozaid, A., Hung, J., Tsang, B., **Motlana, K.**, Al-Ani, R., & Gerlai, R. (2022). Behavioral effects of acute ethanol in larval zebrafish (d. rerio) depend on genotype and volume of experimental well. Progress in Neuro-Psychopharmacology and Biological Psychiatry, 112, 110411. https://doi.org/10.1016/j.pnpbp.2021.110411	
	Poulson, S. J., Aldarraji, A., Arain, I. I., Dziekonski, N., **Motlana, K.**, Riley, R., Holmes, M. M., & Martin, L. J. (2020). Naked mole-rats lack cold sensitivity before and after nerve injury. Molecular Pain, 16, 174480692095510. https://doi.org/10.1177/1744806920955103	
Posters and Presentations at Conferences:	**Motlana, K.**, Khan A., & Mirsattari, S. (2023, October 13). Changes in Cortical Thickness as a Potential Biomarker for Epilepsy in People with First-Time Unprovoked Seizure [Presentation]. Centre for Education Research & Innovation 2023 Research Symposium, Charlottetown, PEI, Canada.	
	Motlana, K., Khan A., & Mirsattari, S. (2023, May 16). Changes in Cortical Thickness as a Potential Biomarker for Epilepsy in People with First-Time Unprovoked Seizure [Poster]. Canadian League Against Epilepsy, Charlottetown PEI, Canada.	

	Motlana, K., Khan A., & Mirsattari, S. (2023, May 16). Changes in Cortical Thickness as a Potential Biomarker for Epilepsy in People with First-Time Unprovoked Seizure [Research Day Presentation]. Clinical Neurological Sciences Research Day, University of Western Ontario, London, ON, Canada.
	Poulson, S. J., Arain I. A., **Motlana, K.**, & Martin, L. J. (2021 June 27-July 1). Observation of Social Companions in Pain Modulates the Pain Experience in Mice [Conference Poster]. 2021 The International Association for the Study of Pain, Amsterdam, NL.
	Poulson, S. J., Arain I. A., **Motlana, K.**, Martin, L. J. (2020, December 8). Sensing Pain Expressions in Mice [Research Day Poster]. 2020 Collaborative Program in Neuroscience 2020 Research Day, Toronto, ON, Canada.